EXPERIMENTAL INVESTIGATION OF HEAT TRANSFER CHARACTERISTICS OF MITR-II FUEL PLATES, IN-CHANNEL THERMOCOUPLE RESPONSE AND CALIBRATION

by

WILLIAM JOSEPH SZYMCZAK

BSNE, Lowell Technological Institute

(1972)

SUBMITTED IN PARTIAL FULFILLMENT OF THE REQUIREMENTS FOR THE DEGREE OF

MASTER OF SCIENCE IN NUCLEAR ENGINEERING

at the

MASSACHUSETTS INSTITUTE OF TECHNOLOGY

September, 1975
(i.e. February 1976)

Signature of Author _____
Dept. of Nuclear Engineering
September 17, 1975

Certified by _____
Thesis Supervisor

Accepted by _____
Chairman, Departmental Committee
on Graduate Students

EXPERIMENTAL INVESTIGATION OF HEAT TRANSFER CHARACTERISTICS OF MITR-II FUEL PLATES, IN-CHANNEL THERMOCOUPLE RESPONSE AND CALIBRATION

by

William J. Szymczak

Submitted to the Department of Nuclear Engineering on September 17, 1975 in partial fulfillment of the requirement for the degree of Master of Science in Nuclear Engineering.

ABSTRACT

The heat transfer process in a simulated MITR-II coolant channel has been experimentally investigated. The experimental model was effectively a flat plate with a rectangularly finned convective surface with constant heat flux input. A one-dimensional analysis of the data was undertaken to determine the effective heat transfer coefficients and surface effectiveness. Standard heat transfer plots were made and results compared to values given in the MITR-II Safety Analysis Report. An experimental surface effectiveness, η_0, of 1.885 ± 0.116 was determined.

The response of stainless steel sheated chromel-alumel thermocouples, 10 mils in diameter, identical to the ones used on the MITR-II thermocoupled fuel element, was investigated. Thermocouple response versus Reynolds number is studied and a determination as to whether the thermocouples were reading fuel plate temperature of fluid temperature is made. These results are required for the interpretation of experimental data to be obtained from the testing of the new MITR-II core.

Supervisors: Dr. David D. Lanning and Dr. James Gosnell

Titles: Professors of Nuclear Engineering

ACKNOWLEDGEMENTS

The author wishes to express his gratitude to Dr. David D. Lanning and Dr. James W. Gosnell, professors of Nuclear Engineering for their support and guidance throughout this endeavor and to the MITR-II Reactor for the financial support tended me during my stay at MIT.

The difficulties encountered in the experimental phase of this thesis cannot be overestimated. It was through the suggestions, skill, and ingenuity of machine shop personnel Francis Woodworth and Kenneth Butler that test section was designed and fabricated. Also, I would like to thank Thomas Greene and John Wasik for their help, instruction, and patience in teaching me the use of the machine shop facilities. Electrical problems were solved with the help of Dave Gwinn, Reactor Electrical Supervisor.

The author would like to give special thanks to the Yankee Atomic Electric Company for the services of Miss Sandra Williams who typed the final manuscript. Drawings were prepared by Leonard Andexler.

Finally, I would like to thank my wife Mary, for her patience, encouragement, and understanding throughout this work.

TABLE OF CONTENTS

LIST OF FIGURES

LIST OF SYMBOLS

A	Fin Cross-Sectional Area, FT^2
A_b	Area of Fin Base, Ft^2
A_{BP}	Back Plate Cross-Sectional Area, Ft^2
A_f	Surface Area of Fin, ft^2
A_s	Surface Area, ft^2
C_1	Constant, 8.02 Ft^3/hr - GPM
C_p	Specific Heat Capacity, BTU/lbm - ^oF
D_H	Hydraulic Diameter, Ft
g	Distance from Fin Tip to Back Plate Thermocouple, Ft
h	Heat Transfer Coefficient, BTU/Hr - Ft^2 - ^oF
I	Thermocouple Installation Parameter, BTU/Hr - ft^2 - ^oF
I	Heater Current, amperes
k	Thermal Conductivity, BTU/HR - Ft - ^oF
k_a	Thermal Conductivity of Aluminum
k_e	Thermal Conductivity of Water
k_s	Thermal Conductivity of Cladding Material
k_t	Weighted Conductivity of Thermocouple Wire
l	Fin Height, ft
m	Fin Efficiency Parameter, hP/K_aA
$\dot{m}$	Flow Rate, lbm/hr
N	Number of Fin-Base Cycles
Nu	Nusselt Number, hD_H/k
P	Fin Perimeter, ft
Pr	Prandtl Number, $C_p\mu/k$
q	Heat Transferred from a Surface, BTU/Hr

q_b	Heat Transferred from the Surface of a Fin, BTU/Hr
q_f	Heat Transferred from the Fin Base, BTU/Hr
q''	Back Plate Heat Flux, BTU/Hr - Ft^2 - ^oF
R	Heater Resistance, ohms
R	Equivalent Thermocouple Wire Radius, Ft
Re	Reynold's Number, PVD_h / μ
Rh	Overall Thermal Resistance, BTU/Hr - Ft^2 - ^oF
T	Temperature, ^oF
T_b	Bulk Fluid Temperature
T_{BP}	Back Plate Temperature
T_f	Fluid Temperature
T_o	Observed Temperature
T_s	Actual Surface Temperature
T_w	Wall Temperature
T_{in}	Channel Inlet Temperature
T_{out}	Channel Outlet Temperature
T_z	Fluid Temperature at Position z in Channel
t	Fin Half-Width, ft
V_f	Fluid Velocity, ft/sec
W	Fin Width, ft
W_p	Channel Wetted Perimeter, Ft
z	Height in Channel, ft
z_t	Distance from inlet to IC Location, Ft
Z	Thermocouple Calibration Factor
η_f	Fin Efficiency
η_o	Surface Effectiveness
Θ_B	Back Plate Temperature Difference, F, $T_w - T_f$

μ Viscosity, lbm/hr - Ft

ρ Density, lbm/ft^3

∂ Thermal Coefficient of Resistivity, $ohm/^{o}F$

CHAPTER 1

INTRODUCTION

The redesign of the Massachusetts Institute of Technology Nuclear Reactor (MITR-II) has been completed and present efforts are mainly directed toward the completion of the construction phase of the modification project. The design phase of the modification to the original MIT reactor (MITR-I) began in earnest in the fall of 1967 when a design group composed of both graduate students and MITR Staff personnel was formed under the direction of the late Dr. T. J. Thompson. It officially ended in May, 1974, when the MITR-I was permanently shutdown and work was started on the construction of the new core.

Just prior to the MITR-I decommissioning, an experimental program to determine the heat transfer characteristics of the finned fuel plates was undertaken. The performance of the finned aluminum plates had been inferred from experimental data obtained for stainless steel plates. A surface effectiveness of 1.486 had been determined for the aluminum case and is reported in the MITR-II SAR (1). A theoretical master's thesis by Taborda (2) concludes that the surface effectiveness for the finned aluminum surface is greater than that reported in the MITR-II SAR and that the correct value should be 1.9. Later, an experiment more closely simulating the actual case was attempted to check the response of surface thermocouples and to check on the surface effectiveness. The first trial at this experiment was by Hollenberg and Momsen (3,4) but the results obtained were inconclusive due to difficulties encountered

with their apparatus. Hence a second experiment was set up and is the basis of the research reported in this thesis.

Once construction of the new core is completed, experimenters will have a valuable tool with which to perform core temperature measurements, namely, the thermocoupled fuel element. Fine chromel-alumel thermocouple wires surrounded by a layer of magnesium oxide insulation are covered with a stainless steel sheath. The diameter of the sheath is 0.010 inches and the thermocouples are grounded at the tip. The thermocouple is attached to fuel plate by being "staked" between the fins. Since it is necessary to accurately know the temperature at the fin root, thermocouples identical to those installed on the actual fuel element are attached to the test channel surface in a similar fashion. Their response versus heat transfer coefficient has been studied and calibration curves have been generated. This work constitutes the second part of this thesis.

The above problems are further presented in Chapter 2 as well as a brief synopsis of the MITR-II design. Previous experimental work and the new experimental apparatus are the subject of Chapter 3. Data reduction and results are given in Chapter 4. Conclusions and suggestions for further work are stated in the last chapter. All data taken is listed in Appendix A. The computer program used to analyze this data is given in Appendix B. Data tables were compiled from the program and are listed in Appendix C.

CHAPTER 2

OBJECTIVES

2.1 General

The main objectives of this research are to verify certain aspects of the thermal hydraulic design of the MITR-II reactor and to investigate the response of the in-channel thermocuples which are to be used in the testing of the new core. To accomplish these objectives, an MITR-II coolant channel was experimentally simulated.

To fully appreciate this simulation, a brief description of the MITR-II reactor and its heat removal system is given. Heat transfer and thermcouple objectives are discussed in the latter part of this chapter.

2.2 MITR-II Reactor

The Massachusetts Institute of Technology Reactor (MITR-II) is a heavy-water reflected and light water cooled and moderated nuclear reactor which utilizes flat-plate type finned aluminum clad fuel elements highly enriched in U-235. The reactor is designed to operate at power levels up to five megawatts. This design differs from the old core, MITR-I, by the use of light water cooling of a closely-packed array of finned plate-type fuel elements and a heavy water, D_2O reflector. The core is contained inside two concentric tanks and core shroud. This arrangement is shown in Figure 2.2.1.

Heat generated by the fission of U-235 is removed by the primary and secondary light water cooling systems. The MITR-II

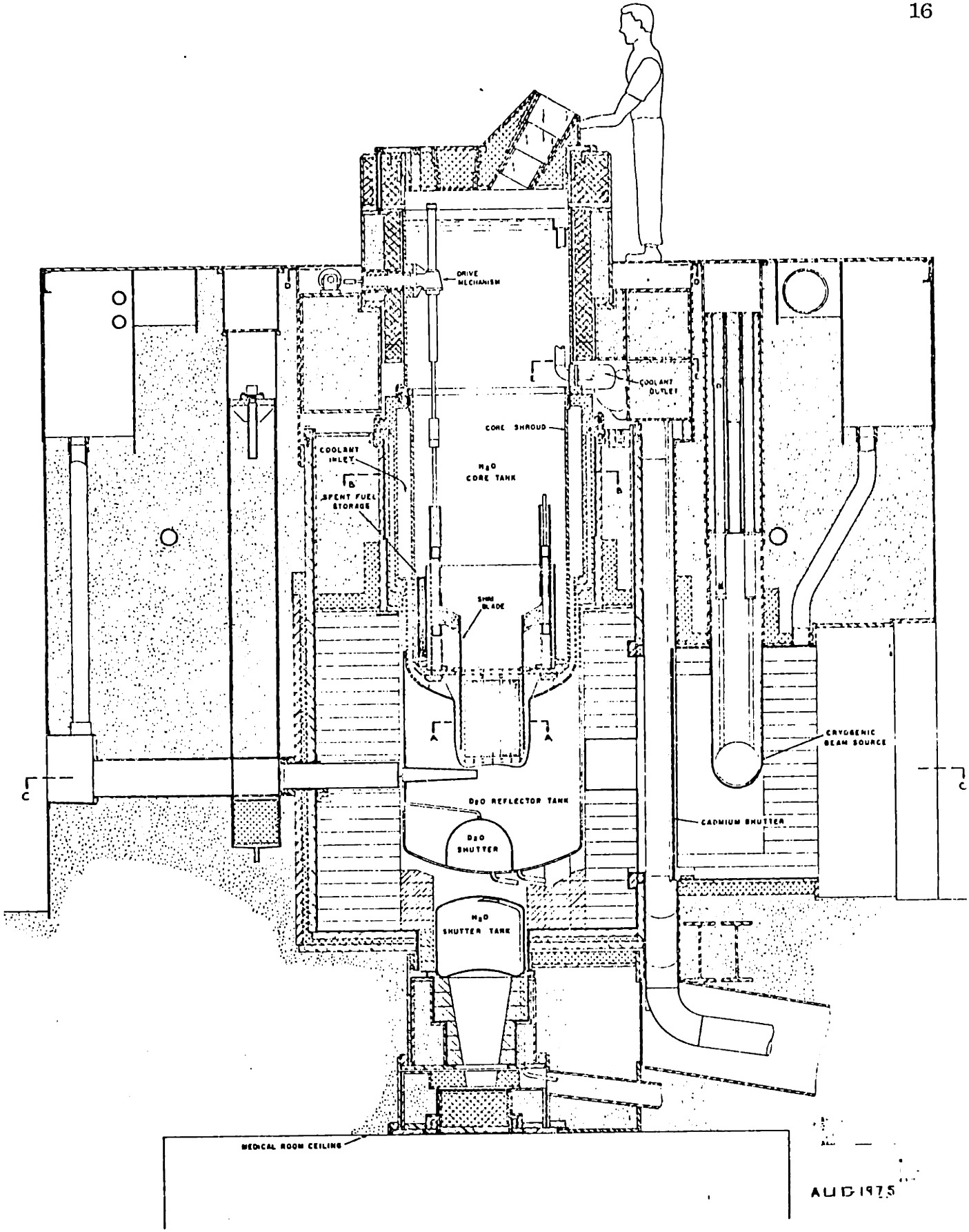

Fig. 2.2.1 Vertical Cross-Section of MITR-II

fuel elements have been specially designed for the high neutron flux compact core. The plates are finned to augment heat transfer.

The finning was necessary to lower clad surface temperatures in the region of peak heat fluxes at the lower edge of the fuel elements. Otherwise, surface temperatures above the incipient boiling point would occur.

A fuel element assembly is shown in Figure 2.2.2. The fuel bearing plates are 0.080 inches thick with longitudinally milled fins on both sides. The fins are 0.010 inches high and 0.010 inches wide separated by 0.010 inch grooves. The spacing between the fuel plates is 0.158 inches which results in a coolant channel 0.078 inches wide, fin-tip to fin-tip. It is this coolant channel which is experimentally simulated in this thesis.

Table 2.2.1 shows MITR-II thermal hydraulic design parameters (taken from Reference (1), Table 3.1-1). In order to simulate the acutal coolant channel and heat flux input, many of the items given in Table 2.2.1 must be adherred to.

First of all, the coolant channel geometry and materials must be duplicated. Secondly, a hydraulic system which provides the necessary range of flow rates is required. Thirdly, a heating system which can duplicate as closely as possible, the heat fluxes experienced in the core is necessary. This last requirement became the most difficult to resolve.

2.3 Heat Transfer Objectives

The heat transfer objectives of this work is to show that the actual effective heat transfer coefficient, $\eta_0 h$ is

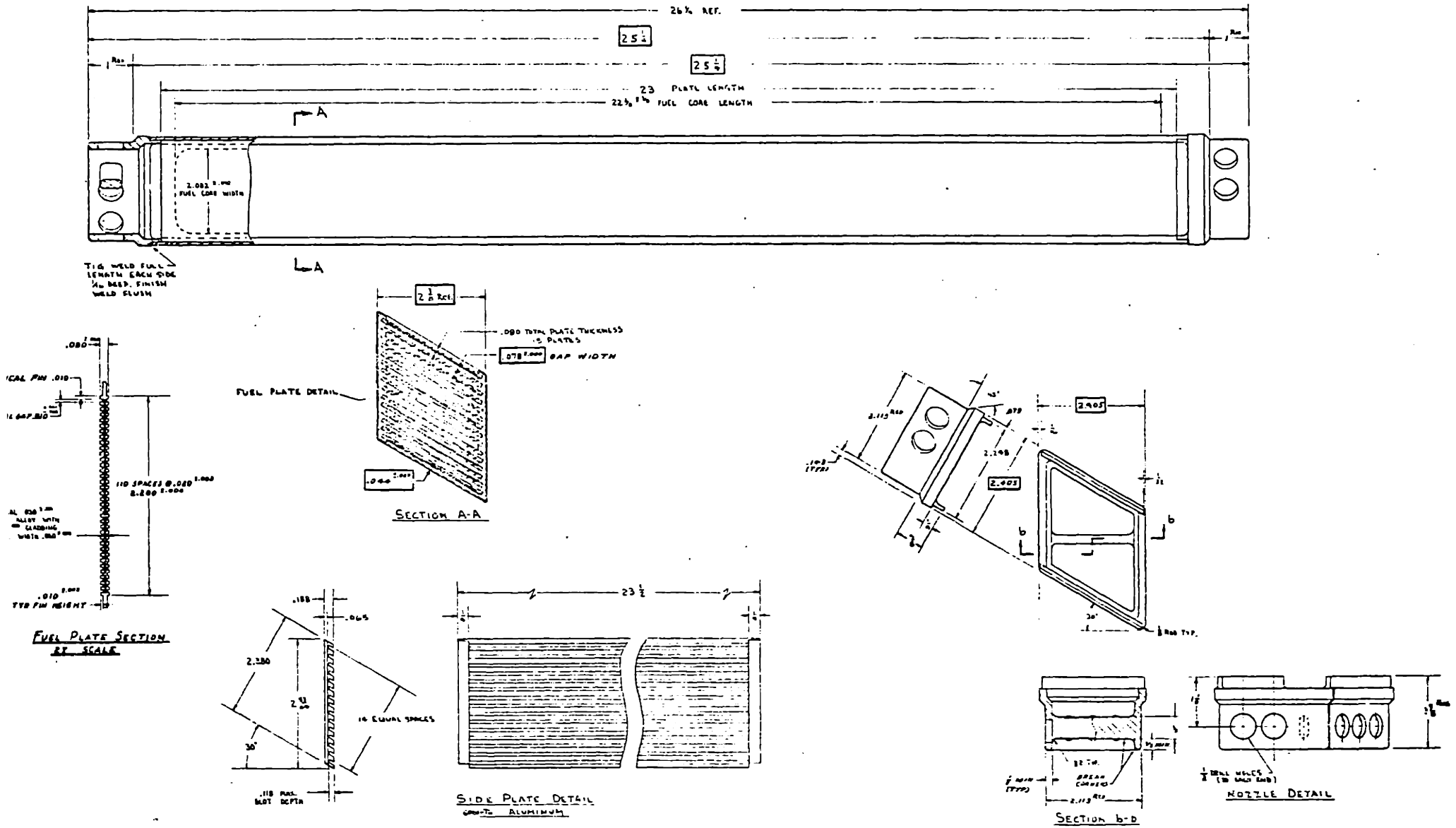

Fig. 2.2.2 MITR-II Fuel Element

TABLE 2.2.1

MITR-II Design Parameters

Pressure Drop Across Fuel Assembly		
Through Fuel Plates		5.0 PSI
Entrance Effect		0.6 PSI
Total		5.6 PSI
Coolant Velocity		8.1 Ft/Sec
Coolant Temperature(Maximum @ 5 Mw and Normal Flow)		
Core Inlet		51.0°C
Core Outlet		60.0°C
Fuel Plates		
Total Height		23 inches
Plate Width		2.552 inches
Height of Fins		0.010±.002 inches
Width of Fins		0.010+.002 inches -.001 inches
Fin Spacing		0.010+.001 inches -.002 inches
Coolant Channel Thickness		
Fin to Fin		0.078±.004 inches
Fin Base to Fin Base		0.098±.008 inches
Flow Area per Channel		0.00141 Ft^2
Heat Flux, 10^5 Btu/Hr-Ft^2		
Average	0.338	0.541 (active volume)
Hot Spot	2.3	2.3
Burnout	15	15
Maximum Surface Temperature		212°F
Incipient Boiling at Hot Spot		248°F

NOTE: The information on this table is taken from Reference (1), Table 3.1-1.

substantially higher than the heat transfer coefficient predicted by the Colburn relation and to show that the actual value of η_0, the surface effectiveness, is greater than the value of 1.486 stated in the MITR-II SAR. These objectives are required in order to confirm this aspect of the thermal hydraulic design. By knowing the actual value of η_0, the degree of conservatism applied to the MITR-II design can be ascertained. In addition to this, the enhanced heat transfer results are needed in the application of the thermocouple investigations conducted in this thesis.

These objectives are achieved through the construction of the test channel described in Chapter 3. Instrumentation is provided such that these parameters, $\eta_0 h$ and h can be readily obtained from the data.

2.4 In-Channel Thermocouple Response Objectives

The proper interpretation of future data obtained from the actual in-channel thermocouples is the main objective in this area of study. The response of the in-channel thermocouples now installed on the thermocoupled fuel element is experimentally inferred from the response of similar thermocouples is a known and controlled installation.

To accomplish this, four similar 10-mil chromel-alumel thermocouples are installed in likewise fashion in the test channel. Temperature readings obtained are used in conjunction with calculated surface temperatures to determine thermocouple response. Data obtained at different test channel flows was assembled to show thermocouple response as a function of the increased heat

transfer coefficient and Reynold's Number. This compilation of thermocouple response data effectively achieved the objectives set forth.

CHAPTER 3

EXPERIMENTAL PROGRAM

3.1 General

As mentioned in Chapter 1, heat transfer data presented in the MITR-II SAR (1) was obtained through experimental work conducted at the MIT Heat Transfer Laboratory. The experiments were carried out by Dennis Spurgeon (5) on longitudinally and transversely finned coolant channels fabricated from stainless steel plates. The decision to augment the heat transfer capability of the new core by using longitudinally finned fuel plates was a direct outcome of his work.

Spurgeon's work laid the foundation for future heat transfer studies. The problem of optimizing the fin spacing remained as well as the questionability of using heat transfer data for electrically heated stainless steel to infer the efficiency of a similarly finned but back plate heated aluminum surface.

A theoretical investigation of these problems was conducted by Taborda (2). Specifically, the heat transfer process in a plate with a rectangularly finned convective surface was studied and fin dimensions were optimized with respect to minimizing fuel clad temperatures. One result of Taborda's thesis was the fact that the surface effectiveness for an aluminum finned surface was found to be approximately 1.9 as opposed to values of 1.486 stated in the MITR-II SAR. Also, Taborda suggested a new experiment which would simulate the actual coolant channel more closely and also

provide for natural circulation studies.

In the spring of 1974, this idea of a new experiment became attractive when the use of in-channel chromel-alumel thermocouples necessitated some form of calibration. Although Taborda's ideas were seriously studied, a new test channel design evolved which almost totally simulated the actual case. This test channel was constructed and ensuing experiments were performed by Bruce Momsen and Ted Hollenberg (3,4). Extreme difficulties were encountered with this new set-up and results were inconclusive. Professor D. D. Lanning, MITR-II Modification Director, expressed his concern for accurate results and subsequently this present work was started.

3.2 Description of Previous Experiments

3.2.1 Spurgeon's Experiment

As mentioned above, Spurgeon (5) conducted heat transfer studies of both flat and finned stainless steel plates. A coolant channel was formed from a stainless steel plate with fins 0.02 inches high, 0.02 inches wide, and separated by 0.04 inches by folding in three times and welding the two edges together. See Figure 3.2.1.1. The channel was heated electrically, with power supplied from the MIT Heat Transfer Laboratory's D.C. generators (maximum output 3000 amps at 24 volts). End blocks were attached to the channel which was sandwiched between an insulating/support block and bolted together. See Figure 3.2.1.2. This final assembly was then incorporated into a flow loop shown in Figure 3.2.1.3.

This experiment set-up was mainly a "proof of principle"

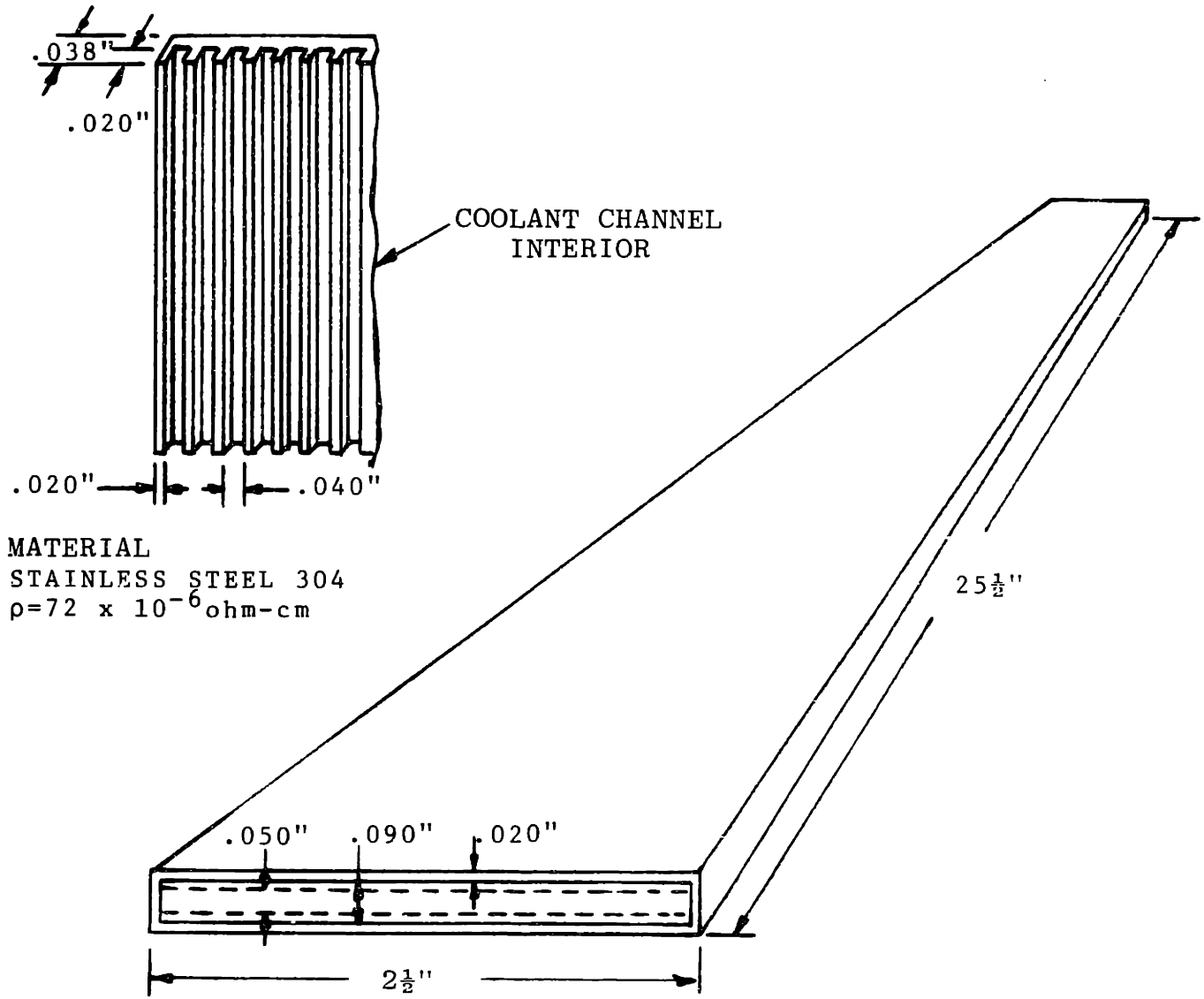

Fig. 3.2.1.1 Spurgeon's Finned Channel

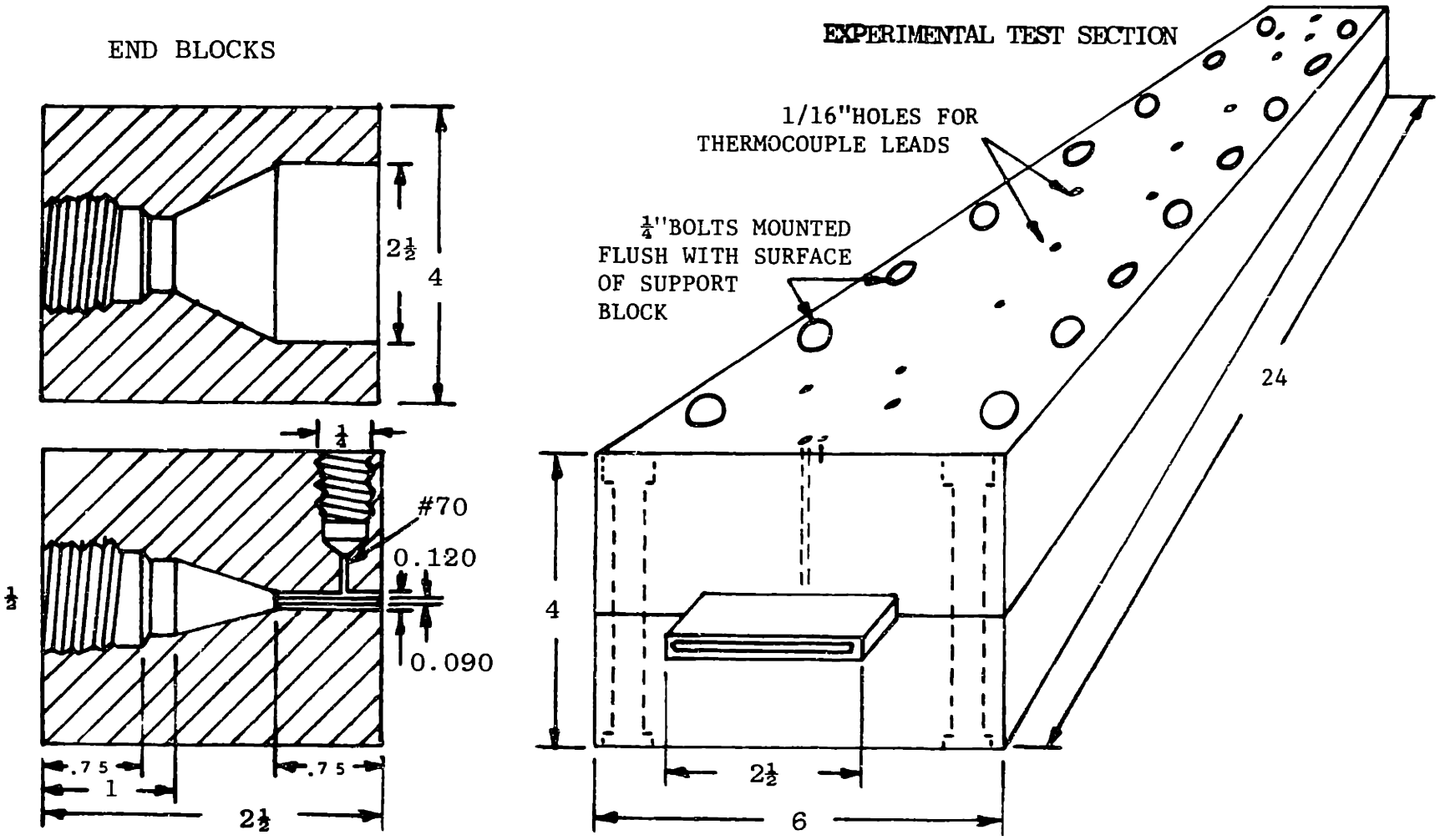

MATERIAL: STAINLESS STEEL

INSULATING/SUPPORT BLOCK MATERIAL: NEMA GRADE G-5

* ALL DIMENSIONS IN INCHES

FIG. 3.2.1.2 Spurgeon's Experimental Test Section

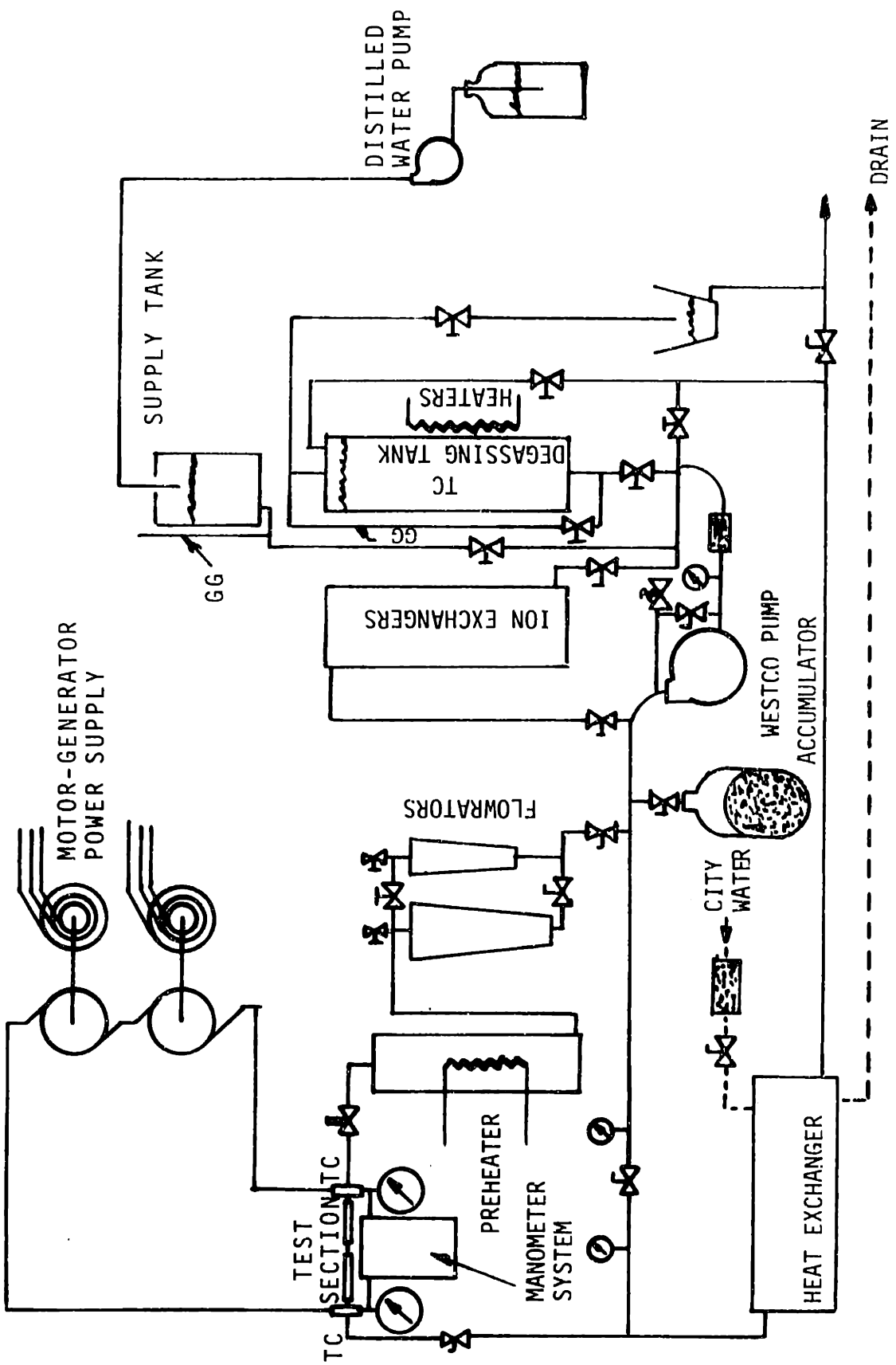

FIG. 3.2.1.3 Schematic Layout of Spurgeon's Experimental Facility

exercise and was not intended to represent a final design. In this respect the finned concept was definitively proved advantageous. However, as far as an actual simulation of a fuel plate (or coolant channel) is concerned, it had three problems inherent to its design and application. First of all, heat was generated throughout the whole plate, including fins. Secondly, stainless steel was used instead of aluminum. And finally, the coolant channel geometry was different from that of the final design.

3.2.2 Heat Transfer Investigations by Hollenberg and Momsen

An experiment to investigate in-channel thermocouples, heat transfer coefficient, and fin effectiveness for the MITR-II fuel plates was the subject of a Bachelor's thesis by Ted Hollenberg (3) and a 22.90 project by Bruce Momsen (4). A cross-section of the test channel used in this experiment is shown in Figure 3.2.2.1. A center strip of stainless steel shim stock, 0.02 inches thick was heated electrically by current from the D.C. generators at the MIT Heat Transfer Laboratory. Surrounding the heater strip was a coating of Teflon 0.004 inches thick to insulate the stainless steel heater strip from the outer aluminum plates. These aluminum plates were finned by the MITR-II fuel fabricator. Two coolant channels were formed when the side blocks were brought together as shown. Sealing the channel was accomplished by a layer of silicon grease deposited on the metal sealing surfaces. Thermocouples were brought in from the sides as shown. Provisions for inlet and outlet piping were made at both ends of the side blocks. The test channel as such was placed in the flow loop

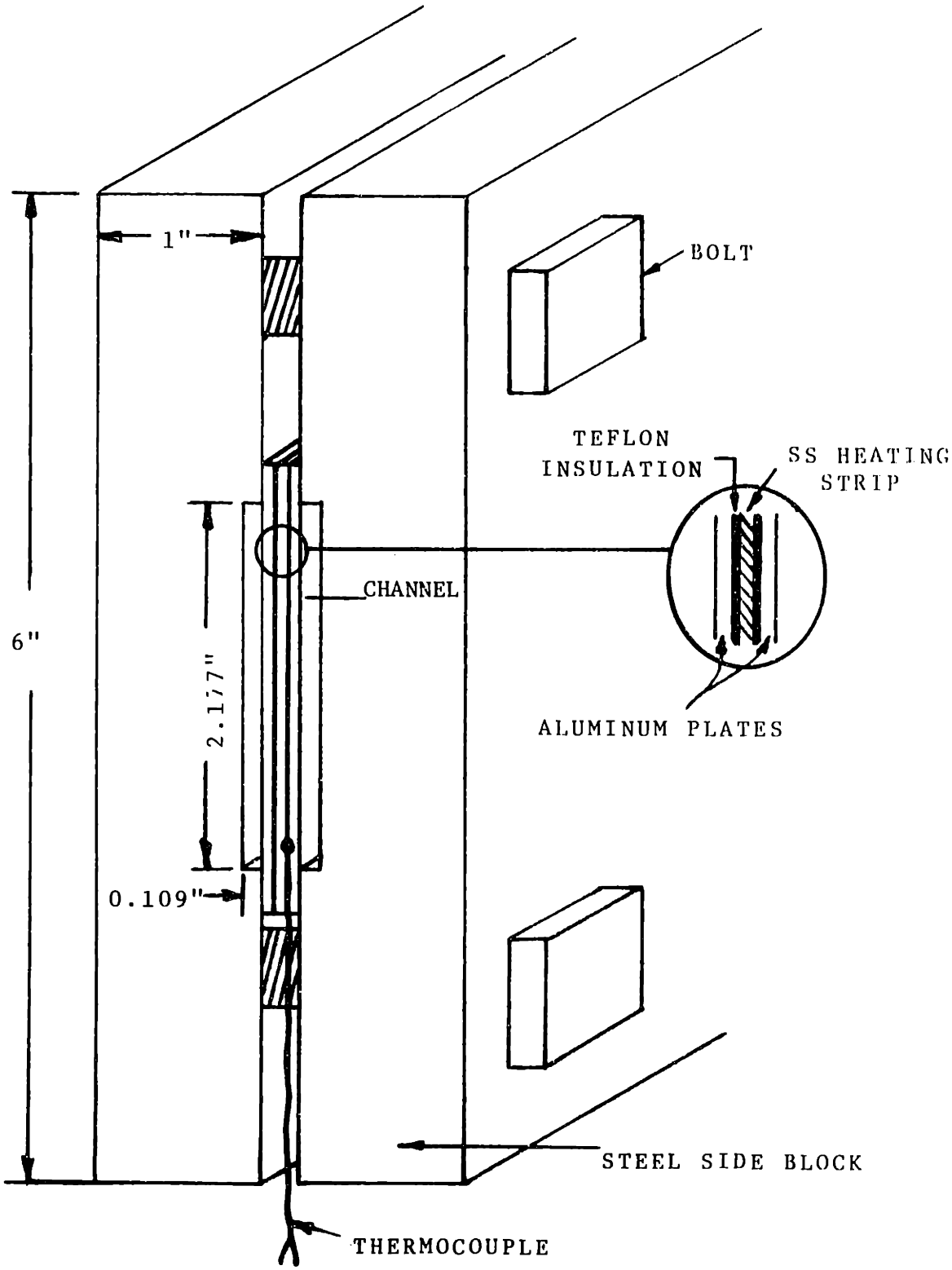

FIG. 3.2.2.1 CROSS SECTION OF HOLLENBERG AND MOMSEN'S TEST SECTION

shown in Figure 3.2.2.2.

The use of this design yielded inconclusive results due to problems encountered with the sandwich type heating arrangement for the finned aluminum plates. The main problem encountered was that of electrically insulating the aluminum plates from the stainless steel heater strip. Bad thermal contact between layers would cause uneven heating. This was evidenced when full power was applied to the test section. The uneven heating caused the temperature to rise nonlinearly in areas of poor thermal contact. Consequently, the Teflon melted. Therefore, the test section could only be operated at low power levels.

Hollenberg and Momsen's inconclusive results can probably be accounted to a phenomenon experienced in this present work. In the low power runs, temperature differences between the fluid and the back plates were small. In solving the applicable heat transfer equation, differences are taken and the results inverted. Consequently, a small error in temperature is greatly magnified.

3.3 Description of New Experiment

3.3.1 General

In the initial phase of this work, an attempt was made to see if salvaging Hollenberg and Momsen's test section was feasible. Eliminating the Teflon insulation would greatly improve the situation but a substitute would be required. Anodizing the back of the aluminum plates was an alternative. This idea was abandoned since any gouging would result in the loss

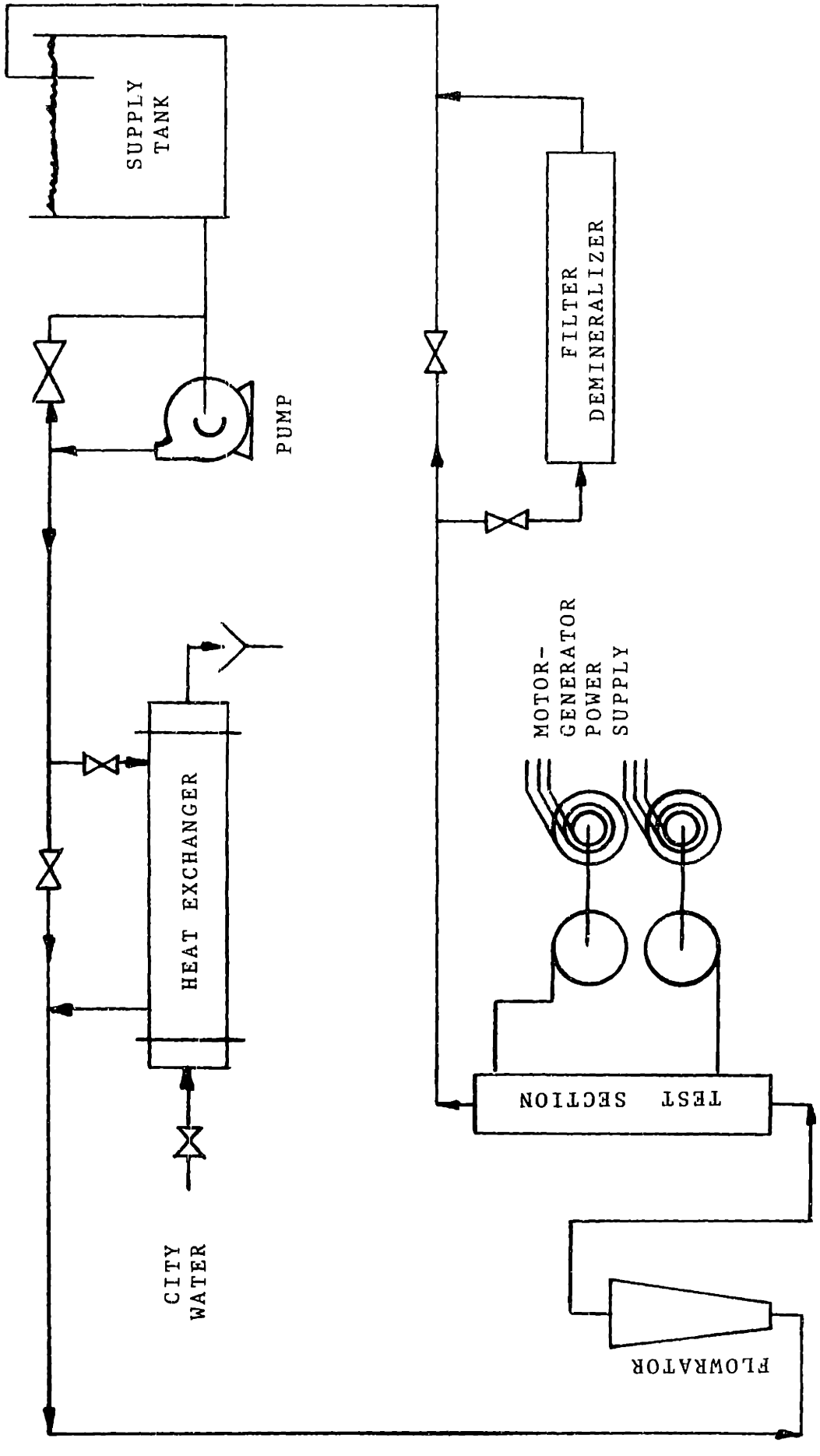

FIG. 3.2.2.2 HOLLENBERG AND MOMSEN'S FLOW LOOP

of electrical insulation and would short out the test section. Also, the problem of thermal contact would not be solved.

It became evident that the sandwich configuration should be abandoned and a new scheme devised if good results were to be obtained. J. H. Brindley (6) approached the problem of calibrating surface attached thermocouples by heating a stainless steel plate brazed to a thick copper block into which high density heaters were embedded. Sheated chromel-alumel thermocouples were used. Brindley reported excellent agreement between experimental and predicted heat transfer coefficients. In light of this, a similar scheme to heat a finned aluminum block was adopted.

3.3.2 Test Channel

A new test channel was fabricated from two 2 x 3 x 28-inch 6061 aluminum blocks using the facilities at the MIT Reactor Machine Shop. The coolant channel is formed when the two halves are brought together and bolted between two 3/8" x 4-1/2" x 30 aluminum backing plates. Figure 3.3.2.1 is a cross-sectional view of the assembly. Two additional 1/2 x 4-1/2 x 12-inch aluminum plates were also installed as stiffeners to prevent the test channel from bowing. Angle irons bolted to the stiffening plates were used to mount the test section in its support stand.

The interior channel surfaces are longitudinally finned. Fin dimensions are the same as those for the MITR-II fuel plates, that is 0.010 x 0.010 x 0.010-inch rectangles. Channel dimensions (see Figure 3.3.2.1) are held as close as possible to actual MITR-II values to ensure an accurate reproduction of the coolant channel.

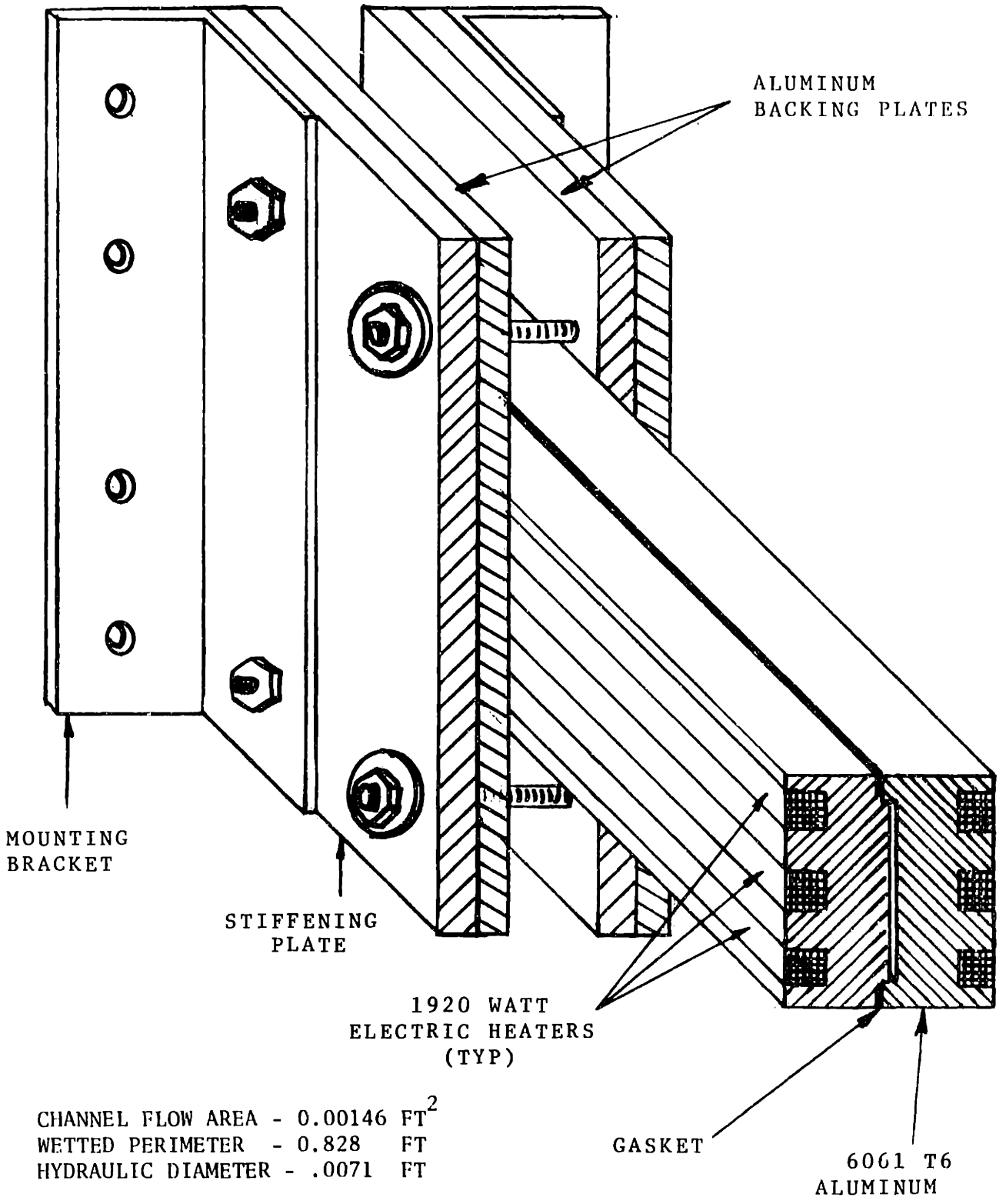

FIG. 3.3.2.1 CROSS SECTIONAL VIEW OF NEW TEST SECTION

Channel flow area, wetted perimeter and hydraulic diameter are also given on Figure 3.3.2.1.

3.3.2.1 Channel Power Requirements

In order to simulate conditions in the actual coolant channel, it is necessary that the six electrical heaters be properly sized. From Table 3.1-1 of the MITR-II SAR (1), the following data is given:

Channel flow area	0.00141 Ft
Average coolant velocity	8.1 Ft/sec
Core inlet temperature (maximum)	51.0 ^{o}C
Core outlet temperature (maximum)	60.0 ^{o}C
Temperature rise (maximum)	16.2 ^{o}F

The channel mass flow rate is then:

$\dot{m} = \rho AV = 61.52 \text{ lbm/ft}^3 \times .00141 \text{ Ft}^2 \times 8.1 \times 3600 \text{ Ft/Hr} = 2529.4 \text{ lbm/Hr}$,

and the heater power required is given by:

$\dot{q} = \dot{m} c_p \Delta T = 2529.4 \text{ lbm/Hr} \times 1.0 \text{ BTU/lbm}^{o}\text{F} \times 16.2^{o}\text{F} = 40976.8 \text{ BTU/Hr}$,

$\dot{q} = 12.00$ Kw.

Six commercial heaters of 2.0 Kw capacity each would therefore be required. A survey of available electric heaters was made and six "Hotwatt" heaters rated at 1920 watts and 220 volts were purchased. Each heater is 1/2" x 1/2" x 24" and would provide a channel similar in length to the actual case.

3.3.2.2 Block Temperature Distribution

A critical design requirement was to insure a uniform one-dimensional heat flux going into the coolant channel. The amount of aluminum between the heaters and the fin surface must be large enough to insure a one-dimensional heat flux. Calculations to

determine the minimum aluminum thickness required dividing the channel cross-section into symmetrical sections and applying the two-dimensional heat conduction equation. The imposed boundary conditions were: 1) uniform heat flux at the heater-aluminum interface and 2) a constant convection coefficient at the channel-fluid boundary. This problem was solved numerically by nodal analysis and a computer program was written to handle the otherwise lengthy calculation. Figure 3.3.2.2.1 shows the section of symmetry used and the resulting temperature distribution. It is seen from Figure 3.3.2.2.1 that 3/4 inches of aluminum between the heater and finned surface is sufficient to provide the desired heat flux distribution.

3.3.3 Hydraulic System

The experimental facility used was the test loop constructed in 1974 by Hollenberg and Momsen at the MIT Heat Transfer Laboratory. A schematic of the loop is shown in Figure 3.3.3.1. The pipes and fittings were made of PVC (polyvinyl chloride). Since the expected fluid temperatures were not too high (less than 150^{o}F), the original designers chose the plastic piping for its ease of installation, corrosion resistance and inexpensiveness. Rayon reinforced hose was used where flexible connections were required.

Demineralized water is circulated from the supply tank by a stainless steel centrifugal pump capable of providing 80 GPM at 100 FT of head. The pump is directly driven by a 5-hp induction motor. From the pump, flow is directed to the heat exchanger. A

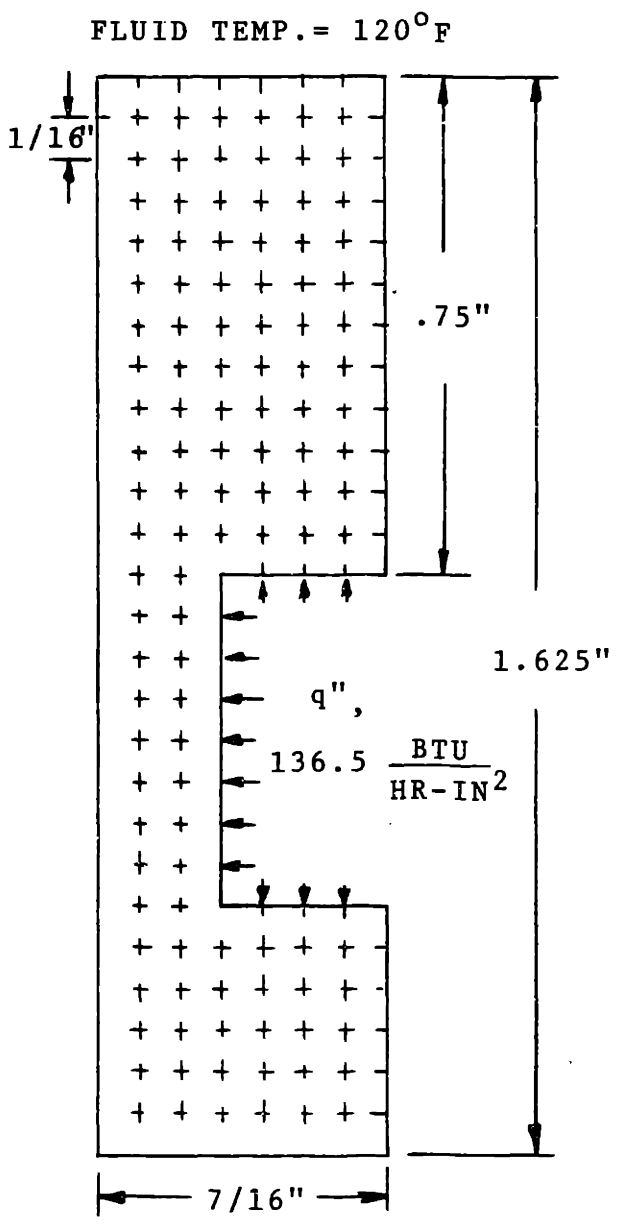

BLOCK
TEMPERATURE DISTRIBUTION
(°F)

134.6	134.6	134.6	134.6	134.6	134.6	134.6	134.6
136.5	136.5	136.5	136.5	136.5	136.5	136.5	136.5
138.4	138.4	138.4	138.4	138.4	138.4	138.4	138.4
140.3	140.3	140.3	140.3	140.3	140.2	140.2	140.2
142.2	142.2	142.2	142.2	142.1	142.1	142.1	142.1
144.1	144.1	144.1	144.0	144.0	144.0	144.0	144.0
146.0	146.0	145.9	145.9	145.8	145.7	145.7	145.6
147.9	147.9	147.8	147.7	147.6	147.5	147.4	147.4
149.8	149.8	149.7	149.5	149.3	149.2	149.1	149.0
151.8	151.7	151.6	151.4	151.1	150.8	150.6	150.6
153.8	153.8	153.6	153.2	152.7	152.4	152.1	152.0
156.0	155.9	155.6	155.2	154.3	153.7	153.4	153.2
158.2	158.1	158.0	157.4	155.7	154.8	154.4	154.2
160.5	160.5	160.6	161.0				
162.6	162.7	163.0	163.7				
164.6	164.8	165.1	165.8				
166.4	166.5	166.9	167.6				
167.9	168.0	168.4	169.2				
169.1	169.3	169.7	170.4				
170.1	170.2	170.7	171.4				
170.8	170.9	171.4	172.3	173.4	174.0	174.3	174.4
171.2	171.3	171.7	172.2	172.9	173.3	173.6	173.6
171.4	171.5	171.8	172.1	172.5	172.8	173.0	173.1
171.6	171.6	171.8	172.0	172.3	172.5	172.7	172.7
171.6	171.7	171.8	172.0	172.2	172.3	172.4	172.5
171.7	171.7	171.8	172.0	172.1	172.2	172.3	172.4
171.7	171.7	171.8	172.0	172.1	172.2	172.3	172.3

FIG. 3.3.2.2.1 BLOCK TEMPERATURE DISTRIBUTION AND SECTION USED IN NODAL ANALYSIS

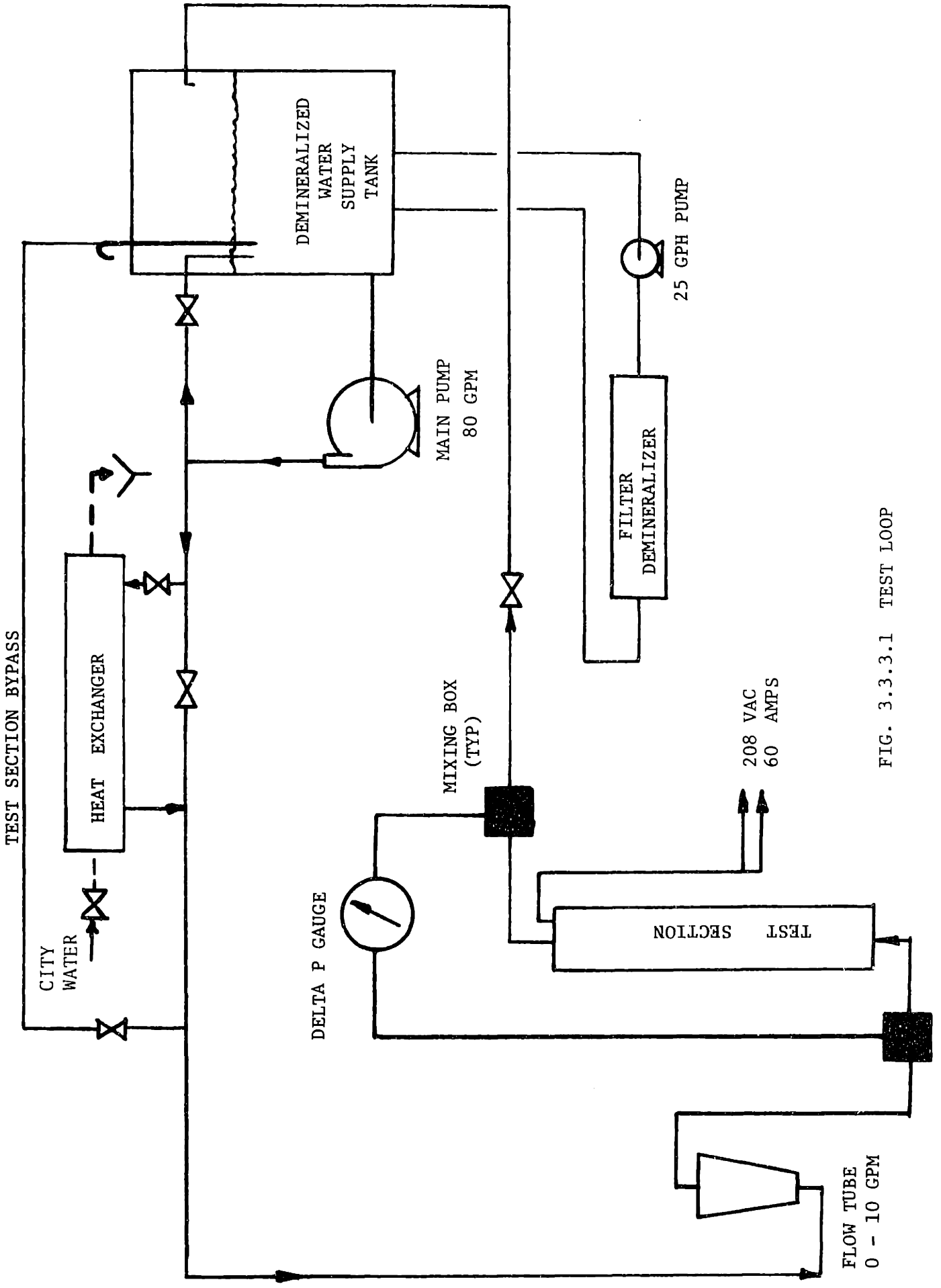

FIG. 3.3.3.1 TEST LOOP

1" Grinnell aluminum diaphragm valve was used to regulate bypass flow which in turn regulates the test section inlet temperature. A 1" gate valve on the heat exchanger inlet line was also used to regulate the fluid inlet temperature. Flow from the heat exchanger was then directed through a Fischer-Porter float tube calibrated for flows from 0-10 GPM, an inlet mixing box and then through the test section. After the test section, fluid flows through the outlet mixing box and then through a control valve back to the supply tank. Test section flow was regulated by the outlet control valve.

The test section bypass line shown was used at low test section flows to limit the amount of hot water in the system. This was accomplished by bypassing most of the flow from the heat exchanger back to the supply tank. Recirculation from the pump served to keep the supply tank at a uniform temperature.

Water from the supply tank was constantly filtered and purified by two Bantam cartridge-type demineralizers in a flow loop separate from the rest of the system. A 25 gallon per hour centrifugal pump was used to provide demineralizer flow.

A Sears 32 gallon heavy duty plastic tank was used as the systems storage tank. Pump suction was siphoned from the tank via a 1" rayon hose. Demineralized water was obtained from the Make-Up Water System at the MIT reactor.

The pressure drop across the test section was measured using a heavy duty (4500 PSIG rating) Barton bellows-type differential pressure gauge with a range of 0-400" H_2O. Pressure taps were located on the inlet and outlet mixing boxes. Test section

absolute pressure was not measured but was for most cases equal to the pressure developed by the pump.

3.3.4 Power Supply and Control

The test section power was taken from the 208 V-3ϕ power line available at the Heat Transfer Laboratory. Each phase is capable of handling 60 amps.

A study was made of available methods of power control. For the heaters connected in a delta configuration as shown in Figure 3.3.4.1, the expected line current would be 32 amps. The cost of a three phase variac capable of handling that amount of current was prohibitive and this course was abandoned. It was possible to install six single phase variacs without balancing chokes in parallel with each heater. This would be very cumbersome and that many variacs were unavailable for prolonged use. It was finally decided to control heater power by changing the wiring. Several power points could then be had with a minimum expenditure. As seen in Figure 3.3.4.1, each heater had its own 10-amp fuse. One hundred percent channel power is obtained in the shown configuration. Fifty percent channel power (only one side heated) was achieved by removing appropriate fuses.

It was found that low channel power settings yielded inconclusive results and only one data set was taken at 1/3 power. This power setting was achieved by wiring the heaters in parallel in a wye configuration.

3.3.5 Instrumentation

In-channel temperatures were measured using stainless steel

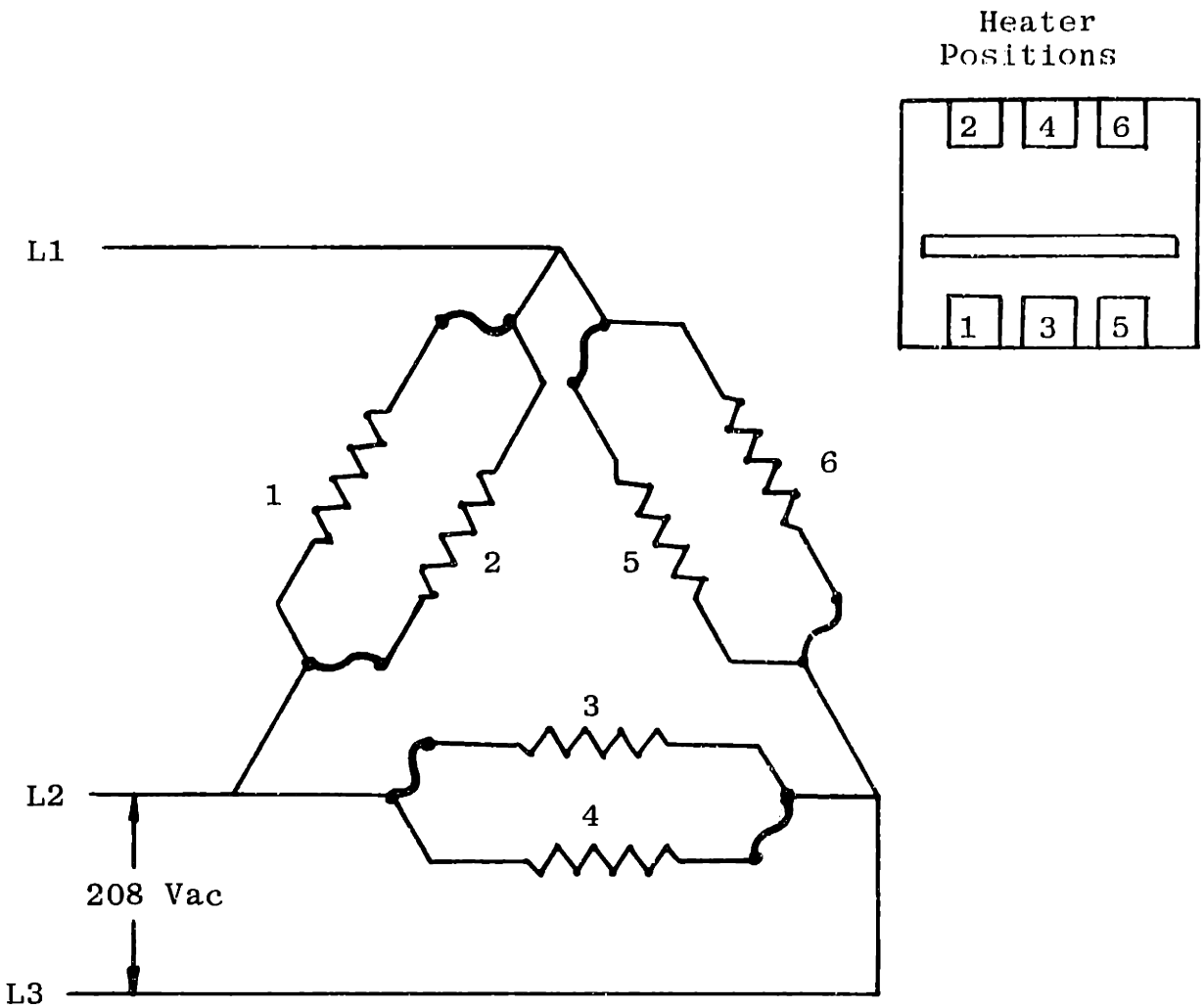

Fig. 3.3.4.1 Heater Wiring Diagram, 100% Power

sheated 10-mil chromel-alumel thermocouples. All other temperatures were measured by chromel-alumel thermocouples made from 28 gage Leeds and Northrup duplex wire. The test section inlet and outlet temperatures were measured by thermocouples directly in the fluid stream located in the mixing boxes shown in Figure 3.3.3.1. These thermocouples were installed in the mixing boxes through 3/8" compression fittings sealed with epoxy.

A Fischer-Porter float tube calibrated for flows of 0-10 gallons per minute provided measurement of the test section flow.

Voltage across the heaters was checked with a Simpson meter to insure power was balanced. Thermocouple voltages were read from a Keithley Digital Voltmeter via two 28 point Honeywell selector switches. The reference junction for the thermocouples was a standard-ice bath using copper extension wires.

3.3.6 Test Section

The test section consisted of a 6061 aluminum channel (described in Section 3.3.2). Inlet and outlet plenums were made at the ends of the female piece by milling grooves as shown in Figure 3.3.6.1. External fluid connections were made to 1/2" half-couplings which were welded into place at each end of the female piece. Staircase-type locating ridges were milled around the outer periphery of both sections which mated with each other when the halves were brought together. Channel sealing was accomplished with a 3/32" rubber gasket (Buna-N) which was placed in the outer step area. When the section was

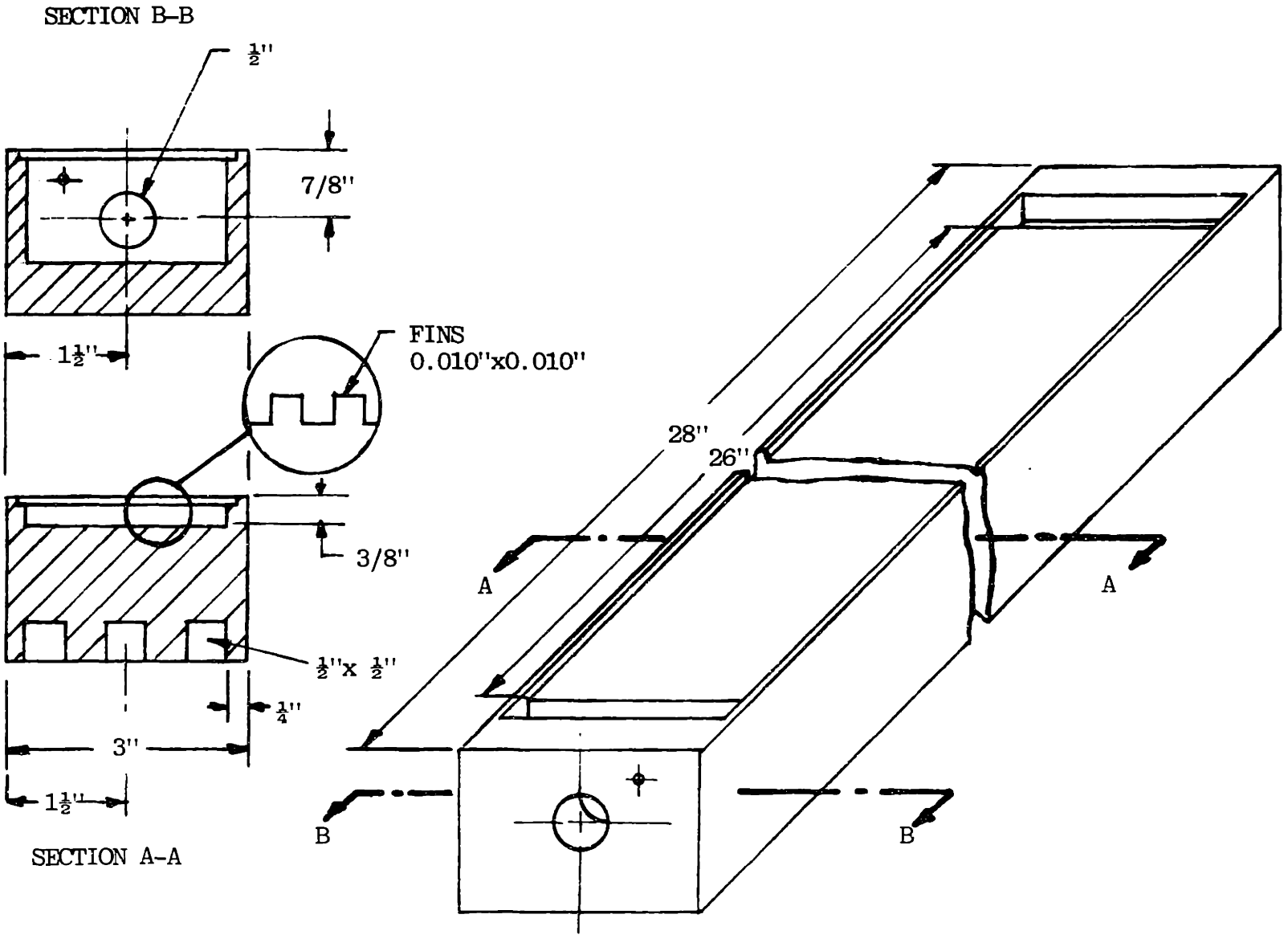

FIG. 3.3.6.1 TEST SECTION FEMALE HALF

bolted together, the gasket was compressed until the inner step surfaces contacted each other. The dimensions of these locating ridges were such that the channel gap would be 0.078 inches wide between tops of the fins. A small layer of silicon grease on the gasket surface was used to aid sealing.

The electric heaters fit tightly into the 1/2" milled groves provided so that thermal expansion would insure good contact with the aluminum.

The test section bolted between the backing plates and stiffening plates was its own support system. Angle irons bolted to the stiffening plates were used to attach the section to its test stand. Once assembled and in place, the test section was insulated with four layers of 1/2" asbestos insulation.

Back plate thermocouples were installed into the sides of both halves by drilling #56 size holes to various depths and then cementing the thermocouples in place. All thermocouples were located 3/8" beneath the finned surface. A total of 28 back plate thermocouples were installed. Figure 3.3.6.2 shows the thermocouple arrangement.

The four 10-mil in-channel thermocouples were introduced into the test section via a 0.045" hole drilled in the outlet plenum which was then sealed with epoxy when the in-channel thermocouples were in place. The location of these thermocouples is shown in Figure 3.3.6.3. The in-channel thermocouples were crimped between the fins. The thermocouple junctions were located as near as possible to a back plate thermocouple location.

After the first two data runs, it was decided to try to cut

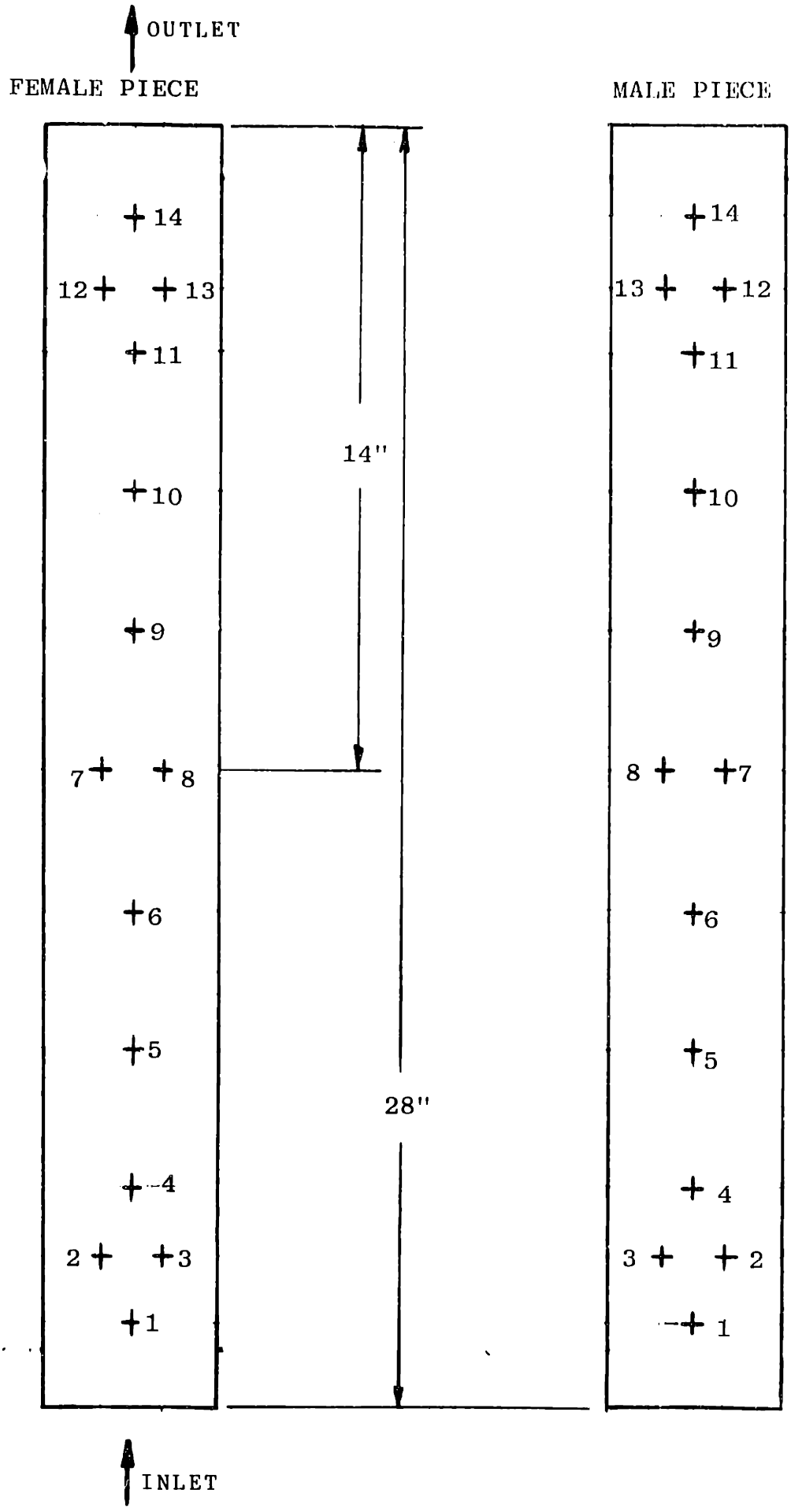

FIG. 3.3.6.2 Back Plate Thermocouple Location

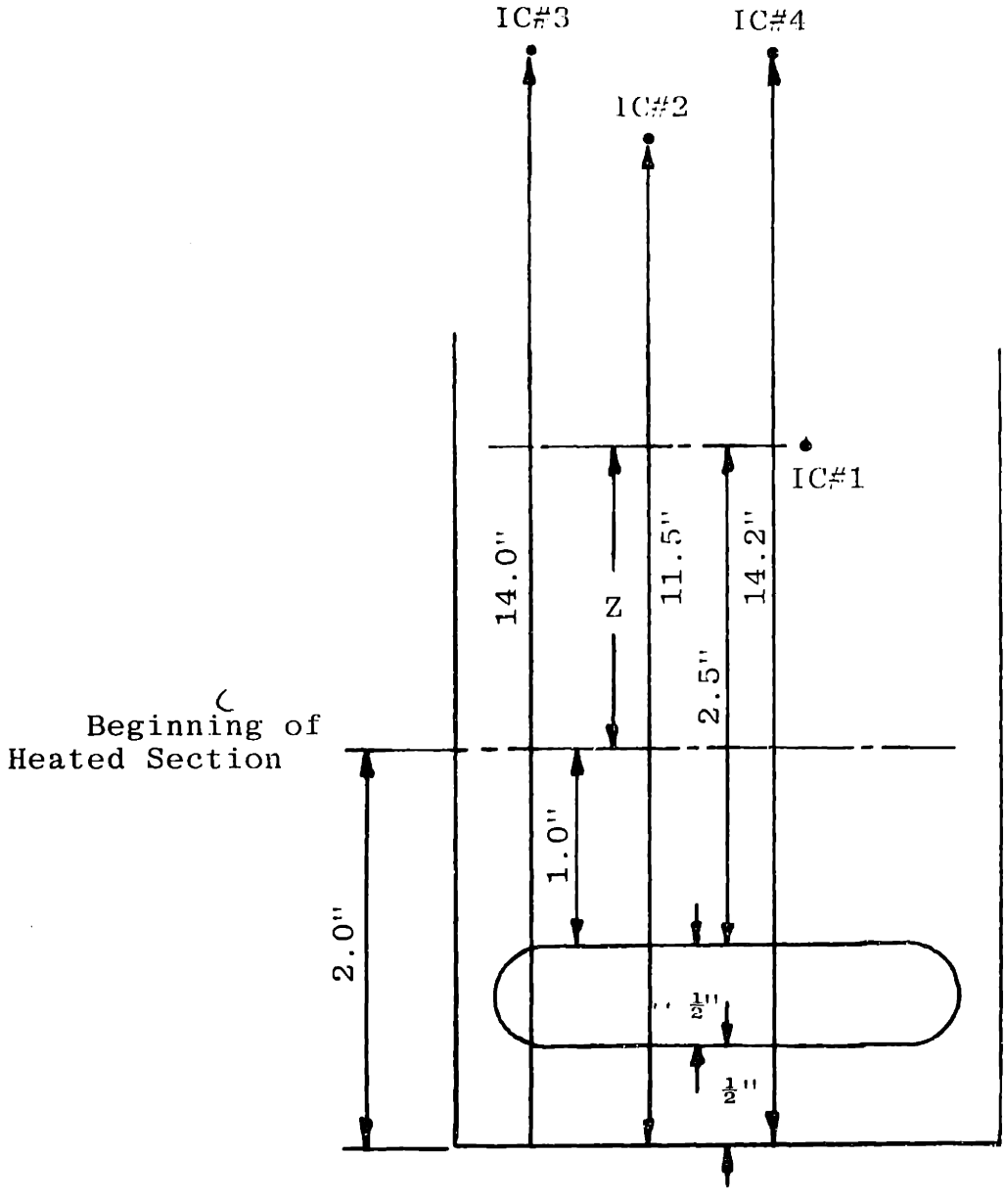

Fig. 3.3.6.3 Inchannel Thermocouple Location

down some of the axial heat conduction which was found near the channel ends. The test section was dismantled. Grooves were milled at the ends to isolate the heated section from the plenums as much as possible. The plenums were also filled with epoxy and re-machined to provide a smaller entrance and exit volume. The epoxy also served as insulation.

3.3.7 Operating Procedure

Before starting the main system pump, flow was established between the filter-demineralize and the H_2O supply tank (Refer to Figure 3.3.3.1). The main pump suction hose was filled with water and immersed in the supply tank to make the siphon. The bottom of the supply tank was 6" above the eye of the pump impeller to provide ample suction. With all system valves closed, the main pump was started and the recirculation valve was immediately opened. Then flow through the heat exchanger and the test section bypass was established. The heat exhanger water was usually dirty so that clean-up was necessary. This was accomplished by allowing 1/2 hour for clean-up with the filter-demineralizer. Once desired water quality was attained, the test section outlet control valve was opened until the desired flow was reached. The test section bypass and pump recirculation valves were then closed. Test section flow was then readjusted.

The electric heaters were then turned on. Flow of city water to the heat exchanger was established when test section inlet temperature reached 95 ^{o}F. The city water valve was usually held at a constant position while the heat exchanger inlet and bypass valves were adjusted until a constant inlet temperature was

achieved for the desired flow. The test section temperatures came to steady-state values approximately five minutes later. Data was then taken.

Data consisted of test section differential pressure and flow rate and all thermocouple readings. Once the readings for a flow point was completed, a new test section flow rate was obtained and the above procedure for setting the inlet temperature was repeated.

At low test section flows, the test section bypass line and pump recirculation lines would be opened to minimize the amount of plastic piping exposed to the hot water.

CHAPTER 4

DATA ANALYSIS, REDUCTION, AND RESULTS

4.1 General

Six data sets were obtained for different test section power settings, consisting of three runs at full power (approximately 11000 watts), two runs at one-half power and one run at one-third power. For each power setting, thermocouple readings were obtained for various flow rates ranging from 1.0 GPM to 10.0 GPM. The analysis of this data is divided into two parts, namely, heat transfer analysis and in-channel thermocouple response analysis. This analysis is presented in the first half of this chapter. All data reduction and results are given the second half of the chapter.

4.2 Heat Transfer Analysis

4.2.1 Heat Transfer Process in a Flat, Heated Plate

The governing equations of the heat transfer process in the MITR-II coolant channel are the classical heat conduction and convection equations:

$$q = -k_a A_{BP} \frac{dT}{dx} \qquad (4.2.1.1)$$

and

$$q = h A_s (T_w - T_f) , \qquad (4.2.1.2)$$

where:

q = heat transferred, BTU's/HR

k_a = thermal conductivity of aluminum, BTU's/HR-FT-^{O}F

h = surface convection coefficient, BTU's/HR-FT^2-^{O}F

A_{BP} = back plate area, FT^2

A_s = surface area, Ft^2

T_w = wall temperature, ^oF

T_f = bulk fluid temperature, ^oF.

Figure 4.2.1.1 illustrates the geometry of the heat transfer process in a heated flat plate. For this situation, Equation 4.2.1 becomes

$$q = \frac{k_a A_{BP} (T_{BP} - T_w)}{g}, \qquad 4.2.1.1.a$$

where

T_{BP} = back plate temperature, ^oF

g = distance between T_{BP} and T_w, Ft.

4.2.2 Heat Transfer From a Finned Surface

In the presence of a finned surface, Equation 4.2.1.2 must be modified to take into account the efficiency of the fins. The derivation of the fin efficiency will not be given here but can be found in Taborda's thesis (2) or in any standard heat transfer text (7,8). For a very rigorous and complete treatment of finned surfaces and extended surfaces in general, the reader is advised to consult the work by A. D. Kraus (9).

Figure 4.2.2.1 shows a cross-sectional view of a typical MITR-II fin. The efficiency of the singular fin can be well approximated by

$$\eta_f = \frac{\tanh\ m\ (l + t)}{ml} \qquad (4.2.2.1)$$

and

$$m^2 = \frac{hP}{k_a A}, \qquad (4.2.2.2)$$

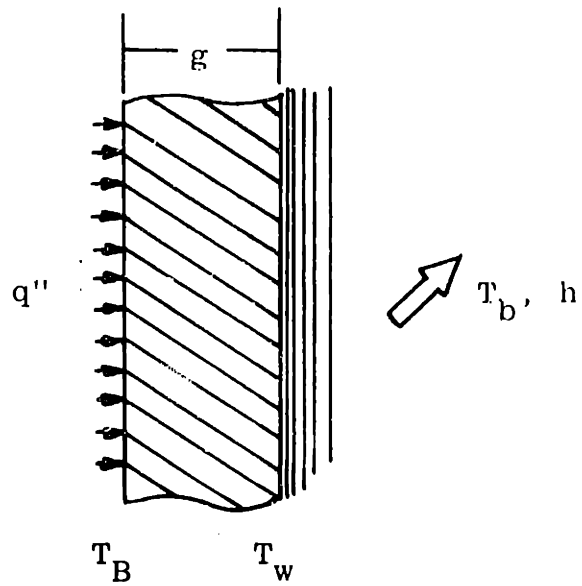

Fig. 4.2.1.1 Flat Plate Geometry Heat Transfer

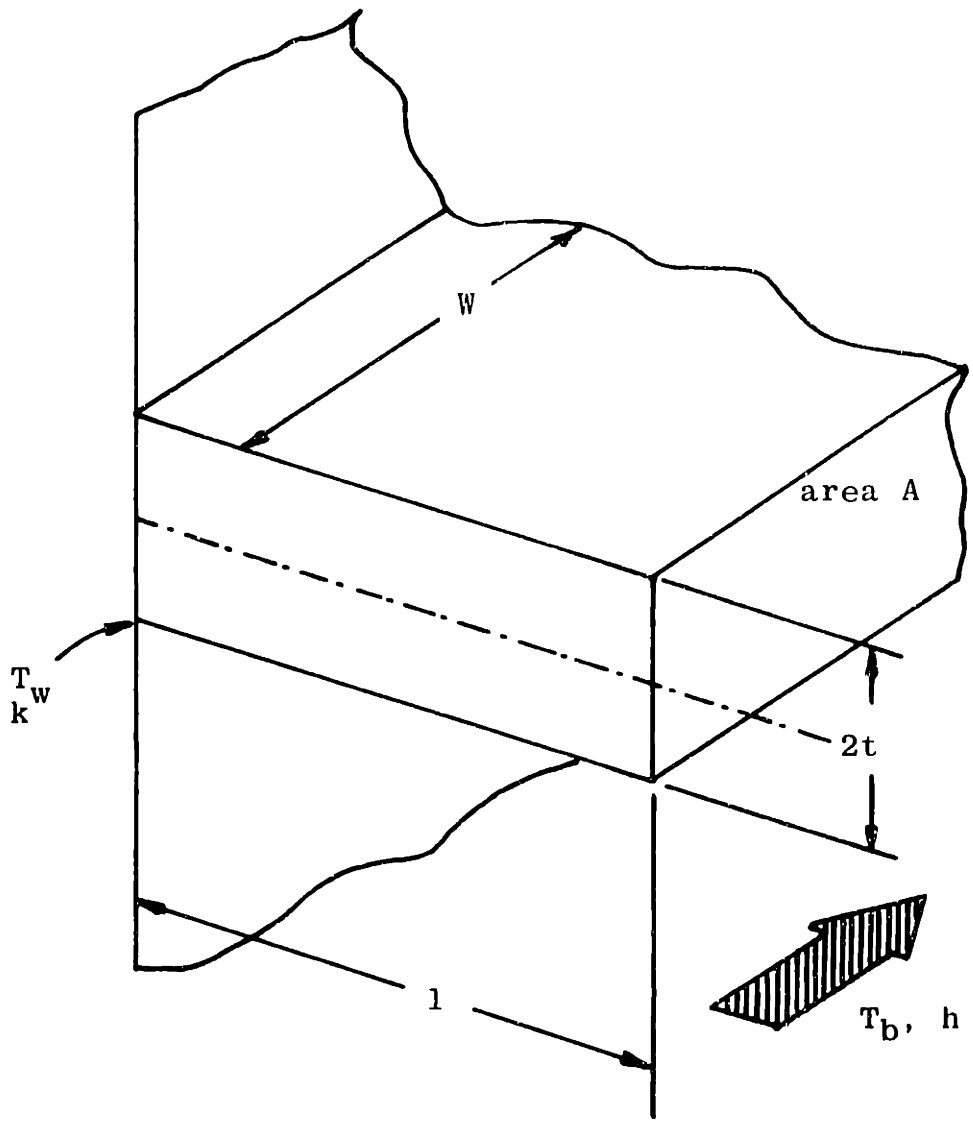

Fig. 4.2.2.1 Fin Geometry

where

h = convective heat transfer coefficient, Btu/Hr-Ft^2-^{o}F

P = fin perimeter, Ft

k_a= thermal conductivity of aluminum, Btu/Hr-Ft-^{o}F

A = fin cross-sectional area, Ft^2.

For the case of Figure 4.2.2.1, Equation 4.2.2.2 becomes

$$m^2 = \frac{h(2t + w)}{k_a tw}, \qquad (4.2.2.3a)$$

which further reduces to :

$$m^2 = h/k_a t, \quad \text{for } w >> t. \qquad (4.2.2.3b)$$

The heat transfer from the fin alone is given by:

$$q_f = h\eta_f A_f(T_w - T_f), \qquad (4.2.2.4)$$

where η_f is the fin efficiency and A_f is the surface area of the fin, Ft^2. Similarly, the heat transfer from the base is given by

$$q_b = hA_b(T_w - T_f), \qquad (4.2.2.5)$$

where A_b is the area of the base, Ft^2. The total heat transferred from the finned surface is the sum of Equations 4.2.2.4 and 4.2.2.5 times the number of repeating cycles n:

$$q_{TOT} = nh(T_w - T_f)[A_b + \eta_f A_f]. \qquad (4.2.2.6)$$

Dividing Equation 4.2.2.6 by the total back plate area, nA_{BP}, an expression for the incident heat flux is obtained:

$$q'' = \frac{q_{TOT}}{nA_{BP}} = h(T_w - T_f)\{\frac{A_b}{A_{BP}} + \frac{\eta_f A_f}{A_{BP}}\}. \qquad (4.2.2.7)$$

The term in brackets on the right hand side of Equation 4.2.2.7 is interpreted as the surface effectiveness and is assigned the symbol η_0 :

$$\eta_o = \frac{A_b}{A_{BP}} + \frac{\eta_f A_f}{A_{BP}} \qquad (4.2.2.8)$$

$$= \frac{\text{heat dissipated by the finned surface}}{\text{heat dissipated by an unfinned surface at the same conditions of } T_w,\ T_f,\ \text{and } h}.$$

Introducing $\Theta_B = T_w - T_f$ and the above definition for the surface effectiveness, Equation 4.2.2.7 simplifies to

$$q'' = \eta_o h \Theta_B = \eta_o h (T_w - T_f). \qquad (4.2.2.9)$$

4.2.3 Experimental Determination of the Enchanced Heat Transfer Coefficient, $\eta_o h$

In this experimental work, the back plate temperature was measured by the thermocouples mentioned in Chapter 3. Therefore, an expression relating T_B, T_f, and $\eta_o h$ is required. This is readily obtained by solving for T_w in Equation 4.2.1.1.a and substituting this expression for T_w into Equation 4.2.2.9.

The heat flux is then given by the familiar form of

$$q'' = \frac{T_B - T_f}{R_{TH}} = \frac{T_B - T_f}{\frac{1}{\eta_o h} + \frac{g}{k_a}}, \qquad (4.2.3.1)$$

where R_{TH} is the overall thermal resistance from T_B to T_f, FT^2-HR - ^oF/BTU. Rearranging Equation 4.2.3.1 gives the desired expression for $\eta_o h$:

$$\eta_o h = \left[\frac{T_B - T_f}{q''} - \frac{g}{k_a}\right]^{-1}. \qquad (4.2.3.2)$$

All the parameters on the right hand side of Equation 4.2.3.2 are either known, experimentally measured or inferred. The thermal resistance of aluminum, g/k_a, is obtained from the test channel geometry and the thermal conductivity of aluminum, k_a, is taken to be constant at 118.36 BTU's/HR -FT - ^oF,

which was evaluated at an average temperature for all data runs. The remaining two parameters, the heat flux and fluid temperature are discussed next.

4.2.4 Fluid Temperature Determination

The temperature rise across the test section is obtained from thermocouples located in the inlet and outlet mixing boxes as shown in Figure 3.3.3.1. The inlet water temperature was held constant at 95^{o}F for all data runs. To evaluate $\eta_o h$ from Equation 4.2.3.2 at a given location in the channel, the fluid temperature as a function of height, z must be known. This is determined by means of an energy balance. Refer to Figure 4.2.4.1. The energy gained by the fluid traveling a distance dz is

$$\dot{m} C_p dT = 2q''wdz. \qquad (4.2.4.1)$$

The corresponding change in temperature is

$$dT = \frac{2q''W\, dz}{\dot{m}C_p}, \qquad (4.2.4.2)$$

and the temperature, Tz, is obtained by integrating Equation 4.2.4.2 to the point of interest:

$$\int_{T_{in}}^{Tz} dT = \int_{o}^{z} \frac{2q''W}{\dot{m}C_p}\, dz, \qquad (4.2.4.3)$$

which becomes:

$$Tz - T_{in} = \frac{2q''Wz}{\dot{m} C_p}. \qquad (4.2.4.4)$$

The total temperature rise is then given by

$$T_o - T_{in} = \frac{2q''Wl}{\dot{m}C_p}, \qquad (4.2.4.5)$$

where l is the total length of the channel. Dividing Equation 4.2.4.4

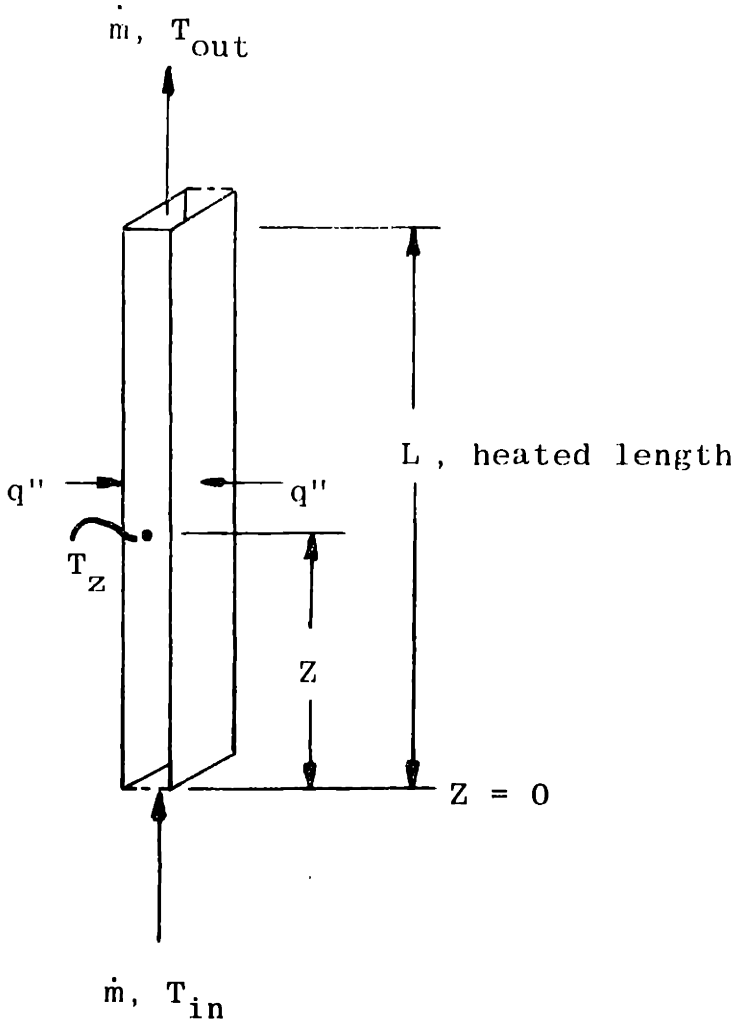

Fig. 4.2.4.1 Model for Fluid Temperature Determination

by Equation 4.2.4.5 and rearranging yields

$$Tz = T_{in} + (T_o - T_{in})\frac{z}{l}, \qquad (4.2.4.6)$$

Two assumptions are made when using Equation 4.2.4.6. The first is the specific heat capacity of water, C_p remains constant. Since the fluid temperature changes encountered in this work are less than 20^oF for the most part, the use of a constant C_p evaluated at average conditions is valid.

The second assumption is that the heat flux is constant along the length of the channel. A certain degree of axial heat conduction was present in all runs. Figure 4.2.4.2 shows the back plate temperature variation with distance up the channel. The temperature gradient is constant through the mid-section which indicates that the second assumption is valid. Another important fact is that the test section was well insulated so the fluid would gain the same amount of total energy regardless of the shape of the heat flux or temperature distributions (symmetry assumed, same amount of total energy but not clear that some error existed in intermediate positions).

4.2.5 Heat Flux Determination

The value of the heat flux used in analyzing the first few data sets was an average value inferred from the fluid temperature rise and channel geometry. It is given by:

$$q'' = \frac{\dot{m}\, C_p \Delta T}{2A_{BP}}. \qquad (4.2.5.1)$$

Preliminary analysis of this data resulted in values for $\eta_o\, Nu/Pr^{1/3}$ above those calculated by the Colburn relation. However, very low surface efficiencies were calculated, in the range of

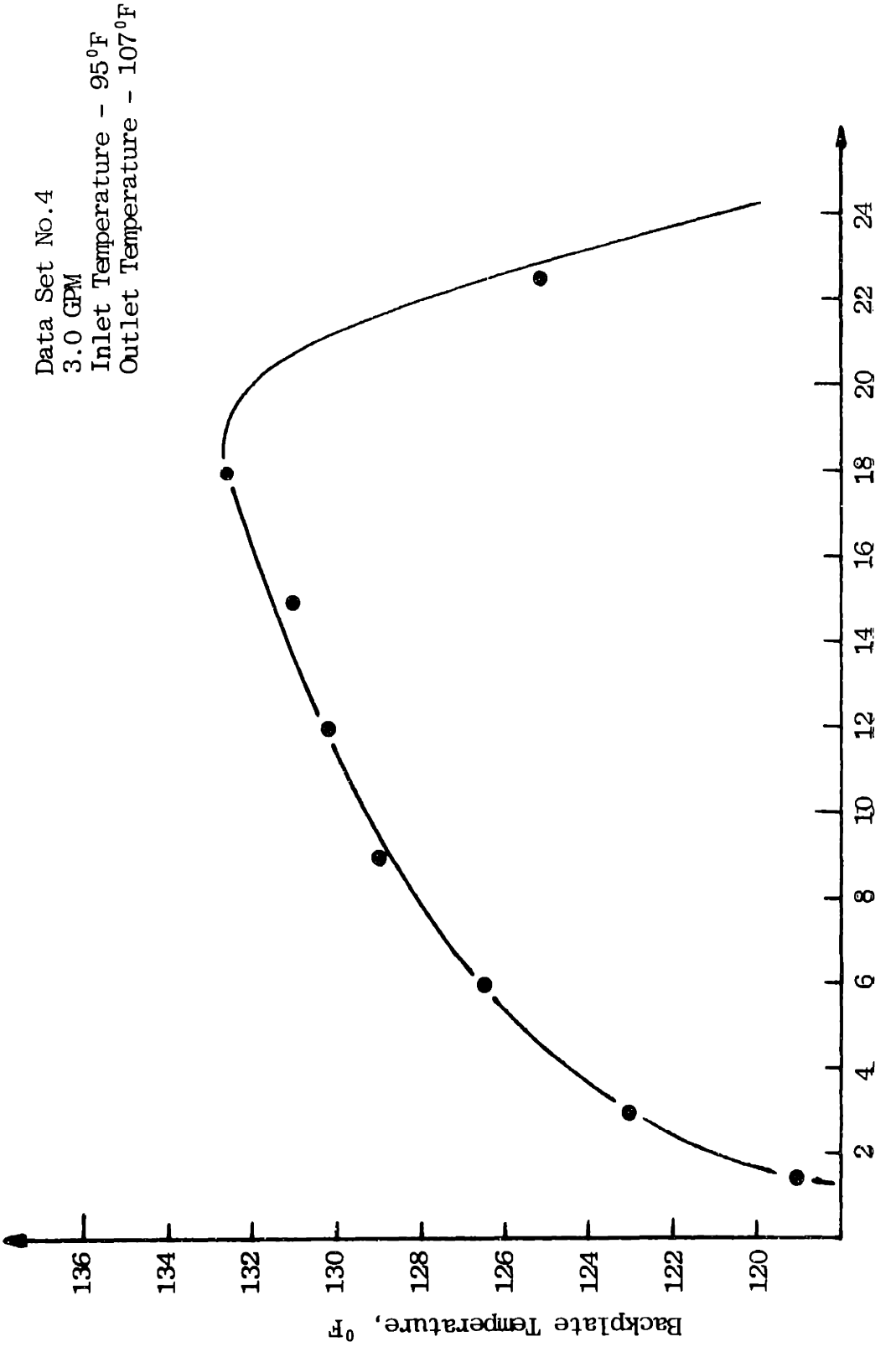

Fig. 4.2.4.2 Backplate Temperature Variation with Channel Position

1.0 to 1.25. The test section was then modified as mentioned in Chapter 3 and thermocouples were attached to the mid-plane to determine the heat flux. In subsequent runs, data from these thermocouples yielded values for the heat flux which were from 5%-20% greater than the average values used.

This discrepancy can be attributed to the fact that the aluminum block temperatures were highest in the mid-plane region. The resistance of the heaters is temperature dependent. Assuming that this dependency is of the following form:

$$R = R_o(1 + \alpha T). \qquad (4.2.5.2)$$

Then the heat deposited in the block would be greatest in the mid-plane region since the heater power is given by I^2R and R would be highest in this region.

For those data sets for which q'' was not determined directly, the average value heat fluxes were multiplied by the ratio of the local to average heat fluxes found in later runs.

4.3 In-Channel Thermocouple Response Analysis

4.3.1 The Thermocouple Problem

The in-channel thermocouple problem briefly mentioned in Chapter 2 is discussed more fully in this chapter. Figure 4.3.1.1 shows the installation of a typical in-channel thermocouple on a fuel element surface. The 0.0005 inch diameter chromel-alumel wires are surrounded by a layer of magnesium oxide insulation and an outer sheath of stainless steel, 0.010 inches in diameter. The thermocouple wires are grounded at the tip which is the measuring junction. The exact location of the tip is of great importance with respect to interpreting the data obtained from the thermocouple. Figures 4.3.1.2 and 4.3.1.3 are examples

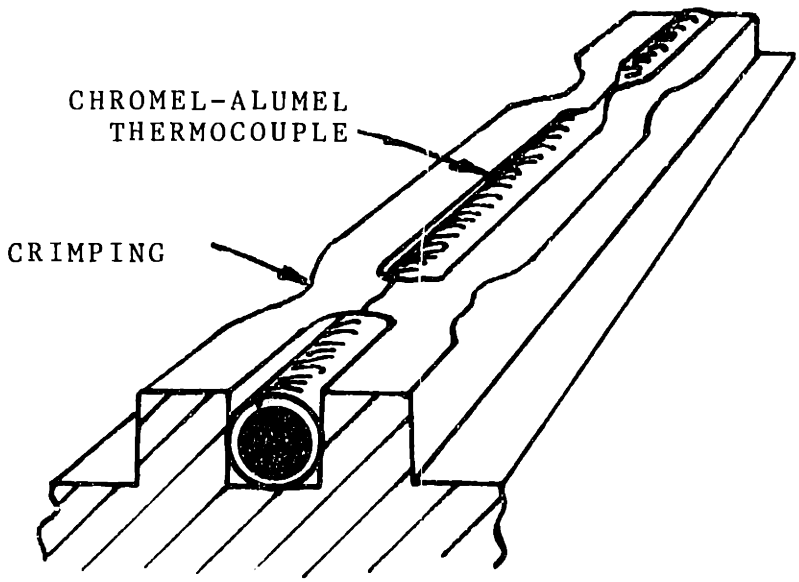

FIG. 4.3.1.1 STAKED INCHANNEL THERMOCOUPLE

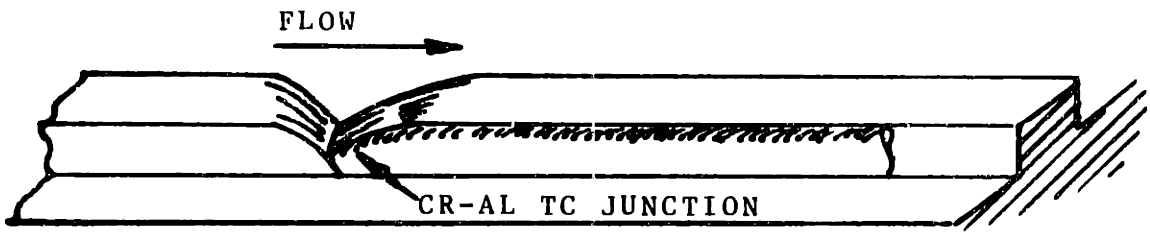

FIG. 4.3.1.2 PROPERLY CRIMPED INCHANNEL THERMOCOUPLE JUNCTION

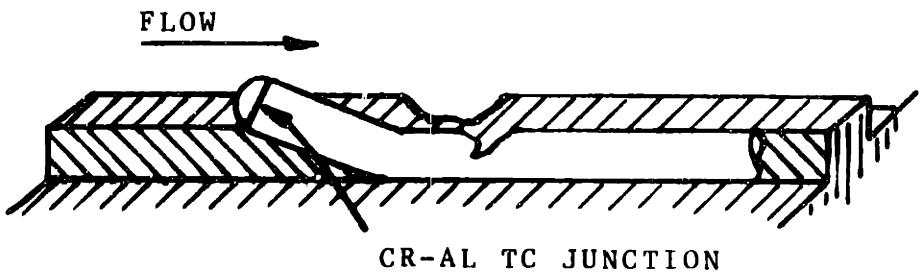

FIG. 4.3.1.3 IMPROPERLY CRIMPED INCHANNEL THERMOCOUPLE JUNCTON

of two possible thermocouple installations. In Case I, the tip or more exactly, the thermocouple junction, is well covered by the fin aluminum in the staking process. This is the most desirable configuration for several reasons, the most important one being the fact that the temperature observed by this thermocouple will approach the actual surface temperature. Secondly, the "staked" down tip is inherently more stable making this thermocouple mechanically stronger than the next case.

Case II represents the most extreme and undesired situation, namely that of the thermocouple junction projecting into the flow as shown. What the observed temperature will be is dependent on the length of the projection; if long enough, it could read the bulk fluid temperature. Most likely, it would project itself only a few thousandths or so above the surface. In this situation, the observed temperature would lie between T_{wall} and T_{fluid}. Mechanical failure of this thermocouple would occur much sooner then in Case I due to flow induced vibration. [IC#3 became inoperative after Data Set 2 was taken. It is felt that the damage occured during the modification of the test section and not during actual operation].

Since the installation of the in-channel thermocouples on the thermocoupled fuel element was not strictly controlled and observation of the installed thermocouples is impossible without dismantling the element, the actual geometry of the MITR-II in-channel thermocouples is not known. Therein lies the dilemma and it is the objective of this thesis to resolve the problem.

As an after thought, this author recommends strict control of such thermocouple installations in the future and that they

be well staked on the surface. To insure good results, the tip of the thermocouple should be inserted into a small hole or indentation on the surface before the aluminum fins are crimped over the thermocouple. In this case the thermocouple may measure a higher temperature than the surface temperature but combining this with convective heat losses from the thermocouple, an observed temperature nearer to T_w will result.

4.3.2 Theoretical and Other Approaches

In the early stages of this work several other approaches to the problem existed other than experimental. They are the theoretical method and electric analogue method. The theoretical method will be presented first.

Browning and Hemphill (10) proposed the model shown in Figure 4.3.2.1 to calculate heat transfer within an attached thermocouple exposed to a coolant stream. The thermocouple was represented as two isolated wires attached to the surface whose temperature is to be measured. The wires were broken down in elements of length as shown and a heat balance was performed for each element. If the initial estimate of the heat flux into the wire were correct, the residual heat flux remaining at the end of the wire would be zero. The heat flux into the thermocouple was adjusted accordingly until the residual became zero.

Although this method seems quite adaptable to the MITR-II thermocouple problem it was not undertaken for the following reasons. Browning and Hemphill in their work used actual measurements of thermocouple installations to supplement their

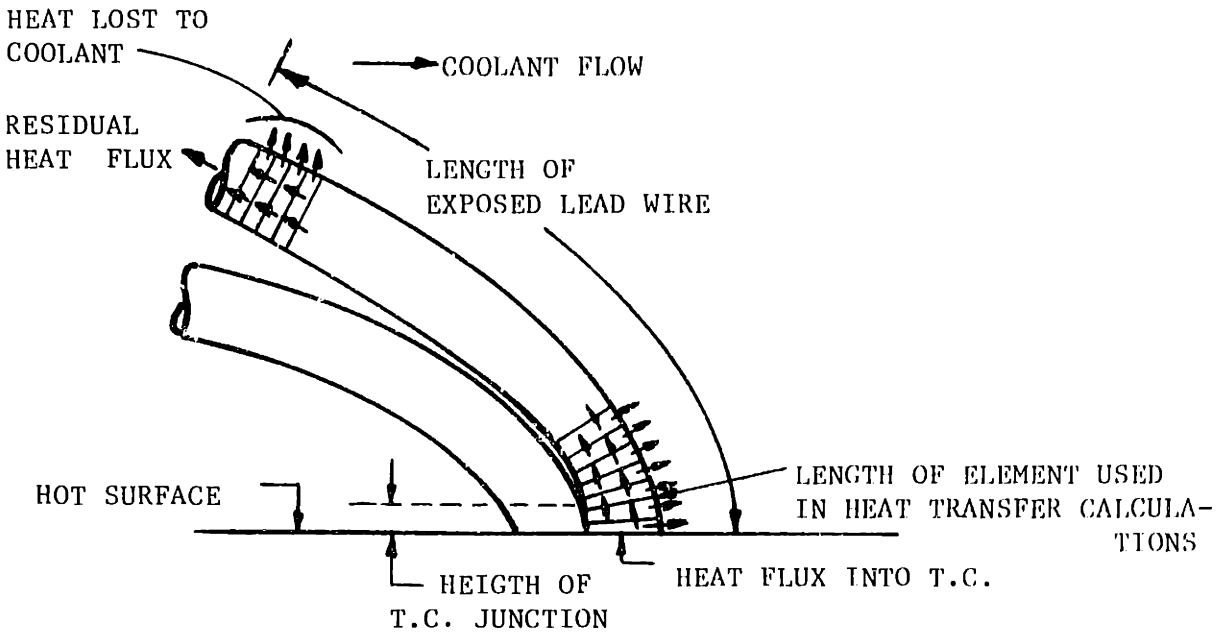

FIG. 4.3.2.1 BROWNINING AND HEMPHILL'S MODEL FOR THERMOCOUPLE HEAT TRANSFER CALCULATIONS

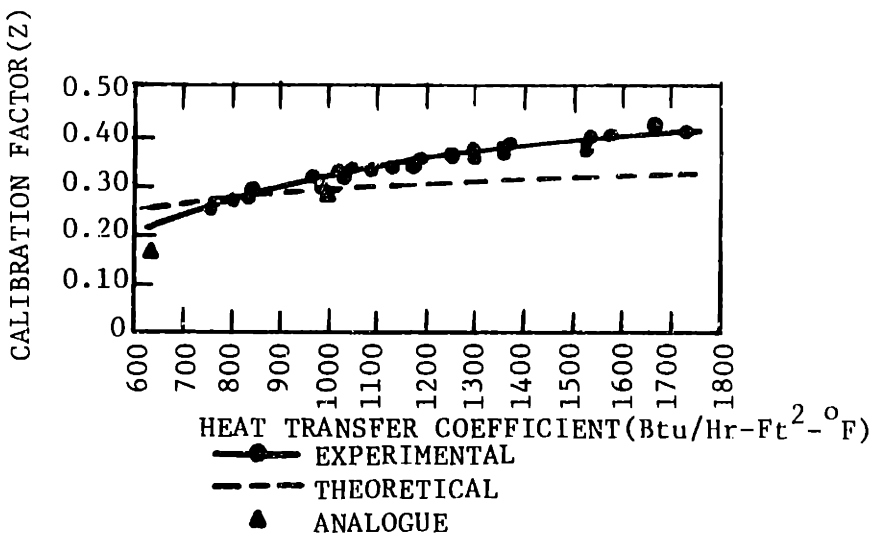

FIG. 4.3.2.2 BRINDLEY'S CALIBRATION FACTOR VS HEAT TRANSFER COEFFICIENT

theoretical work. Again, this was not possible in our case. Secondly, modeling the actual MITR-II case would be very difficult due to the multi-region thermocouple and the amount of contact between the sheath and the surface was unknown and would be an important factor in any calculational scheme.

J. H. Brindley (11) used an electric analogue model of a surface attached thermocouple exposed to a coolant stream on a flat plate fuel element to determine the effects of various parameters, i.e. coolant velocity, coolant temperature on the magnitude of the error associated with the thermocouple assembly. The electrical model was based on the fact that the relative differences in the thermal conductivity between the plate and chromel-alumel thermocouple can be simulated by different thicknesses of stainless steel sheet joined by closely spaced spot welds. Strips of stainless steel, representing the boundary condition on the plate and thermocouple wires, were attached to the part of the analogue representing the convective surface.

Brindley's results are shown in Figure 4.3.2.2 which is taken from his report (11). The ordinate of Figure 4.3.2.2 is a calibration factor given by

$$Z = \frac{T_s - T_o}{T_s - T_b}, \qquad (4.3.2.1)$$

where

T_s = actual surface temperature, ^{o}F

T_o = observed surface temperature, ^{o}F

T_b = bulk coolant temperature, ^{o}F.

Brindley also presents from (12) an analytical prediction for

the calibration factor:

$$Z = \frac{\frac{\pi}{k_s}\sqrt{\frac{ktRh}{8}}}{1 + \frac{\pi}{k_s}\sqrt{\frac{ktRh}{8}}}, \qquad (4.3.2.2)$$

where

k_s = thermal conductivity of cladding material

kt = thermal conductivity of thermocouple wire

R = equivalent thermocouple wire radius

h = heat transfer coefficient or the surface of the thermocouple wire.

Implicit in the above equation and in Brindley's work is the simplifying assumption that the chromel-alumel thermocouple can be simulated by a single wire having a thermal conductivity equal to the weighted thermal conductivity of the thermocouple lead wires and having a cross-sectional area equal to the combined cross-sectional areas of the thermocouple lead wires.

As seen in Figure 4.3.2.2, this expression underestimates the experimentally determined calibration factor by 20% or more for heat transfer coefficients greater than 1000 BTU/hr-Ft^2-^oF. Thus Equation 4.3.2.2 would predict a surface temperature less than the actual temperature and would not be used in a conservative manner.

Once again, this approach was not utilized due to similar reasons presented in the theoretical model. The two cases have been presented to show the continuity in going from an attempt at an analytical solution to the actual experimental work.

4.3.3 Experimental Approach

As mentioned in Section 4.3.1, the geometry of the thermocouple

installation on the thermocoupled fuel element is not known. Since a finned test section was being made to study the heat transfer process, installation of chromel-alumel thermocouples in a similar but perhaps random fashion would yield data from which the performance of the actual in-channel thermocouples could be inferred. The location of these in-channel thermocouples is given in Chapter 3.

4.3.3.1 Thermocouple Calibration Factor

The calibration factor approach is used and three in-channel thermocouples were calibrated. The parameters in Equation 4.3.2.1 again repeated here

$$Z = \frac{T_s - T_o}{T_s - T_f},$$

are all known or calculated guantities. T_o is measured directly. The surface temperature is obtained from the measured back plate temperature and the measured heat flux by

$$T_s = T_B - \frac{q''g}{k}. \qquad (4.3.3.1)$$

The fluid temperature at the IC location is given by

$$T_f = T_{in} + (T_o - T_{in}) \frac{z_t}{l}, \qquad (4.3.3.2)$$

where z_t is the distance from the beginning of the heated section to the thermocouple position. These calibration factors are obtained from the six data dets that were obtained and calibration curves similar to Figure 4.3.2.2 are generated. The installation of each thermocouple in the channel is different enough so that each calibration curve will be different and present

a range in which to work.

4.3.3.2 Installation Parameter, I

With respect to the use of the thermocoupled fuel element in the MITR-II, the calibration curves are of little use if there is no way to link this work with the actual thermocouple installation. In discussions with Professors Gosnell and Lanning, it was indicated that the heat flux out of the thermocoupled fuel element can be estimated. Since most of the in-channel thermocouples are located close to the channel inlet, the fluid temperature would be very close to the inlet temperature. In light of these facts, the following method of characterizing thermocouple installations is adopted.

By subtracting Equation 4.3.2.1 from unity the following expression is obtained:

$$1 - Z = \frac{= T_o - T_f}{T_w - T_f}. \qquad (4.3.3.2.1)$$

The denominator of the above expression is recognized as part of Equation 4.2.2.9 and is given by

$$T_w - T_f = \frac{q''}{\eta_o h}. \qquad (4.3.3.2.2)$$

Substituting this expression into Equation 4.3.3.2.1 and rearranging yields

$$I = \frac{1-Z}{\eta_o h} = \frac{T_o - T_f}{q''}, \qquad (4.3.3.2.3)$$

where I is the installation parameter.

All the quantities on the right hand side of this equation are known. By plotting I versus $\eta_o h$, a characteristic curve for

an in-channel thermocouple can be generated.

The values for q'' in this work are similar to those found in the MITR-II and are in the range of 50,000 BTU/HR-Ft^2-^{o}F. Thus installation curves for the actual in-channel thermocouples can be generated and compared to those found in this experiment. Then calibration factors or curves can be found by interpolation from calibration curves found in this work.

4.4 Heat Transfer Data Reduction and Results

4.4.1 Enchanced Surface Heat Transfer

4.4.1.1 $\eta_o h$ Determination

The general method described above for determining the enhanced heat transfer due to the presence of the longitudinal fins, namely $\eta_o h$, was used in a data reduction program called MITR-II Heat Transfer Study. This program is listed in Appendix (B). For the calculation of $\eta_o h$ at various intervals along the channel, an average back plate temperature at each location was calculated from temperature readings obtained from both male and female back plate thermocouples. This average back plate temperature was used along with the fluid temperature of z_t calculated by Equation 4.2.4.6 and the heat flux measured at the mid-plane to determine $\eta_o h$ at z by Equation 4.2.3.2 again repeated here:

$$\eta_o h = \frac{T_{BP}(z) - T_f(z)}{q''} - \frac{g}{k_a} .$$

The thermal resistance of the aluminum, g/k_a, was found to be 2.5698×10^{-4} ^{o}F - HR - FT^2/BTU for this experiment.

The variation of $\eta_o h$ along the channel is shown in Figure 4.4.1.1 for Data Set No. 6 and 5 GPM flow. A similar variation in heat transfer coefficient with channel position was seen by Spurgeon (5) in his work. The increase in $\eta_o h$ near the channel exit is artificial due to the axial conduction present. The dashed line represents what this author feels the shape should be. The increase in $\eta_o h$ at the channel entrance is expected due to entrance effects creating a higher degree of turbulence.

For each flow point, an average value for the enhanced heat transfer in the mid-section of the channel was obtained from $\eta_o h$ values at positions 6, 7, 8, 9 in the channel (that is 3 inches above and below center line). These average values of $\eta_o h$ are used in subsequent standard heat transfer plots and for the fin efficiency determination.

4.4.1.2 Reynold's Number

Due to some uncertainty in the value of the channel hydraulic diameter, the Reynold's number at the mid-section was found in the following manner. The flow velocity, v , in terms of channel flow, GPM is given by

$$v = \frac{\text{volumetric flow}}{\text{flow area}} = \frac{C_1(GPM)}{A_f}, \quad (4.4.1.2.1)$$

where $C_1 = 8.02032\ Ft^3/HR\text{-}GPM$. The flow area, A_f, in terms of the wetted perimeter and hydraulic diameter is

$$A_f = \frac{W_P D_H}{4}, \quad (4.4.1.2.2)$$

then

$$V_f = \frac{4C_1(GPM)}{W_P D_H}. \quad (4.4.1.2.3)$$

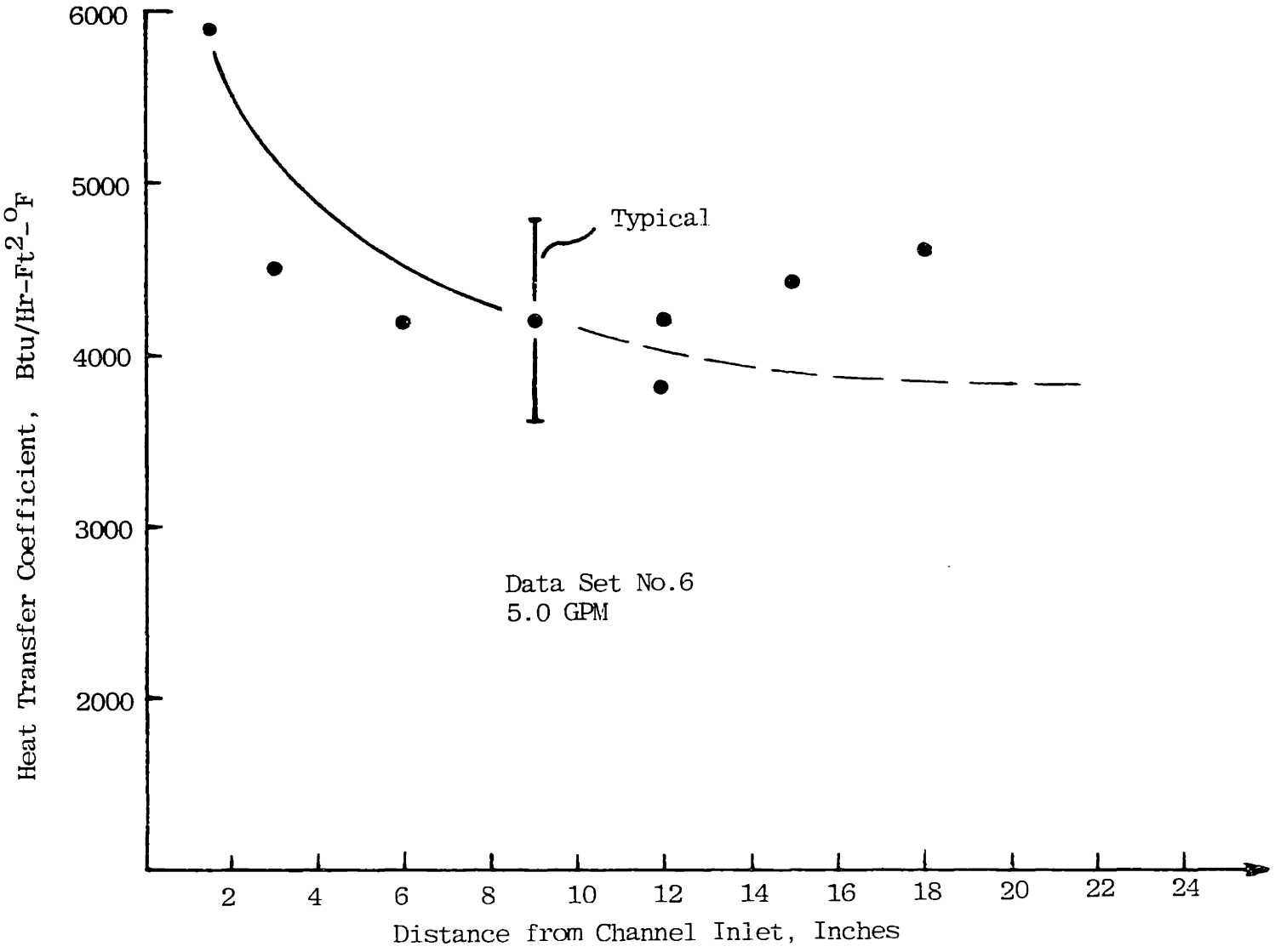

Fig. 4.4.1.1 Heat Transfer Coefficient vs Channel Position

Now the Reynold's number becomes

$$Re = \frac{\rho}{\mu} \times \frac{4C_1(GPM)}{W_p D_H} D_H = \frac{4C_1(GPM)}{W_p} \frac{\rho}{\mu} . \quad (4.4.1.2.4)$$

The wetted perimeter, W_p, for the test channel was found to be 9.934 inches from measurements made of the assembled test section. An expansion in the channel due to temperature and pressure would be less of an effect on W_p than D_H, hence the rationale for using Equation 4.4.1.2.4.

4.4.1.3 Standard Heat Transfer Results

In the presentation of standard heat transfer results, namely $Nu/Pr^{1/3}$ versus the Reynolds, the Nusselt number contains the product $\eta_o h$,

$$Nu = \frac{\eta_o h D_H}{k}. \quad (4.4.1.3.1)$$

Other investigators (2,5) either factored the surface effectiveness out of Equation 4.4.1.3.1 and only compared $hd_H/kPr^{1/3}$ with the Colburn relation. In all cases it was shown that the heat transfer coefficients obtained were above the Colburn prediction. This author feels that using Equation 4.4.1.3.1, the increased heat transfer is readily shown and is the main parameter of interest.

All fluid properties used in subsequent claculations are evaluated at the film temperature to be consistent with the comparison to the Colburn relation which is

$$Nu = 0.023\ Re^{0.8}\ Pr^{1/3}, \text{ where:} \quad (4.4.1.3.2)$$

$$Nu = \frac{hd_H}{Re} = \text{Nusselt Number}$$

$$Re = \frac{\rho_f V d_H}{\mu_f} = \text{Reynold's Number}$$

$$Pr = \frac{C_{pb}\mu_f}{k_l} = \text{Prandtl Number},$$

where f denotes the film condition and b the bulk condition.

The film temperature is given by:

$$T_{film} = \tfrac{1}{2}(T_w + T_f), \qquad (4.4.1.3.3)$$

where T_w and T_f are evaluated at the center of the test channel.

Graphs of $\eta_o Nu/Pr^{1/3}$ versus Reynolds number for data sets 2,3,4,5, and 6 are presented in Figures 4.4.1.3.1 through 4.4.1.3.5. Average values of $\eta_o h$(see Section 4.4.1.1) were used to determine $\eta_o Nu$. On each figure,except Figure 4.4.1.3.2, data points obtained using average q'' values are shown along with data points obtained with measured values of q''. These average values of q'' are based on channel mass flow rate, channel temperature difference and back plate surface area.Figure 4.4.1.3.2 shows only average heat flux data points since the heat flux thermocouples were located on the female side of the test section which was unheated during that run. In all cases, $\eta_o Nu/Pr^{1/3}$ was found to be well above the calculated Colburn relation which is as expected. For Re>4500, the slopes of Figures 4.4.1.3.1-5 are almost parallel to the Colburn relation. This in itself is an indication that the surface efficiency is constant for Re>4500.

For Re<4500, there is a general tail off of $\eta_o Nu/Pr^{1/3}$. One would expect this to happen closer to the transiton Reynolds number (2250) but this does not appear to be the case. Since the abscissa of Figures4.4.1.3.1-5 is more of a bulk Reynolds number, there is a distinct possibility that laminar flow exists between the fins at Reynolds number greater than 2250.

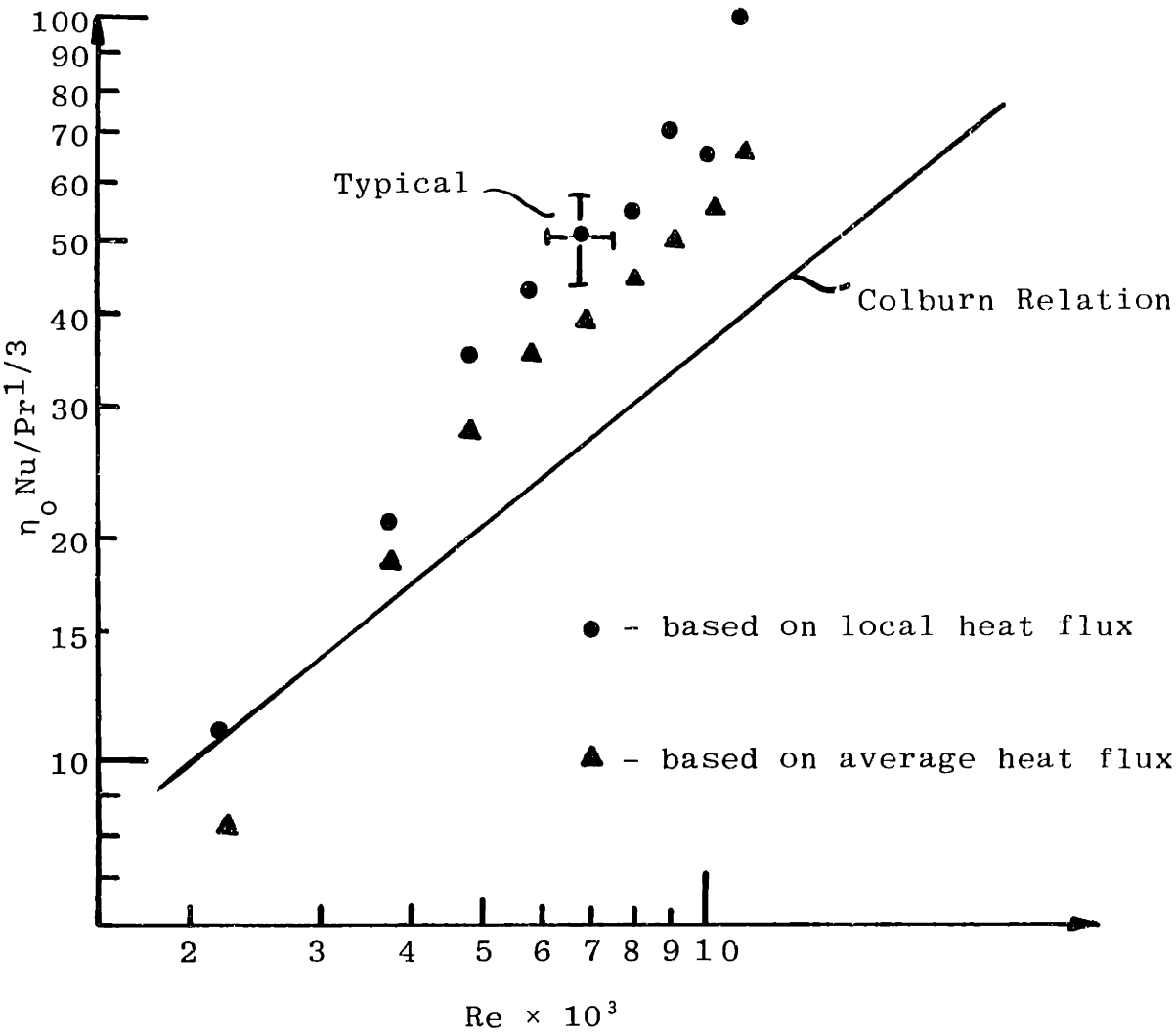

Fig. 4.4.1.3.1 η_0 Nu/Pr$^{1/3}$ vs Reynold's Number for Data Set No.2

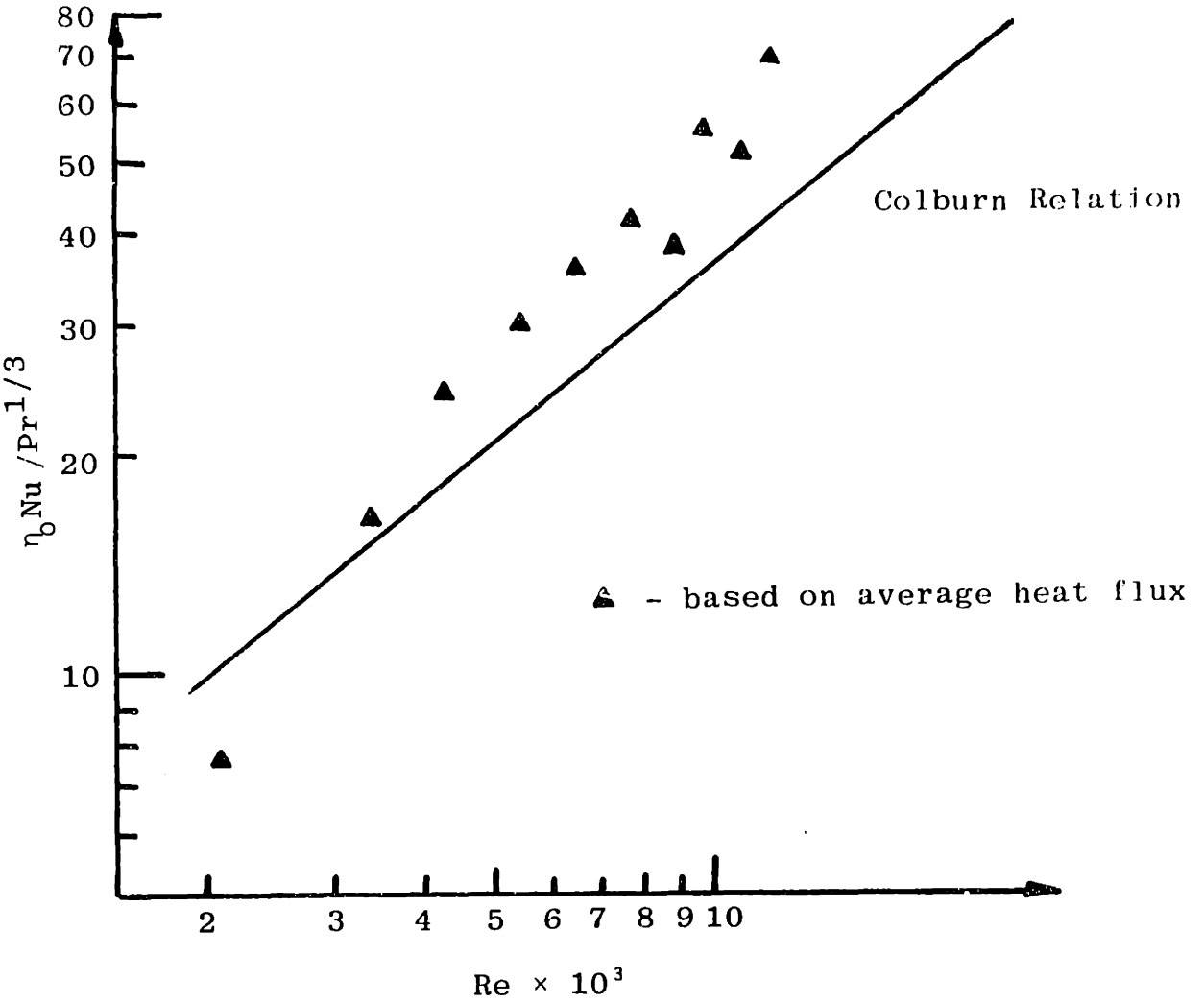

Fig. 4.4.1.3.2 $\eta_o Nu/Pr^{1/3}$ vs Reynold's Number for Data Set No.3

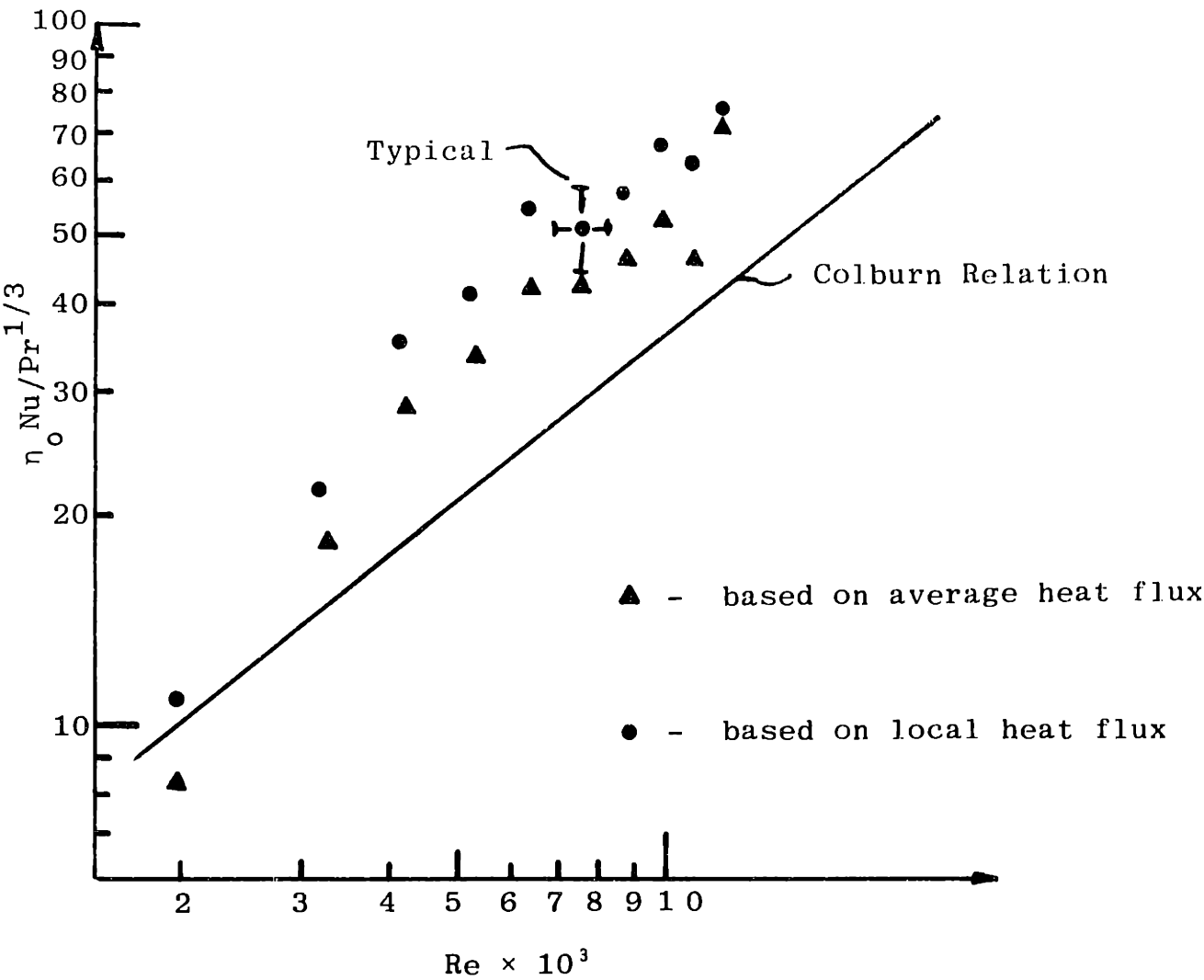

Fig. 4.4.1.3.3 $\eta_o Nu/Pr^{1/3}$ vs Reynold's Number for Data Set No.4

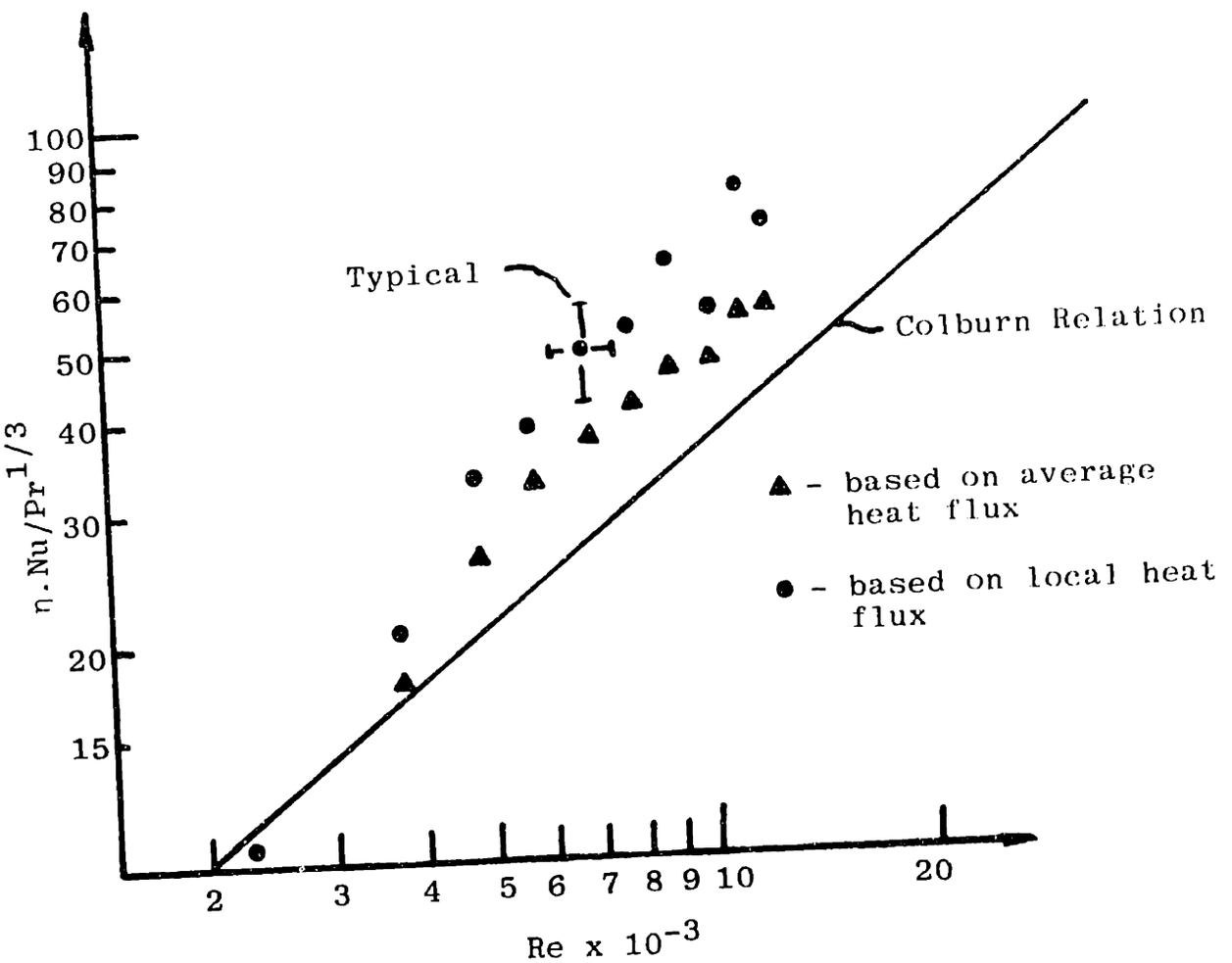

Fig. 4.4.1.3.4 $\eta.Nu/Pr^{1/3}$ vs Reynold's Number for Data Set No.5

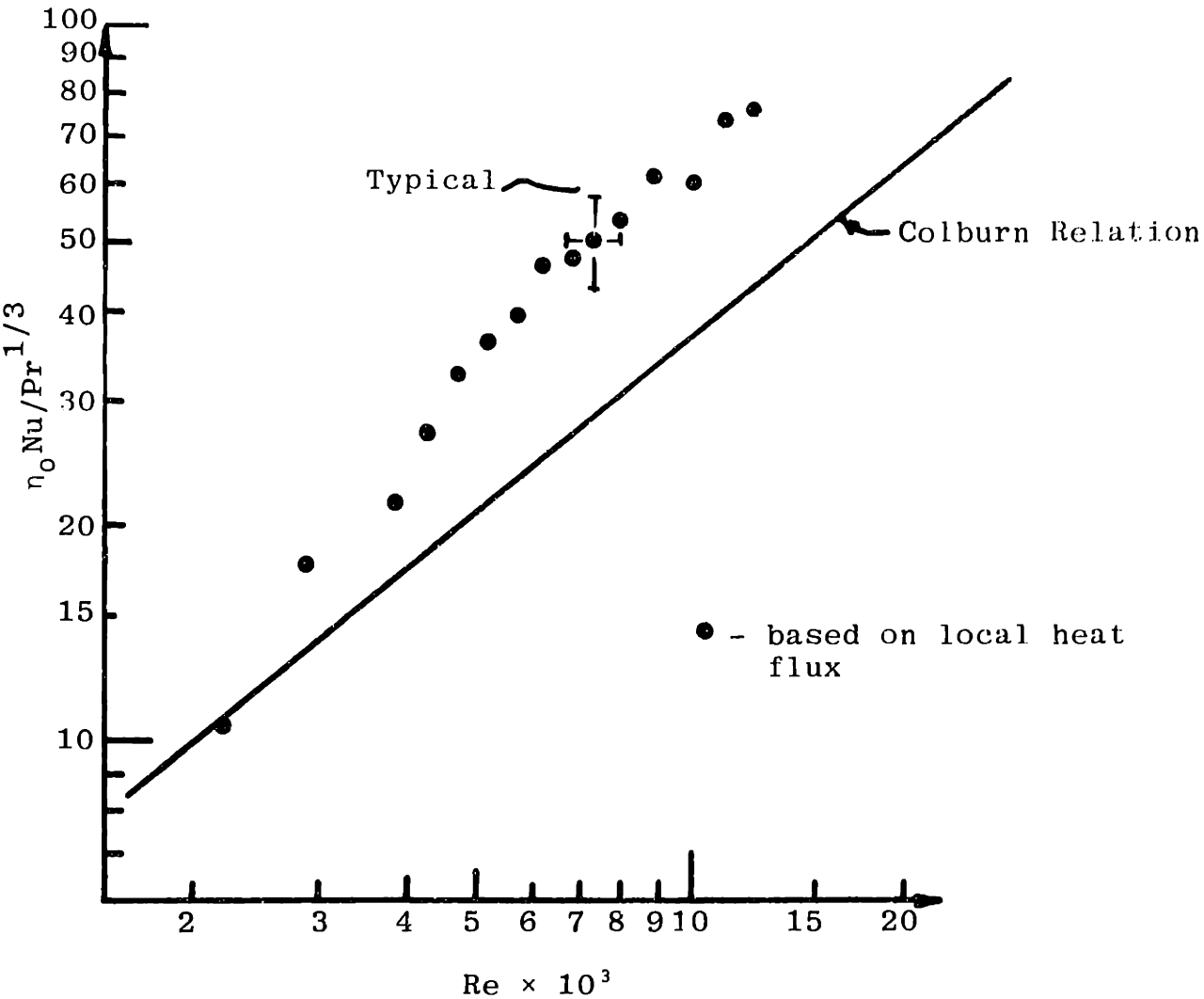

Fig. 4.4.1.3.5 $\eta_o Nu/Pr^{1/3}$ vs Reynold's Number for Data Set No.6

This would explain the drop off at the higher Reynold's number. This phenomenon is given more attention in Section 4.4.2.

Heat transfer results for Data Set 1 are not given. This was a low power run (1/3 power) with both sides of the test channel heated. Consequently, back plate and fluid temperatures approached each other and introduced a large amount of error due to the rature of Equation 4.2.3.2. The calculated values for $\eta_o h$ for Data Set 1 are plotted versus flow rate on Figure 4.4.1.3.6. Values obtained in Data Set 6 are shown for comparison. As can be seen from this figure, once T_{BP} approached T_f, calculated values of $\eta_o h$ skyrocketed. The author found no reason to suspect this data, hence Data Set 1 was not used in any of the analysis.

4.4.2 Surface Effectiveness Determination and Results

Surface effectiveness data was obtained indirectly by calculation of an average overall thermal resistance for each flow point at the channel mid-section and calculation of the heat transfer coefficient, h by the Colburn relation using the values of Re and Pr obtained at the film temperature condition.

Rearranging Equation 4.2.3.2 and inverting it, we have

$$\frac{T_B - T_f}{q''} = R_{th} = \frac{1}{\eta_o}\left[\frac{1}{h}\right] + \frac{g}{k_a} \quad . \qquad (4.4.2.1)$$

By plotting R_{th} versus the calculated Colburn h, we obtain a curve which has a slope of $1/\eta_o$. It should be mentioned however, the slope is not directly equal to $1/\eta_o$ since η_o is a function of h through the fin efficiency η_f. Taborda (2) has shown the slope of this curve is given by

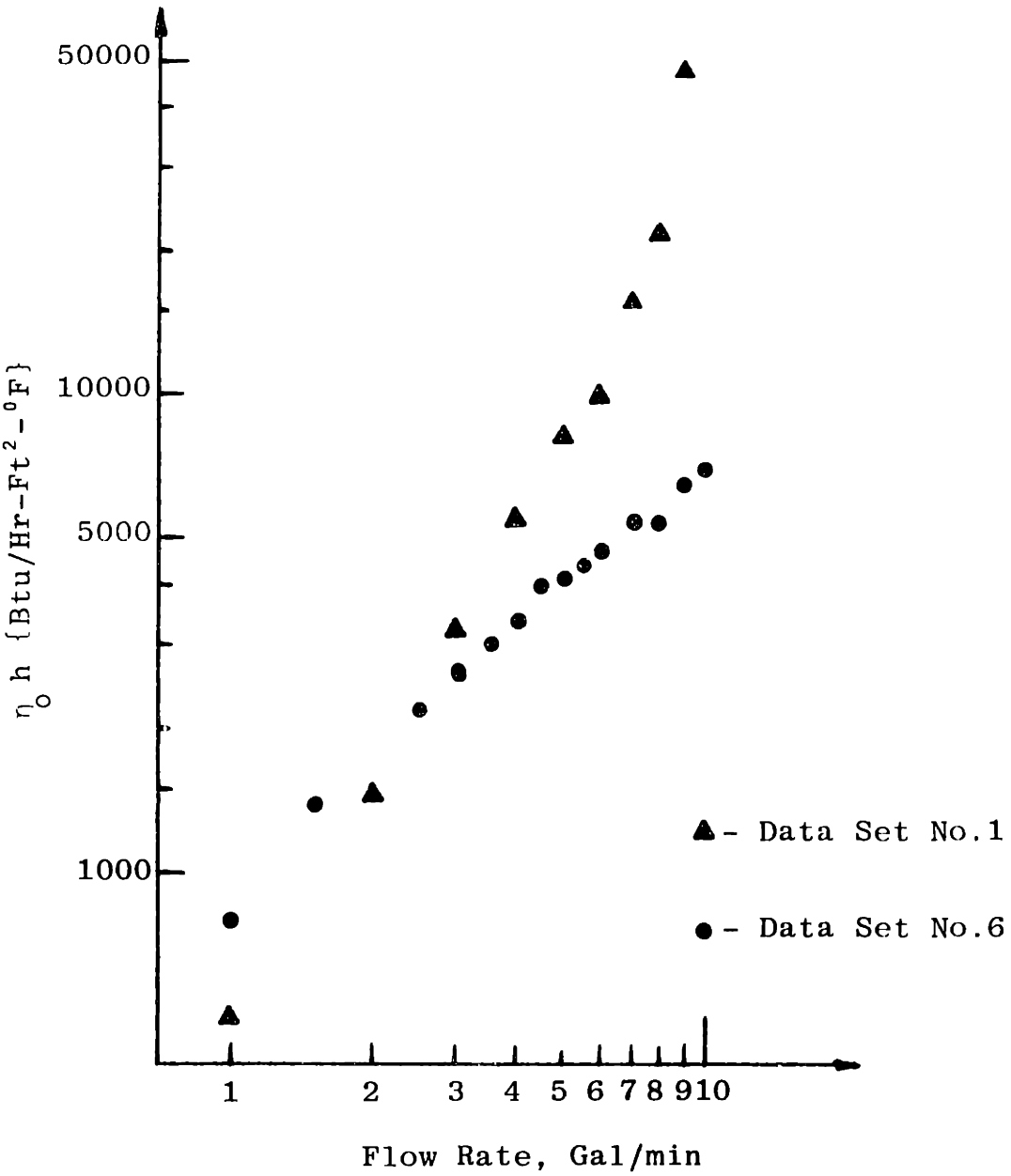

Fig. 4.4.1.3.6 Log $\eta_o h$ vs Log Flow Rate

$$\frac{d(T_B - T_f/q'')}{d(1/h)} = 1/\eta_0 \{1 - \frac{1}{2\eta_0} \frac{A_f}{A_B} [(m(1+t)n_f)^2 + n_f - 1]\}, \quad (4.4.2.2)$$

and recommends that the surface effectiveness be approximated by Equation 4.2.2.8, again repeated here:

$$\eta_o = \frac{A_b}{A_B} + \eta_f \frac{A_f}{A_B}.$$

For the purpose of this thesis, the slope of the Rth versus 1/h curve is close enough to the inverse of η_o to make valid conclusions. Taborda (2) analyzed the case for similar aluminum fins and found justification to make this assumption.

Graphs of Rth versus 1/h are presented for the different data sets in Figures 4.4.2.1-5. The inverse of the bulk Reynold's number is also given on the abscissa of these curves. Again, data points for both average and local heat fluxes are plotted. Only those points obtained with the local values of the heat flux are used to determine η_o.

In all cases, a straight line can be observed for 1/h less than 60. A least square fit was applied to all the data to determine the best line to draw through them. All data points are included in the least square fit. A value for η_o of 1.885 ± 0.116 was found. This value for η_o differs quite drastically from the value of 1.486 given in the MITR-II SAR (2) and is much nearer to the value of 1.9 reported by Taborda (2).

The shape of the Rth versus 1/h calculated tails off at values of 1/h greater than 60. This does not indicate the η_o is changing since the abscissa is based on the Colburn relation and the Reynold's number between the fins maybe in the laminar

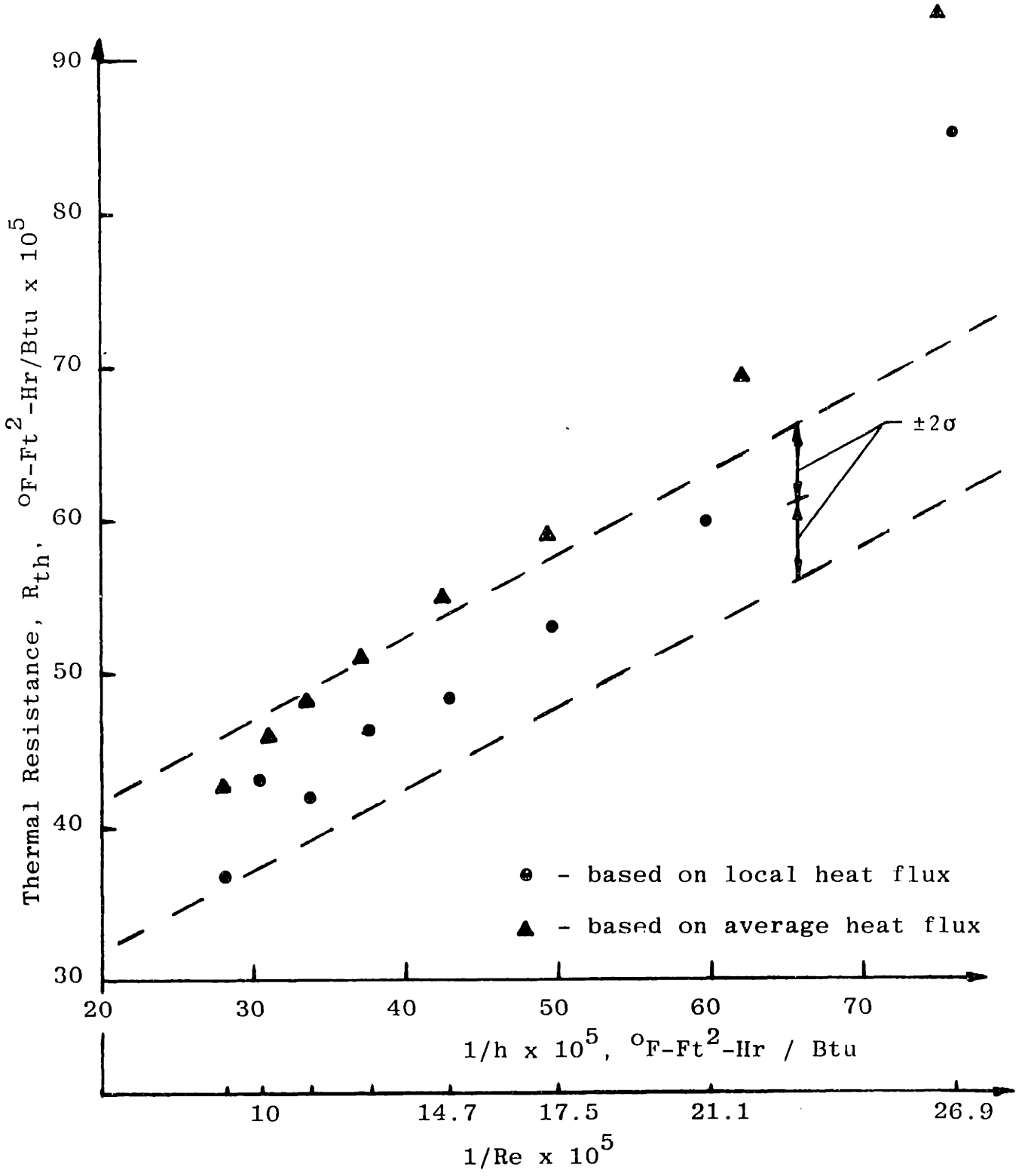

Fig. 4.4.2.1 Thermal Resistance vs 1/h and $1/Re_b$ for Data Set No.2

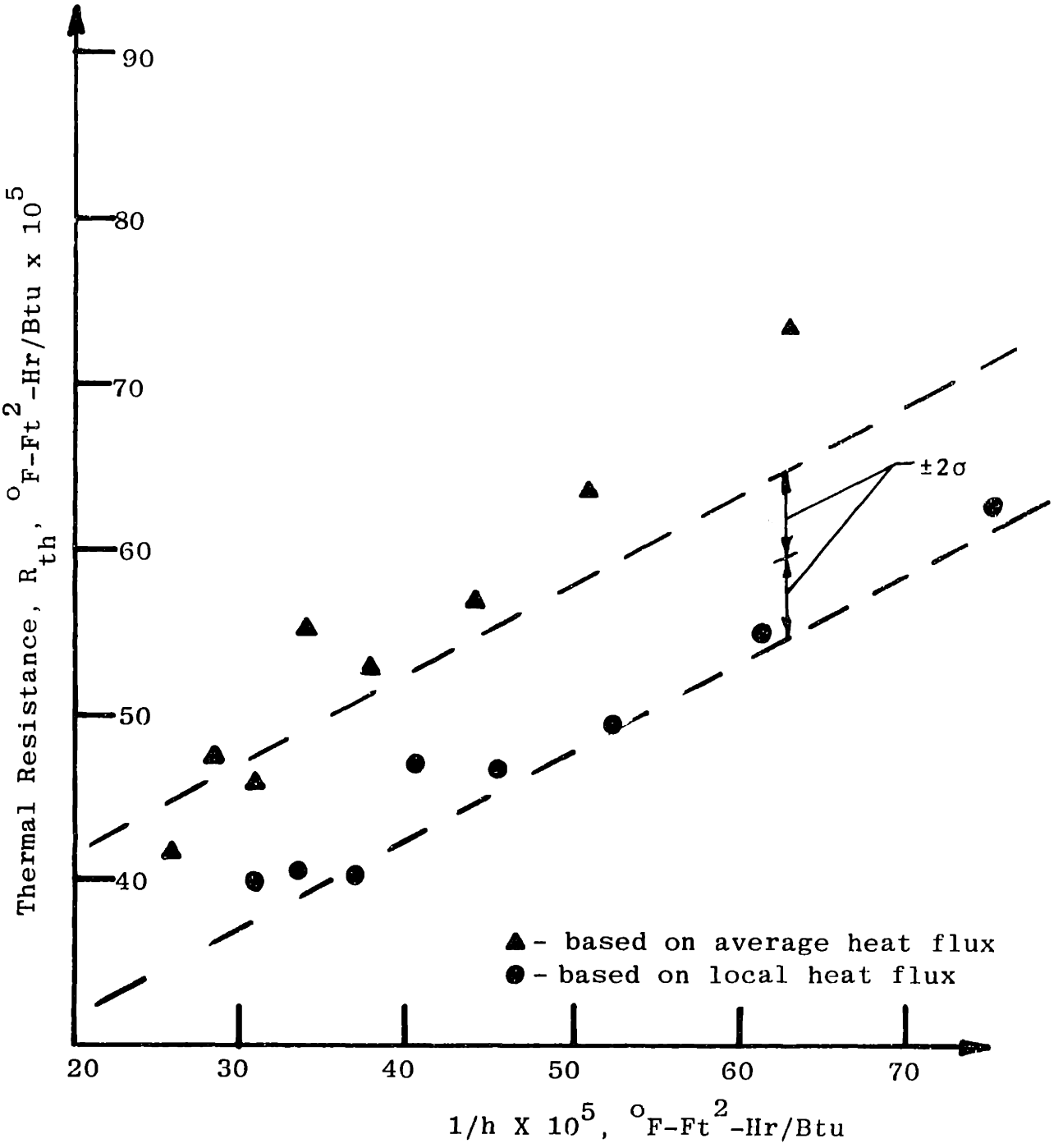

Fig. 4.4.2.2 Thermal Resistance vs 1/h for Data Set No.

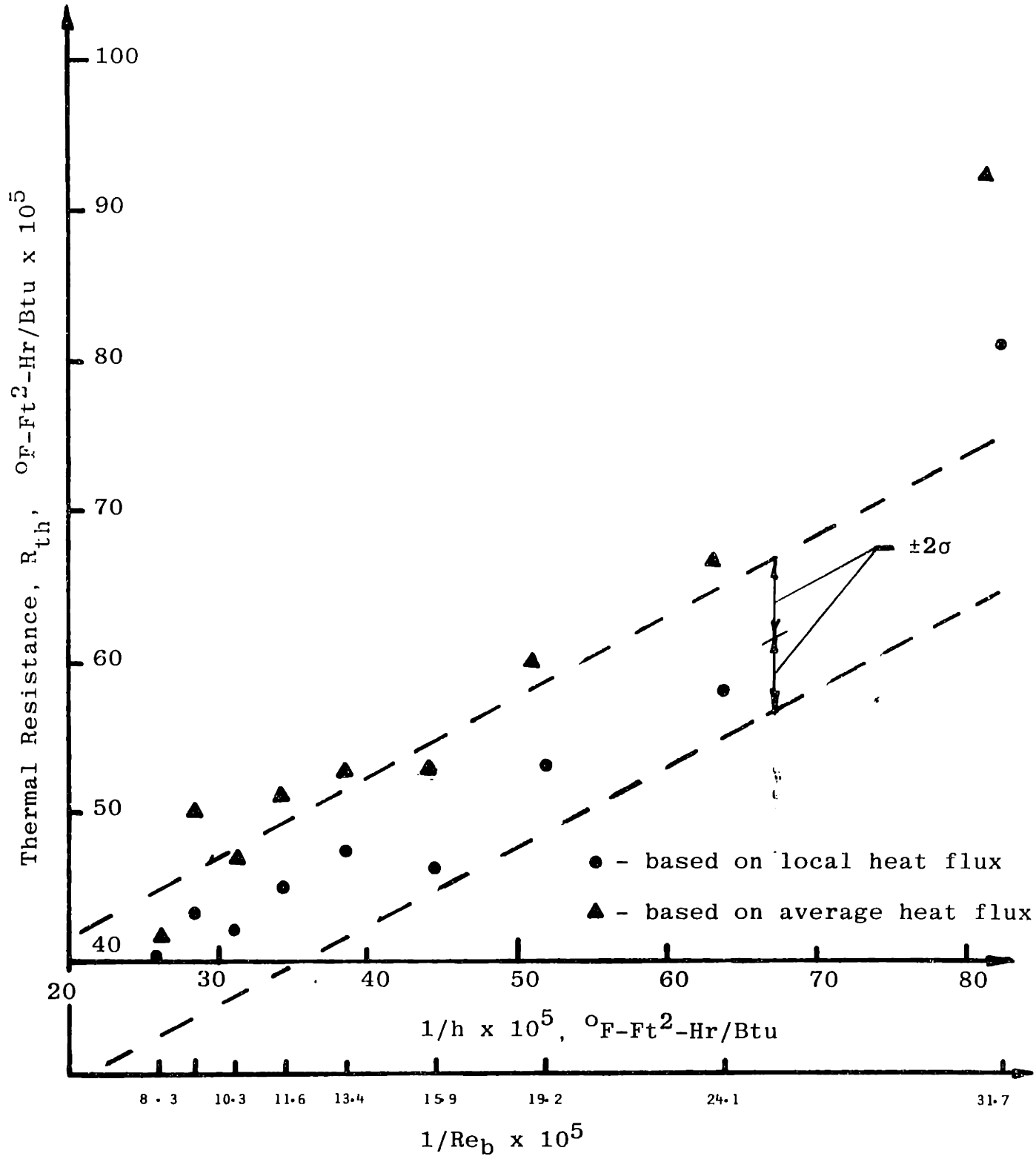

Fig. 4.4.2.3 Thermal Resistance vs 1/h and 1/Re_b for Data Set No.4

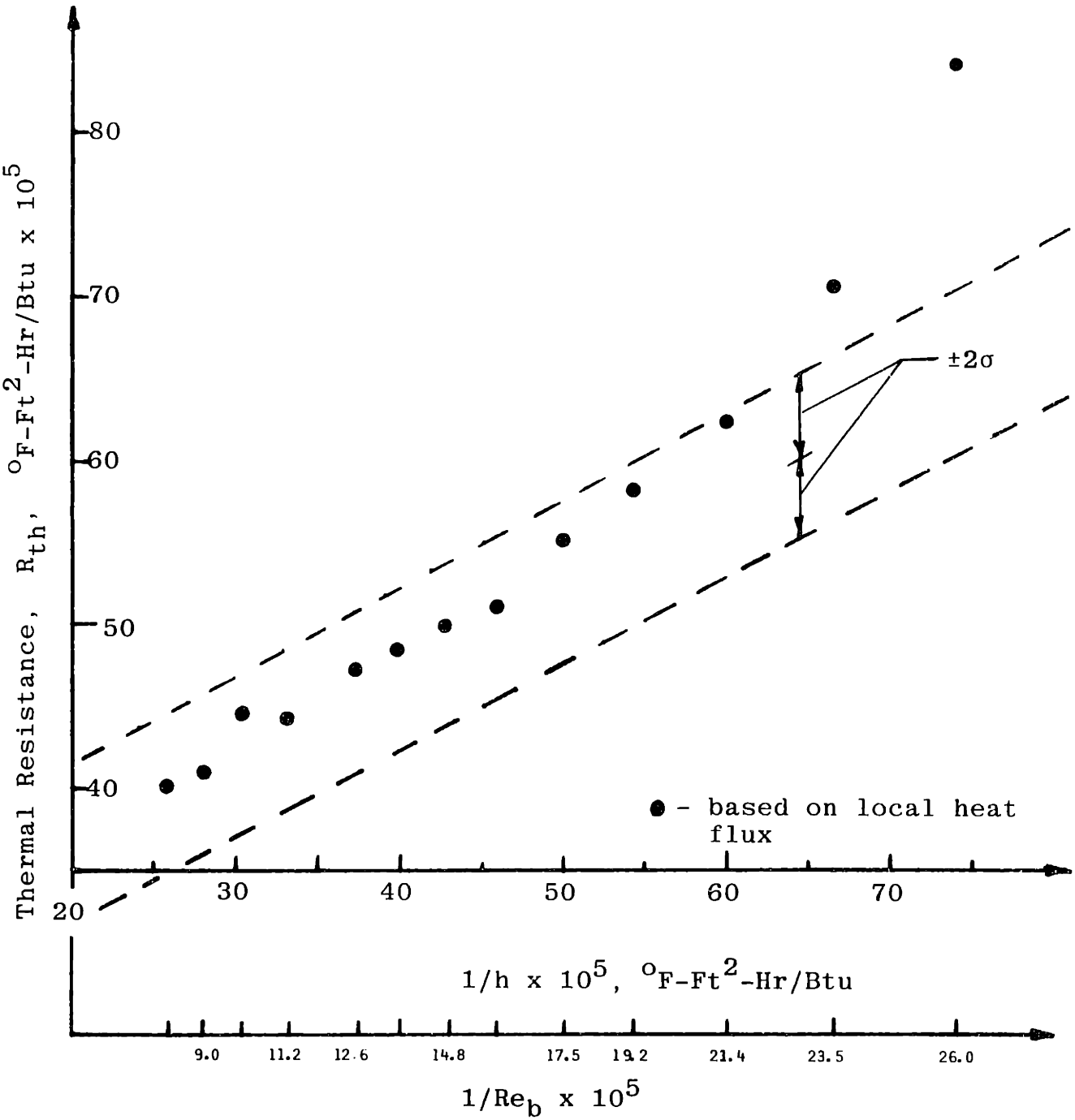

Fig. 4.4.2.5 Thermal Resistance vs 1/h and $1/Re_b$ for Data Set No.6

region. Consider the case when only laminar flow exists in the channel. The Nusselt number takes on a constant asymptotic value for fully developed laminar flow. Kayes (13) has determined this value to be 8.23 for uniform heat flux and high channel aspect ratio. The laminar heat transfer coefficient for this case then given by:

$$h = 8.23 \frac{k}{d_H} \simeq \frac{8.23(.3807 \text{ BTU/hr - ft - }^{\circ}\text{F})}{7.0573 \times 10^{-3} \text{ ft}} = 444 \frac{\text{BTU}}{\text{HR-FT}^2\text{-}^{\circ}\text{F}},$$

and

$$1/h = 225 \times 10^{-5} \frac{\text{Hr - Ft}^2\text{ - }^{\circ}\text{F}}{\text{BTU}} .$$

This value for h was the used in Equations 4.2.2.1 and 4.2.2.8 to determine, η_o. A value very close to 2.0 was obtained. (It should be mentioned that calculation of the actual 1/h is not possible since $\eta_o h$ is the quantity that is measured.)

This indicates that the low flow data points will be shifted to the right of Figures 4.4.2.1.5 for a combination of laminar and turbulent flow. This shift will result in curves of decreased slope and hence, higher values of η_o in this region. Further investigation of the laminar flow between the fins is warranted but is beyond the scope of this thesis.

4.5 In-Channel Thermocouple Data Reduction and Results

The general method of analyzing in-channel thermocouple data has been presented in Section 4.3.3 of this chapter. The experiment initially had four operable in-channel thermocouples. Due to the axial conduction at the beginning of the channel, it was felt that there would be too much uncertainty associated with the values used in calibrating IC#1, located 1.5 inches from the beginning of the heated section and results would be inconsequential. Hence, no results

for IC#1 are presented. IC#3 became inoperative after Data Set 2 when the test section was modified. Only results from Data Set 2 are given for IC#3. Results for the remaining in-channel thermocouples for Data Sets 2,4,5, and 6 are presented. All pertinent IC data is given in Appendix A and Appendix C.

All in-channel thermocouples are located on the female part of the test section and their exact locations are given in Section 3.3.6 of Chapter 3. Only the female back plate temperatures near the IC location are used with the measured heat flux to determine the wall temperatures. In-channel thermocouple temperatures are measured directly.

4.5.1 In-Channel Thermocouple Calibration Curves

The calibration factor for a surface attached thermocouple is given by Equation 4.3.2.1 and is repeated here:

$$Z = \frac{T_w - T_o}{T_w - T_f}.$$

This parameter has been calculated for IC's#2 and 4 at each flow point in Data Sets 2,4,5, and 6 and has been calculated for IC#3 at each flow point in Data Set 2. These calibration factors are plotted against their associated experimental heat transfer coefficient, $\eta_o h$ in Figures 4.5.1.1 through 4.5.1.3.

Figure 4.5.1.1 is the calibration curve for IC#2. As can be seen from this figure, the data spread is rather large with no real definable pattern except for points from Data Set Number 4. To be conservative, the curve on Figure 4.5.1.1 has been drawn to envelope most of the data points. The calibration factor data for IC#3, Figure 4.5.1.2, form a very well defined curve with very little spread from the drawn curve. Once again, the data spread for IC#4,(Figure 4.5.1.3) is large but a general trend is seen. An enveloping curve

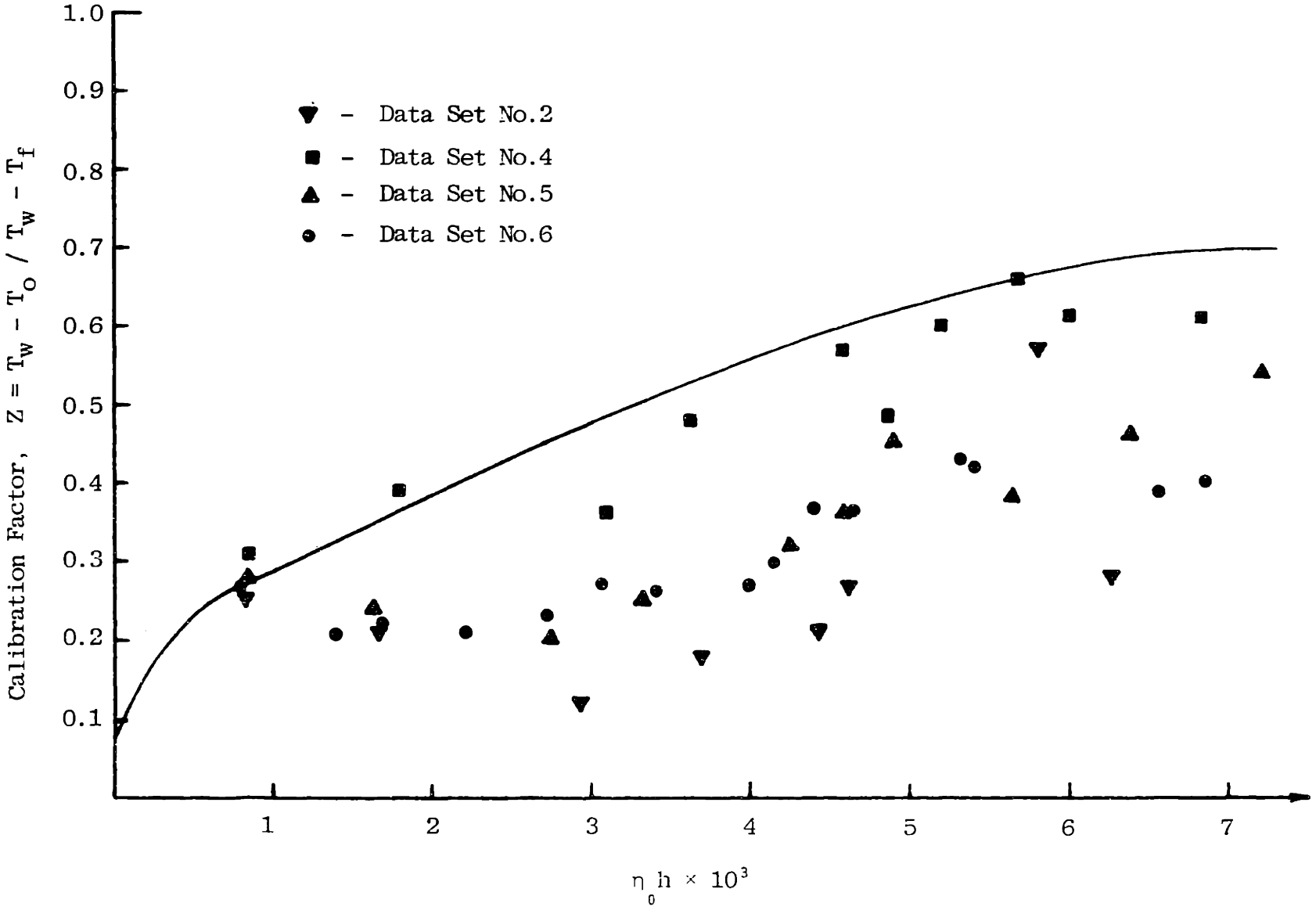

Fig. 4.5.1.1 Calibration Factor, Z vs Experimental $\eta_0 h$ for Inchannel Thermocouple No.2

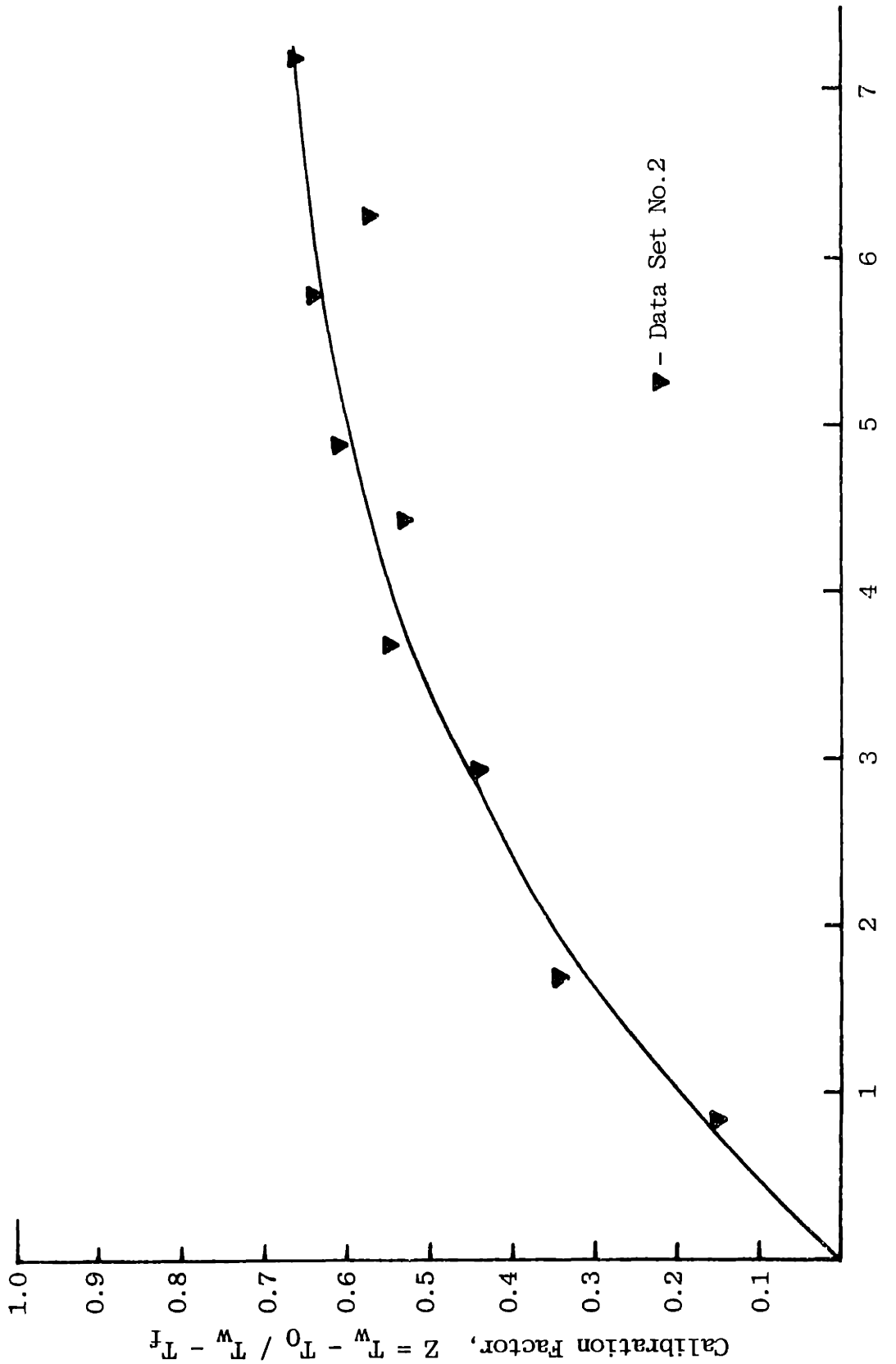

Fig. 4.5.1.2 Calibration Factor Z vs Experimental $\eta_0 h$ for Inchannel Thermocouple No.3

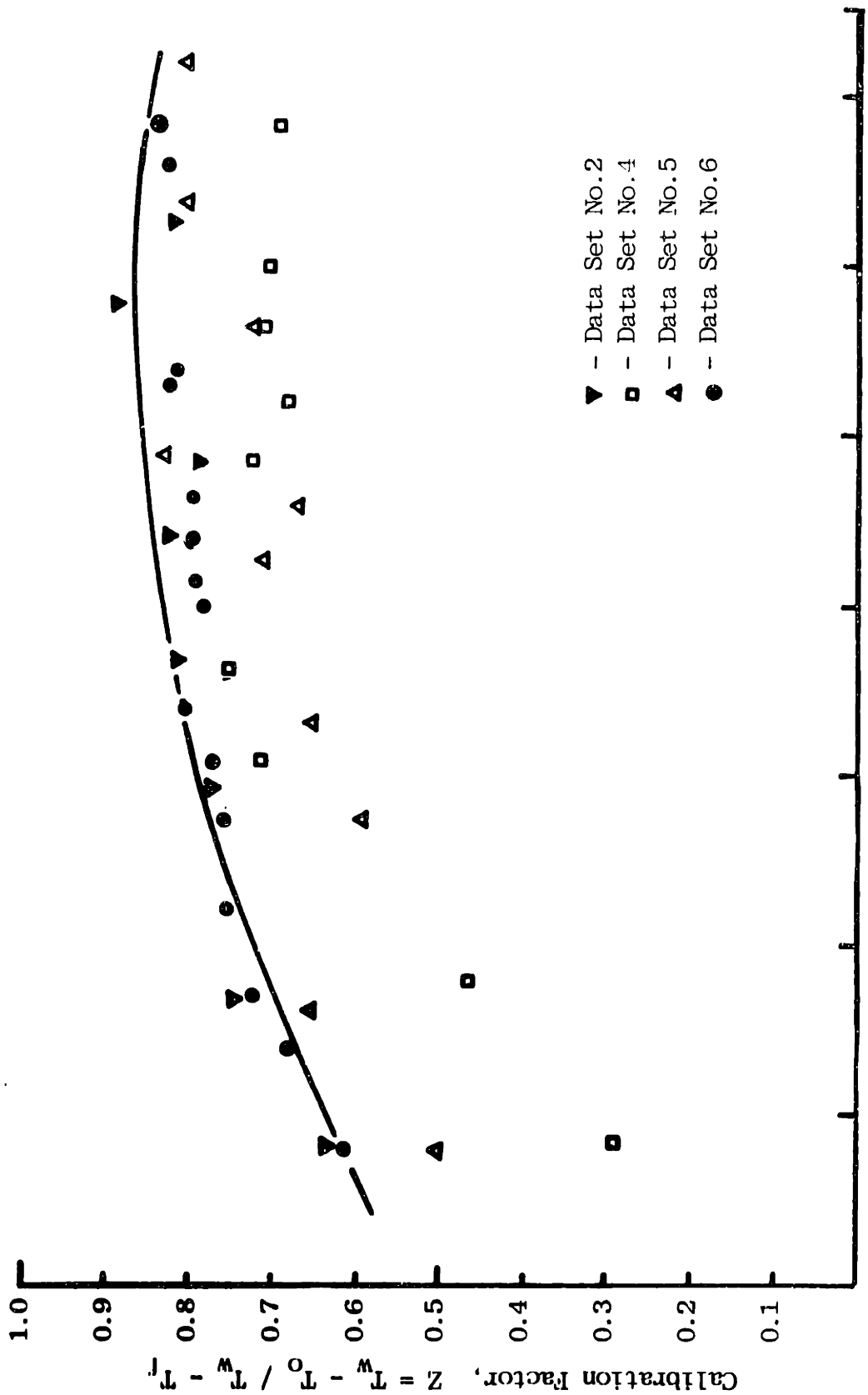

Fig. 4.5.1.3 Calibration Factor Z vs Experimental $\eta_0 h$ for Inchannel Thermocouple No.4

has been drawn to be conservative.

The main reason for drawing the curve through Set No. 4 data points on the IC#2 calibration curve, Figure 4.5.1.1 is the fact that the IC#2 installation very closely resembles that for IC#3. Hence, the similar shaped curve. This fact will be shown in the following section.

4.5.2 Thermocouple Characteristic Curves

A characteristic curve for each in-channel thermocouple can be found by plotting the installation factor I given by Equation 4.3.3.2.3, again repeated here

$$I = \frac{1 - Z}{\eta_o h} = \frac{T_o - T_f}{q''},$$

versus the corresponding experimental heat transfer coefficient. These characteristic curves have been generated for the three in-channel thermocouples and are given in Figures 4.5.2.1-3. The data for each in-channel thermocouple follow the $1/\eta_o h$ relationship rather closely with very little deviation from the drawn in curves. Since the heat flux, observed in-channel TC temperature and fluid temperature are experimentally determined quantities, the error in these curves is small. The drawn in exponential curves were obtained by applying the method of least squares to the logarithms of I and $\eta_o h$ for each figure. A composite of these characteristic exponential curves is given in Figure 4.5.2.4.

As can be seen from Figure 4.5.2.4, in-channel thermocouples 2 and 3 closely resemble each other. The characteristic curve for IC#4 is different from the other two, decreasing much more rapidly with $\eta_o h$. This is to be expected since this TC was not installed as well as the others and had more exposure to the coolant stream.

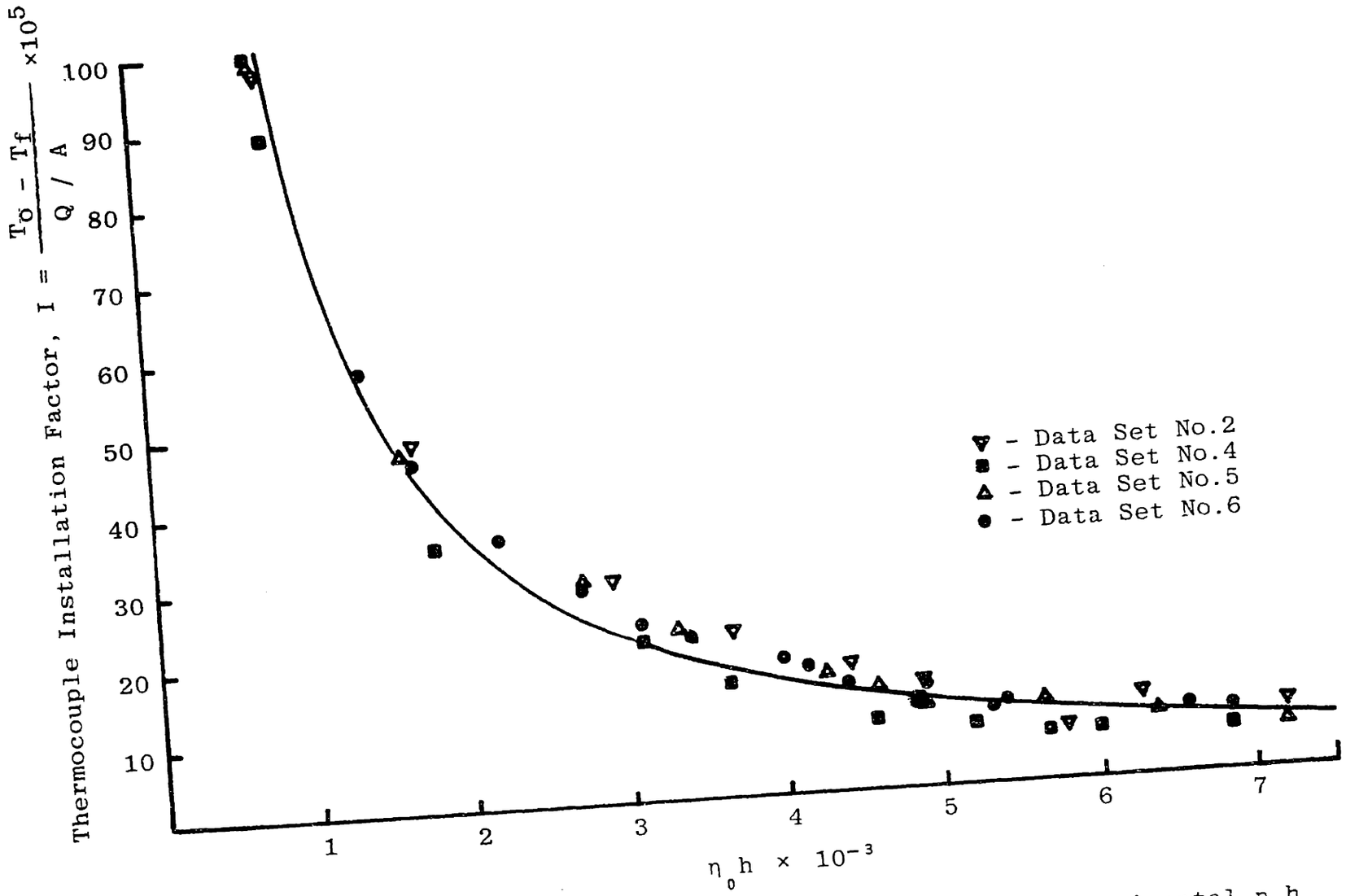

Fig. 4.5.2.1 Thermocouple Installation Factor vs Experimental $\eta_0 h$ for Inchannel Thermocouple No.2

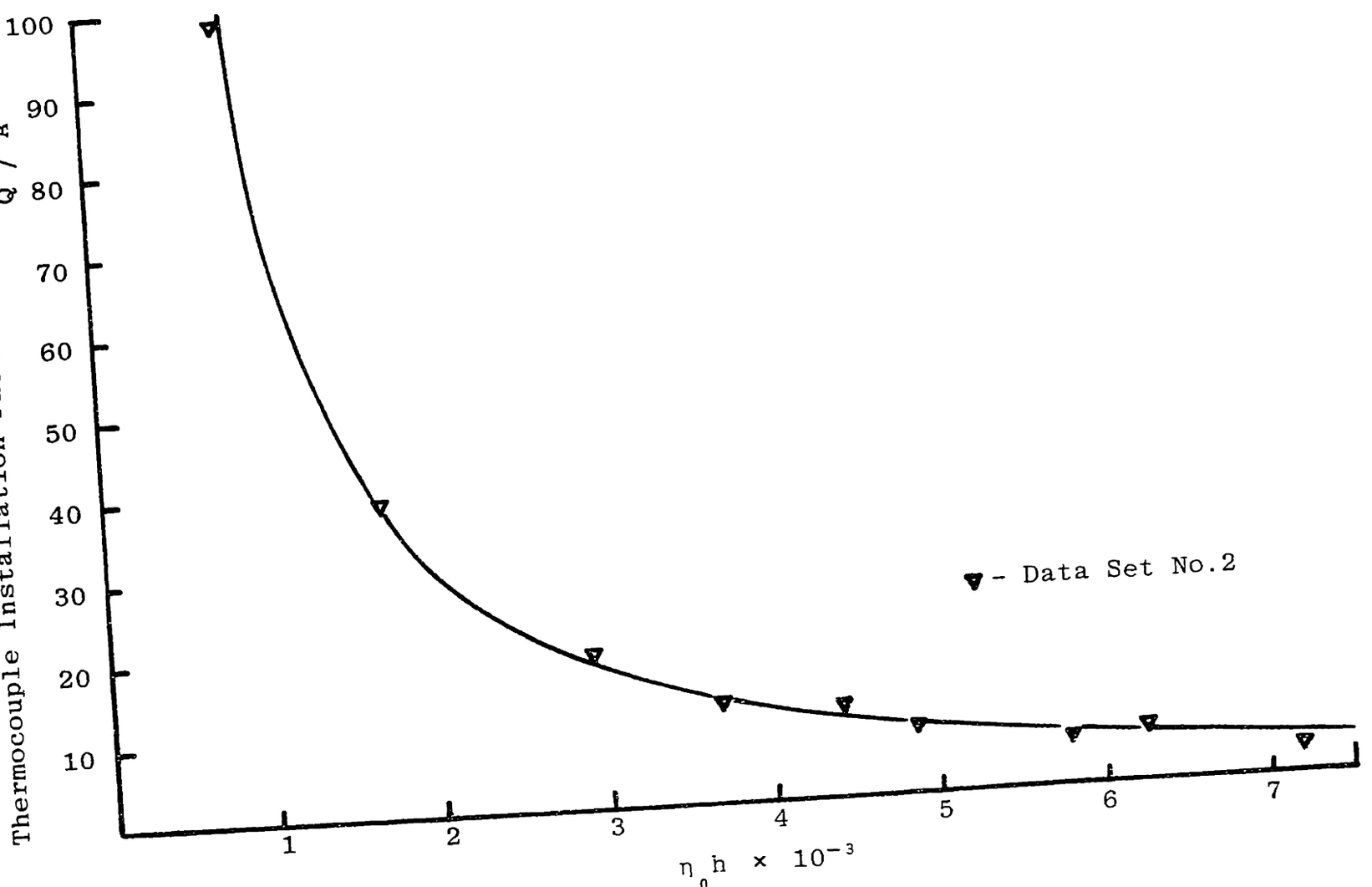

Fig. 4.5.2.2 Thermocouple Installation Factor vs Experimental $\eta_0 h$ for Inchannel Thermocouple No.3

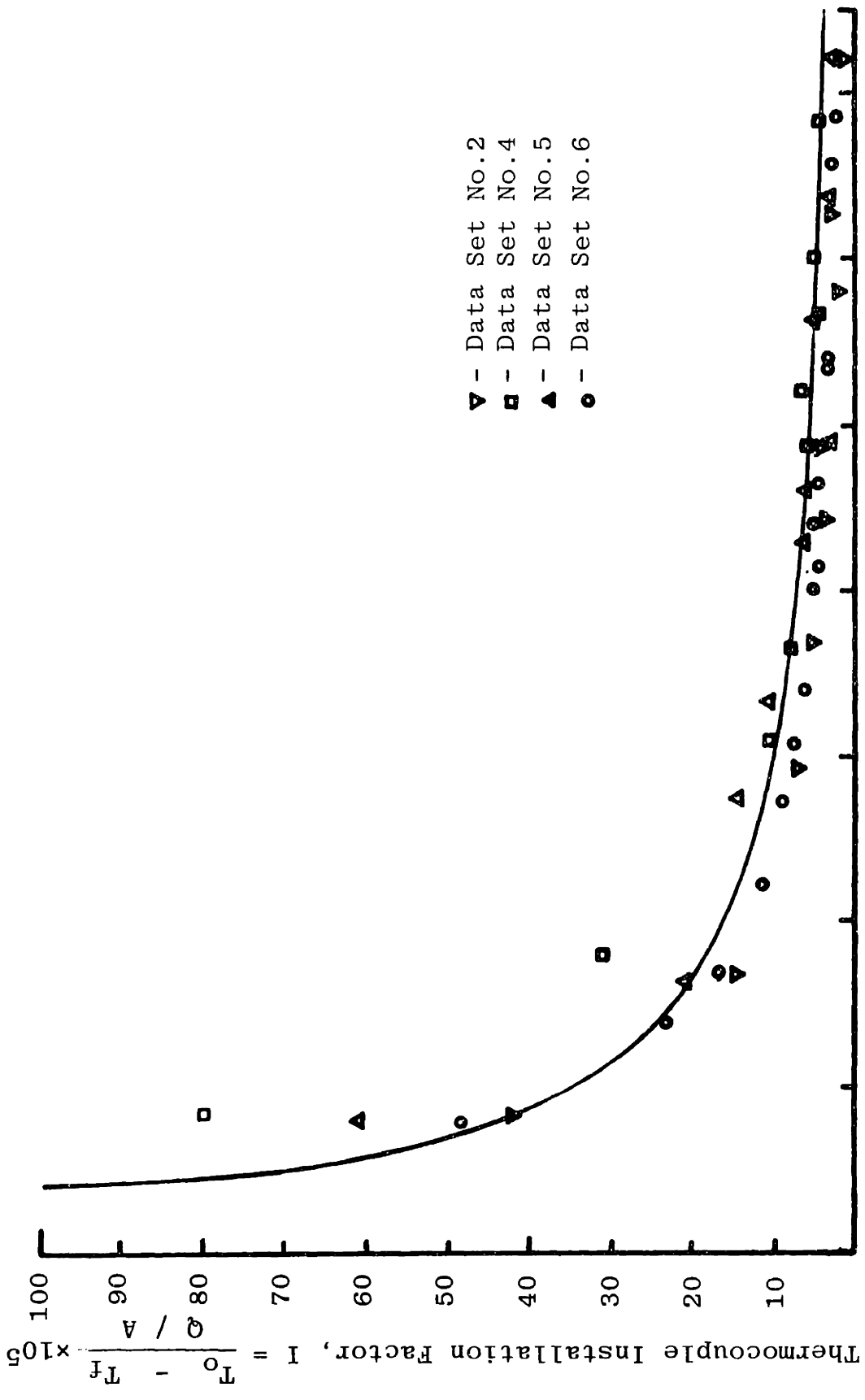

Fig. 4.5.2.3 Thermocouple Installation Factor vs Experimental $\eta_0 h$ for Inchannel Thermocouple No.4

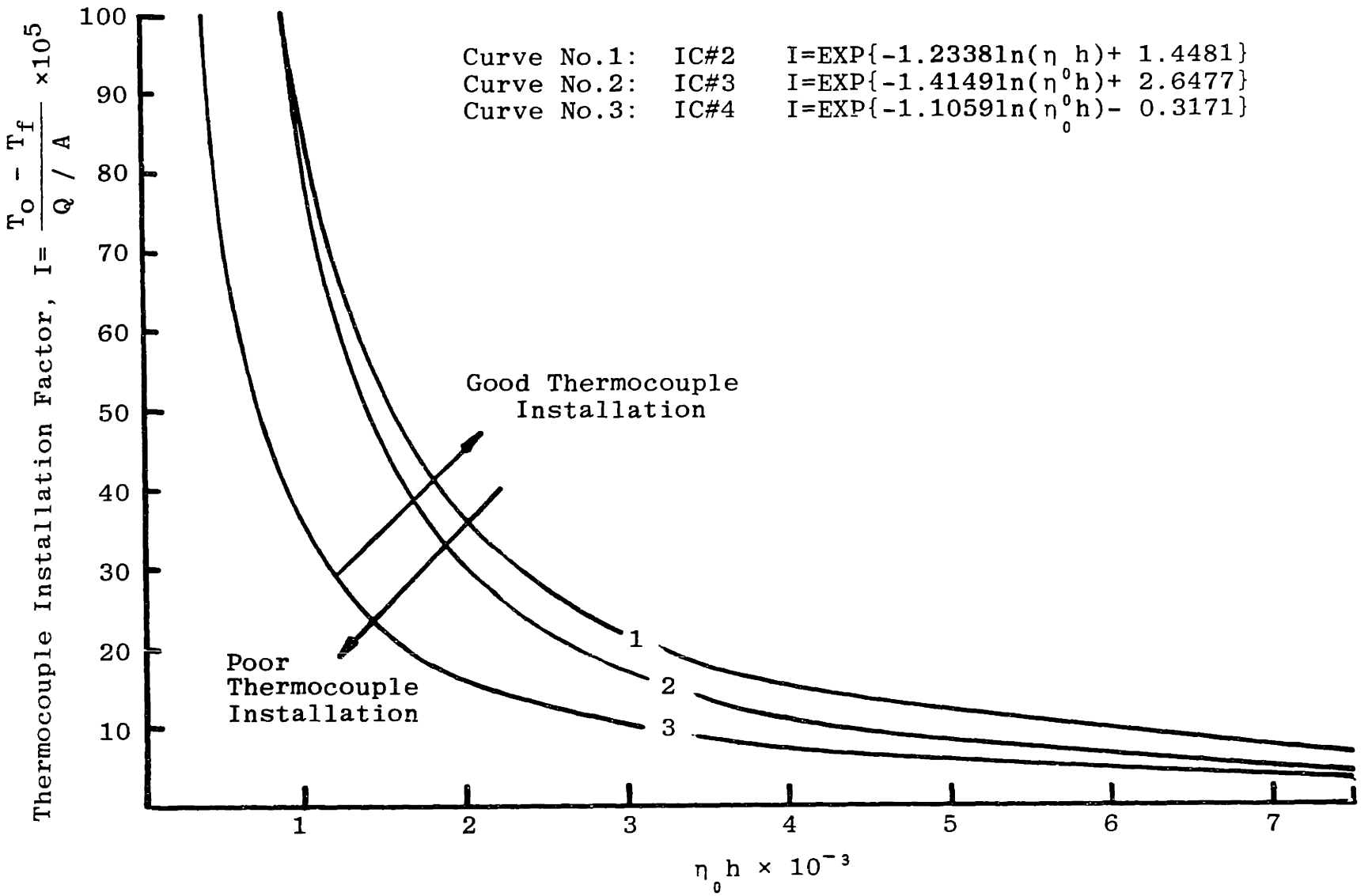

Fig. 4.5.2.4 Thermocouple Installation Factor vs Experimental $\eta_0 h$ for Inchannel Thermocouple Nos. 2,3, and 4

As $\eta_o h$ increased, the observed temperature approached the fluid temperature causing the rapid decline.

4.5.3 Application of Characteristic Curves to MITR-II

As mentioned in Section 4.3.3.2, characteristic curves of the in-channel thermocouples on the thermocouple fuel element are to be generated from the estimated heat flux, fluid temperature and observed temperatures. The procedure then is to go to Figure 4.5.2.4 and locate the relative position of the thermocouple with respect to IC's#2,3, and 4. A well installed thermocouple curve will be to the right of curves 1 and 2 whereas a poorly installed thermocouple curve will be in the region of curve 3. Once the thermocouple is characterized, interpolation of calibration factors from Figures 4.5.2.1-3 becomes necessary.

In order to estimate the magnitude of the difference between the surface temperature and the observed thermocouple temperature, graphs of $(T_w - T_o)$ versus the Reynold's number have been drawn. These are given in Figures 4.5.3.1 and 4.5.3.2. As can be seen from Figure 4.5.3.1, the maximum expected temperature difference between wall and observed temperature for IC's#2 and 3 for Re's greater than 4700 (channel flows greater than 3.0 GPM) is $8^{o}F$ for IC#3 and $6^{o}F$ for IC#2. These values are for heat fluxes in the range of 50,000 BTU/HR - Ft^2 - ^{o}F or a reactor power of $\sim$ 4.5 megawatts.

The temperature difference curve for IC#4 is more clearly defined (Figure 4.5.3.2) but since this thermocouple has the poorest

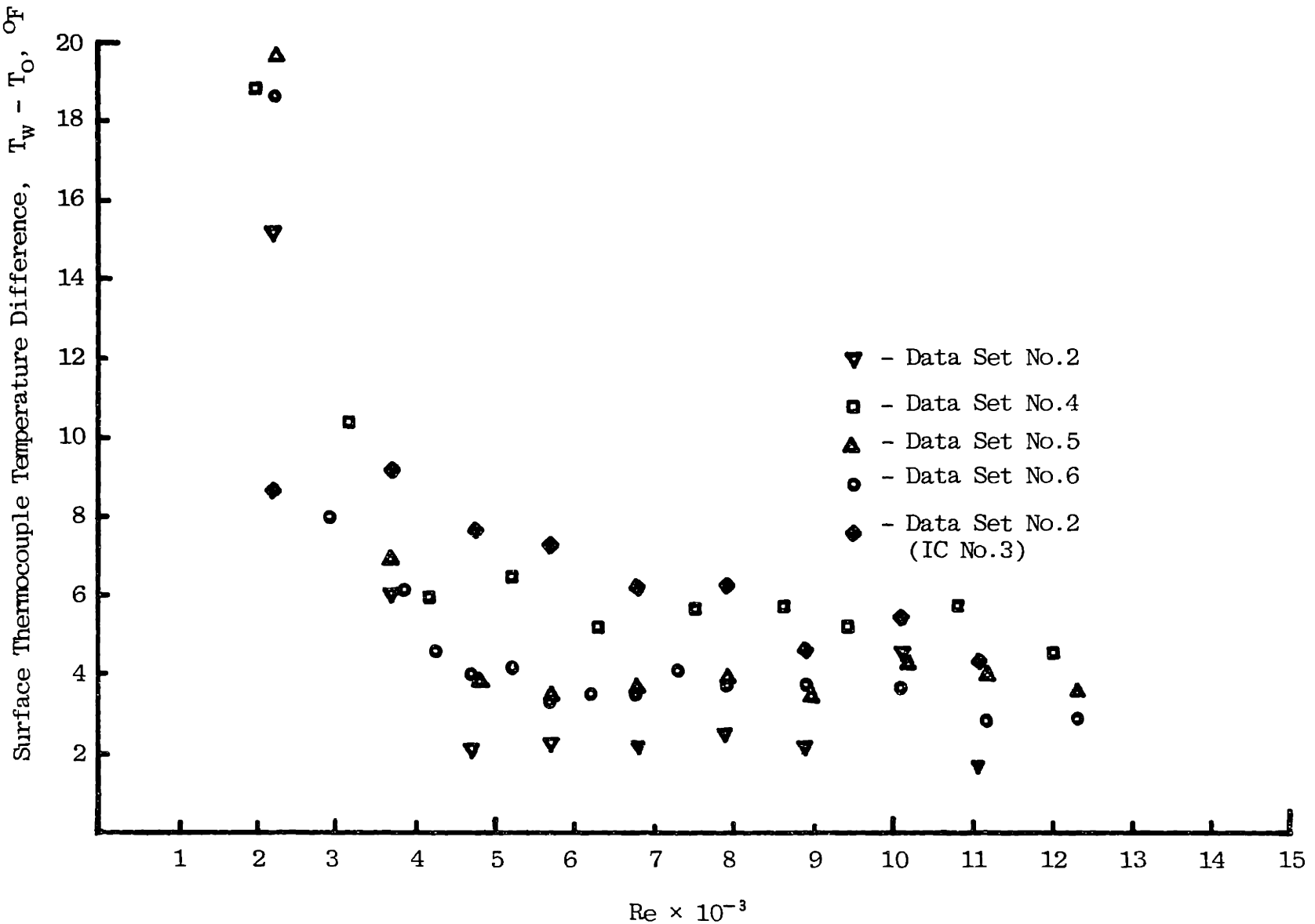

Fig. 4.5.3.1 Surface Thermocouple Temperature Difference vs Reynold's Number for Inchannel Thermocouples Nos.2 and 3

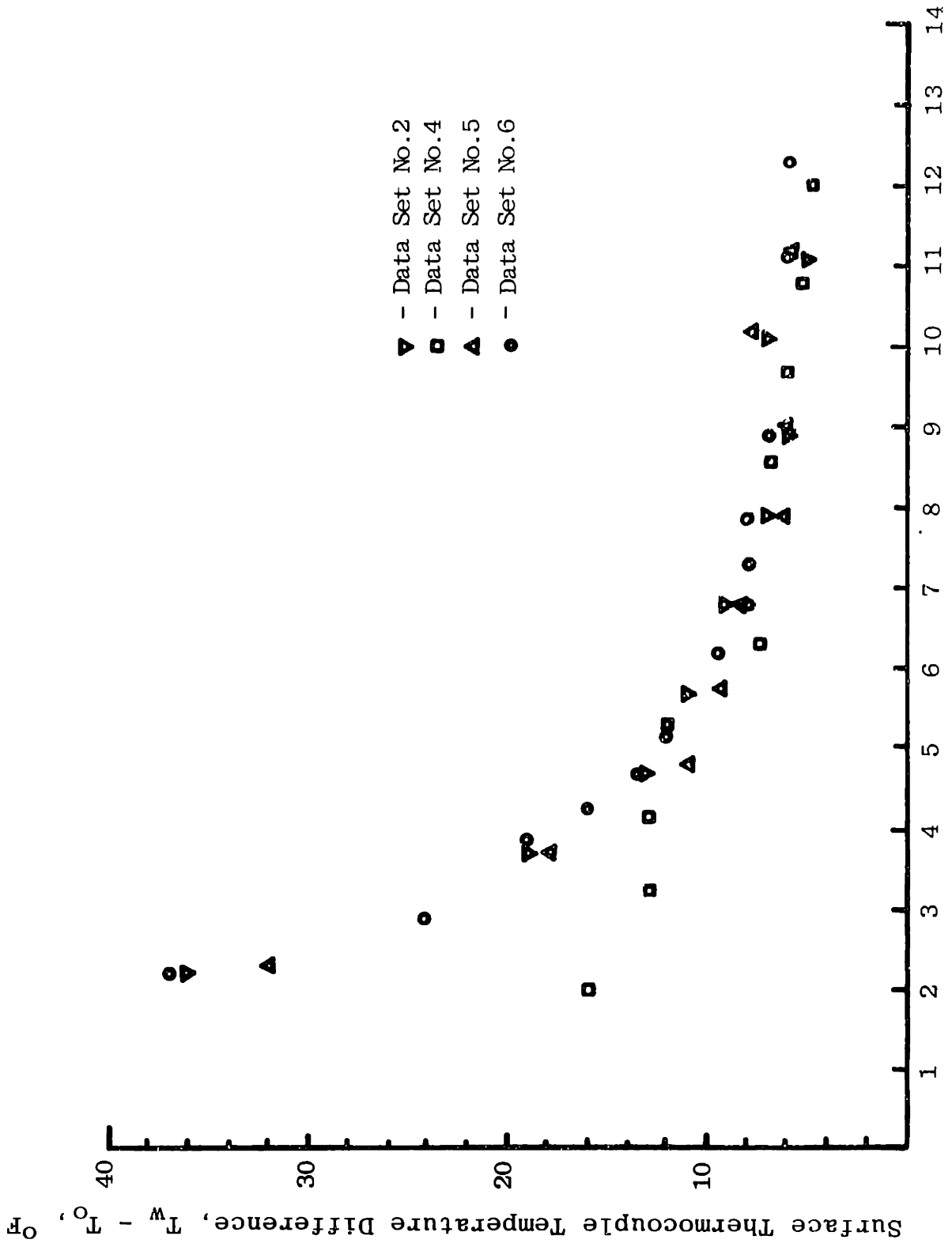

Fig. 4.5.3.2 Surface Thermocouple Temperature Difference vs Reynold's Number for Inchannel Thermocouple No.4

installation, the temperature differences are much higher with a difference of 16°F at Re = 4000 (2.5 GPM) decreasing to approximately 6° F at Re = 12000 (10 GPM).

The maximum surface temperature difference is an important parameter with respect to the use of thermocoupled fuel element. Since clad surface temperature is the limiting factor in the power escalation to 5 Mw for the new MITR-II core and in the natural convection test, Figures 4.5.3.1 and 2 can be used to check if calculated surface temperatures by the method presented above are reasonable.

CHAPTER 5

CONCLUSIONS

The need for experimentally simulating an MITR-II coolant channel was discussed in Chapter 1. After surveying in detail various methods of accomplishing this, a test channel was designed that accurately reproduced actual MITR-II channel dimensions. Power was applied to the test channel through the use of six 1920 watt commercially available electric heaters tightly fitted into the back of the two aluminum blocks which formed the channel. Appropriate instrumentation was used to monitor parameters necessary for the determination of the heat transfer characteristics of the coolant surface and in-channel thermocouple response. Six sets of data were obtained with each set of data containing ten to fifteen flow points. The analysis of this data is presented in Chapter 4.

The primary objective of this thesis was the experimental determination of the surface effectiveness of the MITR-II finned fuel plate. From the analysis of the data in Chapter 4, the value of the surface effectiveness, η_0, was found to be 1.885 ± 0.116. This confirms the results of an earlier thesis by Taborda (2) who obtained a value of 1.9 for the theoretical value of η_0. The agreement between the value of η_0 determined by this experimental work and that determined by Taborda's extensive computer analysis is very good. In light of this agreement, this author recommends that the value of the surface effectiveness as presented in the MITR-II Safety

Analysis Report (1) be changed to reflect the results of this experimental work.

The second objective of this thesis was to study the response of the chromel-alumel in-channel thermocouples. Four thermocouples were attached to the test channel surface in a similar fashion to those attached on the actual thermocoupled fuel element. Each thermocouple was installed differently in order to determine installation effects on thermocouple response. One in-channel thermocouple was damaged and no data was obtained from it.

Installation parameter curves for the remaining three in-channel thermocouples were generated from the data and are presented in Chapter 4. By following the procedure set forth in Chapter 4, experimenters using the thermocoupled fuel element can determine the quality of the thermocouple's installation.

Calibration curves for each in-channel thermocouple are also given in Chapter 4 along with surface-fluid temperature difference curves. For a properly installed thermocouple, the temperature difference between the channel wall temperature and bulk fluid temperature was shown to be less than $8^{o}F$ for channel flows greater than 3.0 GPM. For a poor thermocouple installation, this difference was shown to be less than $16^{o}F$ for channel flows above 2.5 GPM.

Finally, the conservatism in the thermal hydraulic design of the MITR-II fuel plates is evidenced by difference between the experimental value of the surface effectiveness, η_o, found by this research and the value used in the MITR-II SAR (1).

Secondly, in-channel thermocouple response was investigated and a means of characterizing the physical installation was devised. In the future, closer attention should be paid to the installation of such thermocouples.

REFERENCES

1. MITR Staff "Safety Analysis Report for the MIT Research Reactor (MITR-II)," 1970.

2. Taborda-Romero, J., "Design of MITR-II Fuel Plates Heat Transfer in Longitudinal Finned Narrow Channels," MIT Nuclear Engineering Department, S. M. Thesis, September 1971.

3. Hollenberg, T., "The Design of an Experiment to Investigate In-Channel Thermocouples, Heat Transfer Coefficient, and Fin Effectiveness for the MITR-II Fuel Plates," MIT Mechanical Engineering Department, Bachelor's Thesis, June 1974.

4. Momsen, B., Course 22.90 Term Paper Report, June 1974.

5. Spurgeon, D., "Preliminary Design Studies for a High Flux MIT Reactor," MIT Nuclear Engineering Department, Nuclear Engineer Thesis, June 1969.

6. Brindley, J. H., "Experimental Calibration of Thermocouples on Flat Fuel Plates," Transactions of the American Nuclear Society, Vol. 5, No. 2, p. 479,

7. Rohsenow, W. and Choi, H., "Heat Mass and Momentum Transfer," Prentice-Hall Inc., Englewood Cliffs, New Jersey, 1961.

8. Holman, J. P., "Heat Transfer," McGraw-Hill, Inc., 1968.

9. Kraus, A. D., "Extended Surfaces," Spartan Books, 1964.

10. Browning, W. E. Jr. and Hemphill, H. L., "Thermocouples for Measurement of the Surface Temperature of Nuclear Fuel Elements," Paper No. 66, Temperature, Its Measurement and Control in Science and Industry, Vol. 3, Part 2, A.I. Dahl, Editor.

11. Brindley, J. H., "Calibration of Surface Attached Thermocouples on a Flat-Plate Fuel Element by Electrical Analogue Techniques," Transactions of the American Nuclear Society., Vol. 4, No. 1, p. 333,

12. Chapman, Allan J., "Heat Transfer," The Mamillan Co., New York, 1960, p. 392.

13. Kays, W. M., "Convective Heat and Mass Transfer," McGraw-Hill & Company, 1960.

APPENDIX A

EXPERIMENTAL DATA

In the experimental data which follows, Data Sets 2, 5, and 6 are full power runs. Data Sets 3 and 4 are one-half power runs in which only the male or female side of the channel was heated. Data Set 1 was a one-third power run with both sides of the channel being heated.

The data is printed in the following order:

Data Set Number
Date of Experiment
Flow Rate, GPM
Channel Pressure Drop, inches of H_2O
Channel Inlet/Outlet Temperatures*
Male Backplate Temperatures, Positions 1-7
Male Backplate Temperatures, Positions 8-14
Female Backplate Temperatures, Positions 1-7
Female Backplate Temperatures, Positions 8-14
In-Channel Thermocouple Temperatures, IC 1-4
Heat Flux Thermocouple Temperatures, HF 1-4**

*All temperatures in ^{o}F.
**Only for Data Set 6.

```
1
3/11/75
 1.0
  2.0
95.27/119.50
108.00 117.80 117.80 125.00 134.60   0.0  138.50
138.50 138.00 138.50 137.00 134.60 133.50 127.33
117.00 118.15 117.33 124.66 135.00 140.00 140.00
140.33 140.00 140.66 139.50 135.50 135.50 128.00
111.50 125.00 130.00 119.00


1
3/ 8/75
 2.0
  9.0
95.00/107.35
112.25 108.50 108.65 112.20 114.15   0.0  116.65
116.10 117.00 117.73 117.37 116.25 115.00 111.20
100.35   0.0  106.18 108.40 111.75 113.60 115.30
115.02 116.35 117.83 117.47 114.90 115.60 110.67
112.45 108.40 108.15 113.83


1
3/ 8/75
 2.0
  9.5
95.26/107.50
112.25 108.35 108.35 111.75 113.73   0.0  116.15
115.65 116.60 117.33 117.00 115.70 114.55 110.80
100.41   0.0  106.23 109.05 112.18 114.02 115.77
115.68 116.77 118.50 118.00 115.45 116.10 111.04
112.27 108.10 107.73 103.64


1
3/11/75
 3.0
 20.0
95.07/105.20
 99.87 104.35 104.35 106.40 107.30   0.0  109.75
109.33 110.10 110.47 110.17 109.35 108.30 105.30
101.10 105.95 105.25 106.83 108.90 110.40 111.30
111.10 111.75 113.10 112.50 110.70 110.90 107.10
 99.57 103.10 102.65 100.30
```

```
1
3/11/75
 4.0
 35.0
95.13/103.53
 99.43 103.43 103.43 105.00 105.75   0.0  107.30
107.15 107.55 107.90 107.35 106.77 106.10 103.27
100.50 104.85 104.30 106.00 107.20 108.35 109.40
109.20 109.65 110.47 110.00 108.25 108.60 105.15
 98.50 101.00 100.00  99.33


1
3/11/75
 5.0
 42.0
95.09/102.36
 99.18 102.45 102.45 103.91 104.45   0.0  106.09
105.95 106.18 106.41 105.91 105.32 104.45 101.59
100.23 104.32 103.82 105.14 106.50 107.36 108.23
108.09 108.32 109.23 108.55 107.00 107.32 103.91
 98.00  99.59  99.36  98.50


1
3/11/75
 6.0
 71.0
95.07/101.75
 98.80 102.20 102.20 103.47 103.77   0.0  105.25
105.15 105.30 105.45 104.85 104.20 103.53 100.75
100.01 103.90 103.57 104.70 106.00 106.60 107.15
107.00 107.15 108.05 107.25 106.10 106.33 103.23
 97.50  99.00  99.00  98.00


1
3/11/75
 7.0
 92.0
95.20/101.40
 98.70 102.00 102.00 103.23 103.47   0.0  104.70
104.55 104.70 104.75 104.15 103.70 103.10 100.20
100.23 103.91 103.41 104.47 105.65 106.32 106.95
106.82 106.91 107.64 106.95 105.50 105.82 102.64
 97.50  98.50  98.00  97.50
```

```
1
3/11/75
 8.0
115.0
95.00/100.60
 98.35 101.45 101.45 102.70 103.00   0.0  103.90
103.80 103.83 103.87 103.47 103.07 102.20  99.57
 99.83 103.43 103.30 103.90 104.95 105.60 106.13
106.03 106.07 106.57 106.03 104.55 104.80 102.95
 97.00  98.00  97.50  97.00


1
3/11/75
 9.0
138.0
95.00/100.20
 98.00 101.00 101.00 102.20 107.45   0.0  103.47
103.37 103.37 103.40 102.95 102.40 101.50  99.17
 99.73 103.23 102.90 103.66 104.47 105.10 105.70
105.50 105.50 106.13 105.45 103.97 104.20 101.45
 96.50  97.50  97.00  96.50


2
3/15/75
 1.0
  0.0
95.40/158.25
132.00 159.50 160.00 179.50 199.50   0.0  204.33
202.50 203.50 205.50 202.00 196.50 171.50 178.50
120.67 130.33 140.90 168.50 191.00 197.00 198.00
197.50 200.00 205.00 201.67 192.00 193.00 175.00
140.00 169.00 176.33 148.50


2
3/15/75
 2.0
  9.0
95.32/129.50
117.00 134.67 134.67 144.67 150.00   0.0  155.00
154.00 156.00 157.67 156.50 153.00 150.67 139.50
109.20 127.67 125.50 134.00 142.50 147.33 151.50
150.67 154.00 158.00 156.50 150.00 150.67 137.67
115.70 131.00 130.33 119.45
```

```
2
3/15/75
 3.0
 20.0
95.00/118.35
110.93 124.67 124.67 130.33 133.50   0.0  140.00
138.50 140.33 141.50 140.33 137.67 135.50 126.00
105.35 120.20 118.50 124.00 130.00 134.00 137.50
137.00 138.50 142.00 140.33 135.00 135.50 124.33
108.40 119.15 116.50 110.70


2
3/15/75
 4.0
 35.0
95.03/112.76
108.45 120.37 120.43 125.00 127.00   0.0  132.50
131.50 133.00 133.50 132.00 130.00 127.67 118.95
103.70 116.90 115.25 119.75 124.67 127.67 130.33
130.00 131.00 134.33 132.00 127.33 127.67 117.63
105.00 112.80 110.07 106.53


2
3/15/75
 5.0
 52.0
95.03/108.97
107.00 118.26 118.35 121.74 123.48   0.0  128.91
127.61 128.48 128.91 127.61 125.43 123.04 115.04
102.48 114.70 113.48 117.52 121.30 123.90 126.74
125.87 126.74 129.35 127.17 122.61 123.04 113.48
103.33 109.00 107.50 104.00


2
3/15/75
 6.0
 71.0
95.10/106.71
106.27 116.65 116.75 120.23 121.50   0.0  126.00
124.67 125.50 125.50 124.33 122.00 120.40 112.00
102.40 113.40 112.35 115.80 119.65 121.50 124.00
123.00 124.00 126.00 124.00 119.85 120.30 110.83
102.00 106.60 105.00 103.00
```

```
2
3/15/75
 7.0
 91.0
95.00/105.06
105.40 109.10 115.25 118.55 119.80   0.0  124.00
122.50 123.50 123.50 121.50 120.00 117.93 110.07
101.70 112.30 111.10 114.30 117.90 120.10 121.50
121.00 121.00 124.00 121.00 117.43 117.83 108.80
101.00 104.70 103.50 101.50


2
3/15/75
 8.0
112.0
95.03/103.90
104.90 114.20 114.25 117.57 118.35   0.0  122.00
121.00 121.50 121.50 120.20 118.10 116.60 108.50
101.50 111.65 110.63 113.63 117.13 118.80 120.43
120.00 120.20 122.00 119.95 115.95 116.50 107.40
100.50 102.00 102.50 100.50


2
3/15/75
 9.0
136.0
95.13/103.35
104.50 113.67 113.67 117.00 117.50   0.0  121.00
120.27 120.57 120.37 118.75 117.10 115.20 107.30
101.35 111.20 110.37 113.23 116.35 117.83 119.20
118.80 118.95 120.87 118.65 114.65 115.25 106.60
100.00 103.00 101.50 100.00


3
4/24/75
 1.0
  0.0
95.33/127.67
135.00 154.33 154.00 171.50 190.50   0.0  195.33
  0.0  191.00 189.00 182.66   0.0  173.00   0.0
  0.0    0.0   0.0    0.0    0.0    0.0    0.0
  0.0    0.0   0.0    0.0    0.0    0.0    0.0
107.00 122.50   0.0  117.00
```

```
3
4/24/75
 2.0
 10.0
96.00/112.00
120.33 132.00 131.50 139.50 142.50   0.0   144.33
  0.0  144.00 144.33 141.00   0.0  135.50    0.0
  0.0    0.0    0.0    0.0    0.0    0.0     0.0
  0.0    0.0    0.0    0.0    0.0    0.0     0.0
 99.33 109.00   0.0  103.33


3
4/24/75
 3.0
 21.0
94.50/106.00
114.00 123.50 123.00 128.00 129.50   0.0   132.50
  0.0  132.50 132.50 130.00   0.0  125.00    0.0
  0.0    0.0    0.0    0.0    0.0    0.0     0.0
  0.0    0.0    0.0    0.0    0.0    0.0     0.0
 96.00 103.33   0.0   99.33


3
4/24/75
 4.0
 37.0
95.00/103.67
111.50 120.00 119.50 124.00 124.66   0.0   127.66
  0.0  127.33 127.00 124.00   0.0  120.33    0.0
  0.0    0.0    0.0    0.0    0.0    0.0     0.0
  0.0    0.0    0.0    0.0    0.0    0.0     0.0
 96.00 101.50   0.0   98.00


3
4/24/75
 5.0
 55.0
95.00/102.00
110.00 117.66 117.33 121.00 121.50   0.0   124.33
  0.0  124.00 123.50 121.00   0.0  117.33    0.0
  0.0    0.0    0.0    0.0    0.0    0.0     0.0
  0.0    0.0    0.0    0.0    0.0    0.0     0.0
 95.67  98.00   0.0   97.75
```

```
3
4/24/75
 6.0
 75.0
95.00/101.00
109.50 116.50 116.00 119.50 120.00   0.0  123.00
  0.0  122.00 121.50 120.00   0.0  115.50   0.0
  0.0    0.0    0.0    0.0    0.0    0.0    0.0
  0.0    0.0    0.0    0.0    0.0    0.0    0.0
 95.67  99.67   0.0   97.50


3
4/24/75
 7.0
 99.0
95.33/100.00
109.00 115.50 115.50 118.50 119.00   0.0  121.00
  0.0  120.66 120.33 118.50   0.0  114.50   0.0
  0.0    0.0    0.0    0.0    0.0    0.0    0.0
  0.0    0.0    0.0    0.0    0.0    0.0    0.0
 96.00  99.33   0.0  110.67


3
4/24/75
 8.0
120.0
94.50/ 99.33
108.00 114.50 114.00 117.33 117.66   0.0  120.00
  0.0  119.00 118.00 117.00   0.0  113.00   0.0
  0.0    0.0    0.0    0.0    0.0    0.0    0.0
  0.0    0.0    0.0    0.0    0.0    0.0    0.0
 95.33  98.00   0.0   96.50


3
4/24/75
 9.0
148.0
95.00/ 99.00
107.50 114.00 114.00 117.00 117.00   0.0  119.50
  0.0  118.50 118.00 116.00   0.0  112.50   0.0
  0.0    0.0    0.0    0.0    0.0    0.0    0.0
  0.0    0.0    0.0    0.0    0.0    0.0    0.0
 95.67  98.50   0.0   97.00
```

```
3
4/24/75
10.0
173.0
94.50/ 98.50
107.00 113.33 113.33 116.00 116.00   0.0  118.50
  0.0  117.66 117.00 115.00   0.0  111.50   0.0
  0.0    0.0    0.0    0.0    0.0    0.0    0.0
  0.0    0.0    0.0    0.0    0.0    0.0    0.0
 95.33  97.50   0.0   96.00


4
4/25/75
 1.0
  0.0
95.33/124.83
  0.0    0.0    0.0    0.0    0.0    0.0    0.0
  0.0    0.0    0.0    0.0    0.0    0.0    0.0
  0.0  145.00 143.00 158.50 174.00 180.00 179.00
174.00 179.67 189.00 177.00 167.67 167.67   0.0
135.50 149.00   0.0  148.00


4
4/25/75
 2.0
 10.0
95.00/111.00
  0.0    0.0    0.0    0.0    0.0    0.0    0.0
  0.0    0.0    0.0    0.0    0.0    0.0    0.0
  0.0  125.00 124.00 130.33 136.50 139.50 140.67
140.67 142.00 144.33 141.00 134.00 135.00   0.0
113.67 117.33   0.0  117.67


4
4/25/75
 3.0
 21.0
95.33/106.67
  0.0    0.0    0.0    0.0    0.0    0.0    0.0
  0.0    0.0    0.0    0.0    0.0    0.0    0.0
  0.0  119.00 118.00 123.00 126.50 129.00 130.33
130.00 130.67 132.50 129.50 124.00 125.00   0.0
108.50 110.33   0.0  106.33
```

```
4
4/25/75
 4.0
 37.0
95.00/103.33
  0.0     0.0     0.0     0.0     0.0     0.0     0.0
  0.0     0.0     0.0     0.0     0.0     0.0     0.0
  0.0   116.50  115.50  119.00  122.00  124.33  125.00
125.00  125.00  126.50  124.00  119.00  120.00    0.0
105.00  105.50    0.0   103.00


4
4/25/75
 5.0
 56.0
95.00/102.00
  0.0     0.0     0.0     0.0     0.0     0.0     0.0
  0.0     0.0     0.0     0.0     0.0     0.0     0.0
  0.0   114.50  113.67  117.33  120.00  121.50  122.50
122.00  122.00  123.50  121.00  116.50  117.33    0.0
103.67  103.33    0.0   101.50


4
4/25/75
 6.0
 75.0
95.00/100.50
  0.0     0.0     0.0     0.0     0.0     0.0     0.0
  0.0     0.0     0.0     0.0     0.0     0.0     0.0
  0.0   113.33  112.50  115.50  118.00  119.00  120.33
120.33  120.33  121.00  118.50  113.67  114.50    0.0
102.50  101.50    0.0    95.33


4
4/25/75
 7.0
100.0
95.33/100.00
  0.0     0.0     0.0     0.0     0.0     0.0     0.0
  0.0     0.0     0.0     0.0     0.0     0.0     0.0
  0.0   113.33  112.00  113.33  117.67  119.00  120.00
119.50  119.00  120.33  118.00  113.33  114.00    0.0
102.00  101.00    0.0   100.50
```

```
4
4/25/75
 8.0
123.0
95.00/ 99.33
  0.0    0.0    0.0    0.0    0.0    0.0    0.0
  0.0    0.0    0.0    0.0    0.0    0.0    0.0
  0.0  112.50 111.50 114.00 116.50 117.67 118.50
118.00 117.67 119.00 116.50 112.50 112.50   0.0
101.00 100.00   0.0   99.67


4
4/25/75
 9.0
144.0
95.00/ 98.50
  0.0    0.0    0.0    0.0    0.0    0.0    0.0
  0.0    0.0    0.0    0.0    0.0    0.0    0.0
  0.0  111.50 110.67 113.33 115.50 117.00 117.33
117.00 116.50 117.67 115.00 110.67 111.50   0.0
100.50  99.33   0.0   99.00


4
4/25/75
10.0
173.0
95.33/ 99.00
  0.0    0.0    0.0    0.0    0.0    0.0    0.0
  0.0    0.0    0.0    0.0    0.0    0.0    0.0
  0.0  111.50 110.67 113.67 115.00 116.50 117.00
116.50 116.50 117.33 114.50 100.67 111.00   0.0
100.50  99.67   0.0   99.33


5
4/26/75
 1.0
  0.0
95.66/160.33
144.00 166.00 166.00 185.50 206.50   0.0  212.00
  0.0  210.00 211.00 210.33   0.0  199.00   0.0
  0.0    0.0  157.67 176.67 198.67 205.50 205.50
205.00 205.50 209.50 207.00 198.00 198.33   0.0
147.67 172.50   0.0  160.00
```

```
5
4/26/75
 2.0
 10.0
95.00/129.00
124.00 137.67 137.33 147.00 152.00   0.0  156.00
  0.0  156.50 158.00 157.33   0.0  152.00   0.0
  0.0  130.67 128.50 136.50 144.33 148.50 152.50
152.00 154.00 155.00 157.00 151.00 151.50   0.0
117.67 130.33   0.0  122.00


5
4/26/75
 3.0
 21.0
95.33/118.50
117.00 127.33 127.00 132.50 134.33   0.0  140.67
  0.0  141.00 142.50 141.00   0.0  137.00   0.0
  0.0  123.50 121.50 127.00 132.00 136.00 139.00
138.33 140.00 143.50 141.00 136.50 137.33   0.0
110.67 119.50   0.0  114.50


5
4/26/75
 4.0
 37.0
94.50/112.00
113.33 122.00 121.50 126.00 127.67   0.0  133.50
  0.0  133.50 134.33 133.00   0.0  128.50   0.0
  0.0  118.50 117.33 121.00 121.50 128.50 131.00
130.67 131.00 134.33 132.00 127.67 128.00   0.0
106.33 112.50   0.0  108.50


5
4/26/75
 5.0
 55.0
95.00/109.00
111.50 120.00 119.00 123.50 124.33   0.0  129.00
  0.0  129.00 129.50 127.67   0.0  124.33   0.0
  0.0  117.00 115.50 119.00 122.50 125.00 127.00
127.00 127.00 129.50 127.33 124.00 123.50   0.0
104.00 108.50   0.0  105.50
```

```
5
4/26/75
 6.0
 76.0
94.50/106.33
110.33 119.00 120.00 121.00 122.00   0.0  126.50
  0.0  126.00 126.00 124.67   0.0  121.00   0.0
  0.0  115.00 114.00 117.33 120.67 122.50 124.60
124.00 124.33 126.00 124.00 120.33 120.67   0.0
103.50 106.00   0.0  103.67


5
4/26/75
 7.0
 97.0
95.00/105.00
110.00 117.33 117.00 120.00 120.66   0.0  124.66
  0.0  124.00 124.00 122.50   0.0  119.00   0.0
  0.0  114.00 113.33 116.00 117.00 121.00 122.50
122.00 122.50 123.00 121.50 118.00 118.50   0.0
102.50 104.50   0.0  102.50


5
4/26/75
 8.0
121.0
95.00/103.66
109.00 116.50 116.00 119.00 119.50   0.0  123.50
  0.0  122.50 122.00 120.66   0.0  117.33   0.0
  0.0  113.66 112.50 115.50 118.00 120.00 121.00
121.00 120.66 122.50 120.33 121.00 117.33   0.0
100.75 102.00   0.0  100.00


5
4/26/75
 9.0
144.0
95.00/103.00
108.50 115.50 115.00 118.00 118.50   0.0  122.00
  0.0  121.00 121.00 120.00   0.0  116.50   0.0
  0.0  113.33 112.00 114.50 117.33 119.00 120.33
120.00 119.50 121.00 119.00 115.50 116.00   0.0
102.00 103.67   0.0  101.00
```

```
5
4/26/75
10.0
170.0
95.00/102.00
108.00 114.50 114.50 117.33 117.66   0.0  119.00
  0.0  120.33 120.00 118.50   0.0  115.00   0.0
  0.0  112.50 111.50 113.33 116.50 118.00 119.50
118.50 118.50 120.00 117.66 114.00 114.50   0.0
101.25 101.50   0.0  100.50


6
5/ 3/75
 1.0
  0.0
95.33/157.67
137.33 164.00 163.50 182.33 202.50   0.0  207.33
  0.0  205.50 207.00 204.00   0.0  195.67   0.0
  0.0    0.0  154.67 173.33 194.50 201.00 201.33
201.00 201.00 205.00 202.50 194.50 195.00   0.0
145.50 169.50   0.0  151.00
201.67 197.00 201.67 196.50


6
5/ 3/75
 1.5
  5.0
95.00/137.67
130.00 147.00 146.50 159.50 168.50   0.0  171.00
  0.0  171.00 173.00 171.00   0.0  165.00   0.0
  0.0    0.0  136.00 146.50 157.00 161.50 165.00
165.00 167.67 172.00 170.33 163.50 164.00   0.0
125.50 141.00   0.0  128.00
164.67 159.50 167.33 162.50


6
5/ 3/75
 2.0
 10.0
95.00/127.50
123.00 130.33 136.00 144.67 149.00   0.0  153.50
  0.0  154.33 155.50 154.67   0.0  150.00   0.0
  0.0    0.0  127.33 134.33 141.50 146.50 150.33
150.00 151.50 156.00 154.33 148.50 149.50   0.0
117.00 129.00   0.0  119.00
149.00 144.33 151.50 147.00
```

```
6
5/ 3/75
 2.5
 15.0
95.00/121.50
119.00 130.00 129.50 136.00 139.00   0.0  144.67
  0.0  145.50 147.00 146.00   0.0  141.50   0.0
  0.0    0.0  123.00 128.50 134.67 139.00 142.50
142.00 144.00 147.33 145.50 140.33 141.00   0.0
112.50 122.50   0.0  114.00
141.50 137.00 144.00 139.00


6
5/ 3/75
 3.0
 20.0
94.75/117.00
116.00 125.50 125.00 130.67 133.00   0.0  138.50
  0.0  139.00 140.33 139.50   0.0  135.50   0.0
  0.0    0.0  119.50 124.33 130.00 133.50 137.00
136.50 137.33 140.67 139.00 134.33 135.00   0.0
109.00 117.30   0.0  110.40
136.00 131.00 137.67 133.00


6
5/ 3/75
 3.5
 29.0
95.00/114.00
114.00 123.00 123.00 127.67 129.50   0.0  135.00
  0.0  135.50 136.50 135.50   0.0  131.00   0.0
  0.0    0.0  118.00 122.00 127.00 130.33 133.50
133.00 134.00 136.50 134.67 130.33 131.00   0.0
107.50 114.00   0.0  108.30
132.50 127.67 134.33 129.50


6
5/ 3/75
 4.0
 38.0
95.00/112.00
113.00 121.00 121.00 125.00 127.00   0.0  132.00
  0.0  132.50 133.00 132.00   0.0  128.00   0.0
  0.0    0.0  117.00 120.67 124.67 127.67 130.33
130.00 130.67 133.50 131.00 127.33 127.67   0.0
106.16 112.00   0.0  106.47
130.00 125.00 131.00 126.50
```

```
6
5/ 3/75
 4.5
 46.0
95.00/110.13
111.50 120.67 120.00 124.00 125.00   0.0  130.00
  0.0  130.00 130.67 129.50   0.0  126.00   0.0
  0.0    0.0  115.50 118.50 123.00 126.00 128.00
127.67 128.00 130.67 129.00 124.67 125.50   0.0
105.00 110.00   0.0  105.30
127.67 123.00 129.50 124.33


6
5/ 3/75
 5.0
 56.0
95.00/108.50
111.00 119.00 119.00 122.50 124.00   0.0  128.00
  0.0  128.00 128.50 127.33   0.0  124.00   0.0
  0.0    0.0  114.50 118.00 121.50 124.33 126.50
126.00 126.50 128.50 127.00 123.00 123.50   0.0
104.00 108.50   0.0  104.00
126.00 121.50 127.67 122.50


6
5/ 3/75
 5.5
 66.0
95.00/107.50
110.67 118.50 118.00 121.50 122.50   0.0  127.00
  0.0  127.00 127.33 126.00   0.0  122.50   0.0
  0.0    0.0  114.00 117.67 121.00 123.50 125.00
124.67 125.00 127.33 125.50 121.00 122.00   0.0
103.67 107.00   0.0  103.63
125.00 120.33 126.50 121.00


6
5/ 3/75
 6.0
 75.0
95.33/106.67
110.67 118.00 117.67 121.00 122.00   0.0  126.00
  0.0  126.00 126.00 124.67   0.0  121.00   0.0
  0.0    0.0  113.67 117.00 120.33 122.50 124.33
124.00 124.00 126.00 124.33 120.00 121.00   0.0
103.57 106.30   0.0  103.27
124.33 119.50 125.00 120.33
```

```
6
5/ 3/75
 7.0
 98.0
95.00/104.50
109.50 116.50 116.00 119.00 120.00   0.0  123.50
  0.0  123.00 123.50 121.50   0.0  118.50   0.0
  0.0    0.0  111.50 115.00 118.00 120.33 121.50
121.00 121.00 123.00 121.00 117.33 118.00   0.0
102.15 104.00   0.0  101.45
121.50 117.00 122.50 117.33


6
5/ 3/75
 8.0
121.0
95.00/103.67
109.00 115.50 115.50 118.00 119.00   0.0  122.50
  0.0  121.50 121.50 120.67   0.0  117.33   0.0
  0.0    0.0  112.50 114.50 117.33 119.00 120.67
120.33 120.33 122.00 120.00 116.00 117.00   0.0
101.70 103.30   0.0  100.95
120.67 116.00 121.00 117.00


6
5/ 3/75
 9.0
145.0
95.00/102.50
108.00 114.50 114.50 117.33 116.67   0.0  121.00
  0.0  120.67 120.33 119.00   0.0  116.00   0.0
  0.0    0.0  111.00 113.67 116.50 118.00 119.50
119.00 118.50 120.33 118.00 114.50 115.00   0.0
101.00 102.50   0.0  100.10
119.50 114.50 120.33 115.50


6
5/ 3/75
10.0
172.0
95.00/102.00
107.50 114.00 114.00 117.00 117.00   0.0  120.00
  0.0  119.50 119.00 118.00   0.0  114.50   0.0
  0.0    0.0  110.67 113.33 115.50 117.33 118.50
118.00 117.67 119.00 117.33 113.33 114.00   0.0
100.65 102.00   0.0   99.73
118.50 113.67 119.50 114.20
```

APPENDIX B

DATA REDUCTION PROGRAM

The computer program used to analyze the data given in Appendix A is listed in the following pages. Output from the program for two flow points from Data Set No.6 is also given to show the type of information generated by the program.

The facilities at the MIT Information Processing Center were used to run the computer program.

```
C
C
C
C
C
C
C ******************************************************************
C
C     DATA REDUCTION PROGRAM-MITR-II HEAT TRANSFER STUDY
C
C     INPUT PARAMETERS:
C
C     RHO-AVERAGE DENSITY, LBM/FT**3
C     KAL- THERMAL CONDUCTIVITY OF ALUMINUM, BTU/HR-FT-F
C     XAL-THICKNESS OF ALUMINUM
C     C1-CONVERSION FACTOR,FT**3/HR/GPM
C     ABP- BACK PLATE AREA, FT**2
C     L - LENGTH OF HEATED SECTION
C     CP- HEAT CAPACITY OF WATER,BTU/LBM-F
C     NDATA - NUMBER OF DATA SETS
C     ISET - DATA SET NUMBER
C     FLOW - CHANNEL FLOW RATE, GPM
C     T1 - TEST SECTION INLET TEMPERATURE, DEGREES F
C     T2 - TEST SECTION OUTLET TEMPERATURE, DEGREES F
C     M - MONTH
C     ID - DAY
C     IY - YEAR
C     PDROP - TEST SECTION PRESSURE DROP, INCHES OF WATER
C     QM - LOCAL HEAT FLUX, BTU/HR-FT**2-F
C     TBPM(14) - MALE SECTION BACK PLATE TEMPERATURE, DEGREES F
C     TBPF(14) - FEMALE SECTION BACK PLATE TEMPERATURES, DEGREES F
C
C ******************************************************************
C
      REAL MDOT, KAL, L
      DIMENSION HM(14),HF(14),HBAR(14),TBPM(14),TBPF(14),TBAR(14),Z(14),
     1TF(14),THERM1(14),THERM2(14),THERM3(14)
C ******************************************************************
C
C     READ PARAMETERS FIXED FOR ENTIRE CALCULATION
C
C ******************************************************************
      READ(5,10) RHO,KAL,XAL,C1,ABP,L,CP
      READ(5,10) (Z(N),N=1,14)
   10 FORMAT(7F10.6)
C ******************************************************************
C
C     DEFINE NUMBER OF DATA SETS, NDATA
C
C ******************************************************************
      NDATA = 2
      RAL=XAL/KAL
      DO 200 K=1,NDATA
```

```
C ***************************************************************************
C
C     READ IN INPUT PARAMETERS
C
C ***************************************************************************
      READ(5,20) ISET
   20 FORMAT(I2)
      READ(5,30) FLOW,T1,T2,M,ID,IY
   30 FORMAT(3F10.6,3I2)
      READ(5,35) PDROP
   35 FORMAT(F10.6)
      READ(5,36) QM
   36 FORMAT(F10.2)
      READ(5,40) (TBPM(N),N=1,14)
      READ(5,40) (TBPF(N),N=1,14)
   40 FORMAT(7F10.6)
C ***************************************************************************
C
C     BEGIN CALCULATIONS
C
C ***************************************************************************
      DELT=T2-T1
      MDOT=C1*FLOW*RHO
      Q=MDOT*CP*DELT
      QA=QM
      IF(ISET.EQ.4) GO TO 45
      QB=0.5*Q/ABP
      GO TO 46
   45 QB=Q/ABP
   46 RQ=QA/QB
      DO 100 N=1,14
      TF(N)=T1+(Z(N)*DELT/L)
      IF(TBPM(N).GT.0.0.AND.TBPF(N).GT.0.0) GO TO 50
      IF(TBPM(N).EQ.0.0.AND.TBPF(N).GT.0.0) GO TO 60
      IF(TBPM(N).GT.0.0.AND.TBPF(N).EQ.0.0) GO TO 70
      IF(TBPM(N).EQ.0.0.AND.TBPF(N).EQ.0.0) GO TO 80
   50 TBAR(N)=0.5*(TBPM(N)+TBPF(N))
      RMT=(TBPM(N)-TF(N))/QA
      RFT=(TBPF(N)-TF(N))/QA
      RBAR=(TBAR(N)-TF(N))/QA
      THERM1(N)=RMT
      THERM2(N)=RFT
      THERM3(N)=RBAR
      HM(N)=1.0/(RMT-RAL)
      HF(N)=1.0/(RFT-RAL)
      HBAR(N)=1.0/(RBAR-RAL)
      GO TO 100
C
   60 RFT=(TBPF(N)-TF(N))/QA
      THERM2(N)=RFT
      THERM1(N)=0.0
      THERM3(N)=THERM2(N)
      HF(N)=1.0/(RFT-RAL)
```

```
      HM(N)=HF(N)
      HBAR(N)=HF(N)
      TBAR(N)=TBPF(N)
      GO TO 100
   70 RMT=(TBPM(N)-TF(N))/QA
      THERM1(N)=RMT
      THERM2(N)=0.0
      THERM3(N)=THERM1(N)
      HM(N)=1.0/(RMT-RAL)
      HF(N)=HM(N)
      HBAR(N)=HM(N)
      TBAR(N)=TBPM(N)
      GO TO 100
   80 HM(N)=0.0
      HF(N)=0.0
      HBAR(N)=0.0
      TBAR(N)=0.0
      THERM1(N)=0.0
      THERM2(N)=0.0
      THERM3(N)=0.0
  100 CONTINUE
      SUM1=0.0
      DO 101 I=1,14
  101 SUM1=SUM1+THERM3(I)
      AVG14=SUM1/14.0
      SUM2=0.0
      DO 102 ICE=6,9
  102 SUM2=SUM2+THERM3(ICE)
      AVG49=SUM2/4.0
      SUM3=0.0
      DO 103 INK=6,9
  103 SUM3=SUM3+HBAR(INK)
      AVGH=SUM3/4.0
C *****************************************************************************
C
C     PRINT RESULTS
C
C *****************************************************************************
      WRITE(6,110) ISET
  110 FORMAT(1H1//50X,15HDATA SET NUMBER,1X,I2//)
      WRITE(6,120) M,ID,IY,Q,FLOW,MDOT,QA,PDROP,RQ
  120 FORMAT(50X,17HDATE.............,I1,1H/,I2,1H/,I2/50X,17HPOWER.....
     1.......,F8.2,8H  BTU/HR/50X,17HFLOW.............,F4.1,19H GALLONS
     2PER MINUTE/50X,17HMASS FLOW.........,F8.2,7H  LB/HR/50X,17HHEAT FLU
     3X.........,F8.2,16H  BTU/HR-FT**2-F/50X,17HPRESSURE DROP.....,F5.1,2
     4X,15HINCHES OF WATER/50X,17HHEAT FLUX RATIO..,F7.4//////////)
      DO 135 J=1,14
  135 WRITE(6,140) J,Z(J),TBPM(J),TBPF(J),TBAR(J),HM(J),HF(J),HBAR(J),TF
     1(J)
  140 FORMAT(20X,I2,2X,F4.1,2X,3(F6.2,2X),3(E12.5,2X),2X,F6.2)
      WRITE(6,145) AVGH
  145 FORMAT(/20X,35HAVERAGE ETA*H, POSITIONS 6 THRU 9= ,E12.5)
      WRITE(6,148)
```

```
148 FORMAT(1H1//////)
    WRITE(6,150)
150 FORMAT(///44X,19HTHERMAL RESISTANCES/24X,15HF/(BTU/HR-SQFT)//1X,4H
   1POS.,9X,4HMALE,13X,6HFEMALE,11X,7HAVERAGE/)
    DO 155 JAY=1,16
155 WRITE(6,160) JAY,THERM1(JAY),THERM2(JAY),THERM3(JAY)
160 FORMAT (20X,I2,10X,3(E12.5,5X))
    WRITE(6,170) AVG16,AVG49
170 FORMAT(/20X,17HOVERALL AVERAGE= ,E12.5/1X,31HAVERAGE OF POSITIONS
   16 THRU 9= ,E12.5)
200 CONTINUE
    STOP
    END
```

DATA SET NUMBER 6

DATE.....5/ 3/75
POWER.....33508.23 BTU/HR
FLOW..... 5.0 GALLONS PER MINUTE
MASS FLOW..... 2488.06 LB/HR
HEAT FLUX.....49051.76 BTU/HR-FT**2-F
PRESSURE DROP.... 56.0 INCHES OF WATER
HEAT FLUX RATIO.. 1.1584

TC NO.	PCS.	BACK PLATE TEMPERATURES MALE	FEMALE	AVERAGE	ETA*H MALE	FEMALE	AVERAGE	BULK FLUID TEMP
1	0.0	111.00	0.0	111.00	0.14451E+05	0.14451E+05	0.14451E+05	95.00
2	1.5	119.00	0.0	119.00	0.46492E+04	0.46492E+04	0.46492E+04	95.84
3	1.5	119.00	114.50	116.75	0.46492E+04	0.81070E+04	0.59094E+04	95.84
4	3.0	122.50	118.00	120.25	0.37141E+04	0.56337E+04	0.44768E+04	96.69
5	6.0	124.00	121.50	122.75	0.37676E+04	0.46630E+04	0.41678E+04	98.38
6	9.0	0.0	124.33	124.33	0.42062E+04	0.42062E+04	0.42062E+04	100.06
7	12.0	128.00	126.50	127.25	0.35950E+04	0.40391E+04	0.38041E+04	101.75
8	12.0	0.0	126.00	126.00	0.42125E+04	0.42125E+04	0.42125E+04	101.75
9	15.0	128.00	126.50	127.25	0.41024E+04	0.46909E+04	0.43769E+04	103.44
10	18.0	128.50	128.50	128.50	0.45548E+04	0.45548E+04	0.45548E+04	105.13
11	21.0	127.33	127.00	127.16	0.61998E+04	0.64696E+04	0.63319E+04	106.81
12	22.5	0.0	123.00	123.00	0.17915E+05	0.17915E+05	0.17915E+05	107.66
13	22.5	124.00	123.50	123.75	0.13122E+05	0.15148E+05	0.14063E+05	107.66
14	24.0	0.0	0.0	0.0	0.0	0.0	0.0	108.50

AVERAGE ETA*H, POSITIONS 6 THRU 9= 0.41499E+04

THERMAL RESISTANCES
F/(BTU/HR-SQFT)

TC NO.	MALE	FEMALE	AVERAGE
1	0.32619E-03	0.0	0.32619E-03
2	0.47208E-03	0.0	0.47208E-03
3	0.47208E-03	0.38034E-03	0.42621E-03
4	0.52623E-03	0.43449E-03	0.48036E-03
5	0.52241E-03	0.47144E-03	0.49692E-03
6	0.0	0.49473E-03	0.49473E-03
7	0.53515E-03	0.50457E-03	0.51986E-03
8	0.0	0.49438E-03	0.49438E-03
9	0.50075E-03	0.47017E-03	0.48546E-03
10	0.47654E-03	0.47654E-03	0.47654E-03
11	0.41828E-03	0.41155E-03	0.41492E-03
12	0.0	0.31281E-03	0.31281E-03
13	0.33319E-03	0.32300E-03	0.32810E-03
14	0.0	0.0	0.0

OVERALL AVERAGE= 0.40918E-03
AVERAGE OF POSITIONS 6 THRU 9= 0.49861E-03

DATA SET NUMBER 6

DATE.....5/ 3/75
POWER.....34128.75 BTU/HR
FLOW..... 5.5 GALLONS PER MINUTE
MASS FLOW..... 2736.87 LB/HR
HEAT FLUX.....49051.76 BTU/HR-FT**2-F
PRESSURE DROP.... 66.0 INCHES OF WATER
HEAT FLUX RATIO.. 1.1374

TC NO.	POS.	BACK PLATE TEMPERATURES MALE	FEMALE	AVERAGE	ETA*H MALE	FEMALE	AVERAGE	BULK FLUID TEMP
1	0.0	110.67	0.0	110.67	0.16007E+05	0.16007E+05	0.16007E+05	95.00
2	1.5	118.50	0.0	118.50	0.48503E+04	0.48503E+04	0.48503E+04	95.78
3	1.5	118.00	114.00	116.00	0.51026E+04	0.87388E+04	0.64431E+04	95.78
4	3.0	121.50	117.67	119.58	0.39777E+04	0.57696E+04	0.47089E+04	96.56
5	6.0	122.50	121.00	121.75	0.41678E+04	0.47765E+04	0.44514E+04	98.13
6	9.0	0.0	123.50	123.50	0.43769E+04	0.43769E+04	0.43769E+04	99.69
7	12.0	127.00	125.00	126.00	0.37318E+04	0.44015E+04	0.40391E+04	101.25
8	12.0	0.0	124.67	124.67	0.45358E+04	0.45358E+04	0.45358E+04	101.25
9	15.0	127.00	125.00	126.00	0.42352E+04	0.51192E+04	0.46355E+04	102.81
10	18.0	127.33	127.33	127.33	0.47396E+04	0.47396E+04	0.47396E+04	104.38
11	21.0	126.00	125.50	125.75	0.65781E+04	0.70509E+04	0.68063E+04	105.94
12	22.5	0.0	121.00	121.00	0.29275E+05	0.29275E+05	0.29275E+05	106.72
13	22.5	122.50	122.00	122.25	0.15447E+05	0.18333E+05	0.16767E+05	106.72
14	24.0	0.0	0.0	0.0	0.0	0.0	0.0	107.50

AVERAGE ETA*H, POSITIONS 6 THRU 9= 0.43968E+04

THERMAL RESISTANCES
F/(BTU/HR-SQFT)

TC NO.	MALE	FEMALE	AVERAGE
1	0.31946E-03	0.0	0.31946E-03
2	0.46316E-03	0.0	0.46316E-03
3	0.45297E-03	0.37142E-03	0.41219E-03
4	0.50839E-03	0.43031E-03	0.46935E-03
5	0.49692E-03	0.46634E-03	0.48163E-03
6	0.0	0.48546E-03	0.48546E-03
7	0.52496E-03	0.48418E-03	0.50457E-03
8	0.0	0.47745E-03	0.47745E-03
9	0.49310E-03	0.45233E-03	0.47271E-03
10	0.46797E-03	0.46797E-03	0.46797E-03
11	0.40901E-03	0.39881E-03	0.40391E-03
12	0.0	0.29115E-03	0.29115E-03
13	0.32173E-03	0.31153E-03	0.31663E-03
14	0.0	0.0	0.0

OVERALL AVERAGE= 0.39755E-03
AVERAGE OF POSITIONS 6 THRU 9= 0.48505E-03

APPENDIX C

DATA TABLES

The following data tables were compiled from the experimental data given in Appendix A and the results of the data reduction program given in Appendix B. The various heat transfer and inchannel thermocouple results presented in graphical form in this thesis are taken from these tables.

Data Tables 1 through 8 give the pertinent experimental heat transfer parameters. Flow rates are in GPM, all temperatures are in ^{o}F, and the remaining parameters are in English engineering units.

Data Tables 9 through 17 give the results of the inchannel thermocouple response analysis. The units of the parameters in these tables are the same as those in Data Tables 1 through 8.

**** DATA TABLE NO.1 ****

FLOW RATE	HEAT FLUX	WALL TEMP	FILM TEMP	FLUID TEMP	RE	PR	$\eta_o h$	THERMAL RESIST.	NU/$PR^{1/3}$	COLBURN 1/h
1.0	39427	190.5	158.6	126.8	2241	2.74	616	0.19E-02	8.10	0.12E-02
2.0	42883	141.8	127.9	112.4	3728	3.44	1479	0.93E-03	18.60	0.76E-03
3.0	43943	127.0	116.8	106.7	4836	4.02	2286	0.69E-03	27.50	0.62E-03
4.0	44489	119.6	111.8	103.9	5814	4.49	3000	0.59E-03	35.00	0.49E-03
5.0	43723	116.0	109.0	102.0	6900	4.74	3407	0.55E-03	39.10	0.42E-03
6.0	43699	114.2	107.5	100.9	8061	4.91	3868	0.51E-03	44.10	0.37E-03
7.0	44175	110.9	105.5	100.0	9069	5.09	4435	0.48E-03	50.00	0.34E-03
8.0	44514	109.4	104.4	99.5	10186	5.18	4900	0.46E-03	55.00	0.31E-03
9.0	46409	107.9	103.6	99.2	11300	5.27	5908	0.43E-03	66.00	0.28E-03

Note: The above parameters are based on average heat flux values and have been calculated from data given in Data Set No.2.

**** DATA TABLE NO.2 ****

FLOW RATE	HEAT FLUX	WALL TEMP	FILM TEMP	FLUID TEMP	RE	PR	$n_o h$	THERMAL RESIST.	NU/PR$^{1/3}$	COLBURN 1/h
1.0	50324	187.6	157.2	126.8	2221	2.80	839	.15E-02	11.04	0.12E-02
2.0	46515	140.8	126.6	112.4	3720	3.43	1686	.85E-03	21.15	0.76E-03
3.0	51475	125.0	115.8	106.7	4735	4.10	2936	.60E-03	35.08	0.60E-03
4.0	50259	118.6	111.0	103.9	5728	4.55	3691	.50E-03	42.90	0.50E-03
5.0	50650	114.3	108.1	102.0	6788	4.83	4427	.48E-03	50.60	0.43E-03
6.0	49336	111.7	106.3	100.9	7891	4.99	4870	.46E-03	55.17	0.38E-03
7.0	51941	108.9	104.5	100.0	8912	5.18	6269	.42E-03	70.32	0.34E-03
8.0	48472	108.4	103.9	99.5	10096	5.22	5784	.43E-03	64.74	0.30E-03
9.0	52000	105.8	102.5	99.2	11101	5.30	7205	.38E-03	102.40	0.28E-03

Note: The above parameters are based on local heat flux values and have been calculated from data given in Data Set No.2.

**** DATA TABLE NO.3 ****

FLOW RATE	HEAT FLUX	WALL TEMP	FILM TEMP	FLUID TEMP	RE	PR	$\eta_0 h$	THERMAL RESIST.	NU/PR$^{1/3}$	COLBURN 1/h
1.0		184.9	148.2	111.5	2100	2.98	591	.20E-02	7.66	0.12E-02
2.0		134.0	119.0	104.0	3384	3.80	1331	.10E-02	16.23	0.80E-03
3.0		121.4	110.8	100.2	4281	4.57	2094	.74E-03	24.28	0.63E-03
4.0		116.5	107.9	99.3	5410	4.84	2643	.64E-03	30.18	0.51E-03
5.0		113.0	105.6	98.5	6492	5.06	3186	.57E-03	35.95	0.44E-03
6.0		113.4	104.9	98.0	7700	5.13	3692	.53E-03	41.52	0.38E-03
7.0		110.5	104.1	97.7	8862	5.21	3373	.55E-03	37.80	0.34E-03
8.0		107.5	102.3	96.9	9817	5.39	5000	.46E-03	55.53	0.31E-03
9.0		107.9	102.4	97.0	11083	5.37	4582	.46E-03	50.93	0.28E-03
10.0		105.6	101.0	96.5	12126	5.46	6193	.42E-03	68.56	0.26E-03

Note: The above parameters are based on average heat flux values and have been calculated from data given in Data Set No.3.

**** DATA TABLE NO.4 ****

FLOW RATE	HEAT FLUX	WALL TEMP	FILM TEMP	FLUID TEMP	RE	PR	$\eta_o h$	THERMAL RESIST.	NU/PR$^{1/3}$	COLBURN 1/h
1.0	37011	167.0	138.5	110.1	1986	3.18	646	0.18E-02	8.25	0.13E-02
2.0	40148	131.0	117.0	103.0	3237	4.00	1514	0.92E-03	18.23	0.81E-03
3.0	42684	119.4	106.7	101.0	4234	4.63	2454	0.67E-03	28.39	0.63E-03
4.0	41800	114.3	106.7	99.2	5300	4.95	2932	0.60E-03	33.26	0.52E-03
5.0	43911	111.0	104.7	98.5	6393	5.15	3733	0.53E-03	41.92	0.44E-03
6.0	41403	109.7	103.7	97.8	7544	5.25	3760	0.53E-03	42.10	0.38E-03
7.0	41015	109.2	103.4	97.7	8757	5.28	4092	0.51E-03	45.70	0.34E-03
8.0	43461	107.1	102.1	97.2	9797	5.39	4796	0.47E-03	53.17	0.31E-03
9.0	39521	107.0	101.9	96.8	10983	5.43	4176	0.50E-03	46.34	0.28E-03
10.0	46043	104.9	101.0	97.2	12030	5.51	6413	0.41E-03	70.81	0.26E-03

Note: The above parameters are based on average heat flux values and have been calculated from data given in Data Set No.4.

**** DATA TABLE NO.5 ****

FLOW RATE	HEAT FLUX	WALL TEMP	FILM TEMP	FLUID TEMP	RE	PR	$\eta_o h$	THERMAL RESIST.	$NU/PR^{1/3}$	COLBURN 1/h
1.0	47241	164.4	137.2	110.1	1970	3.21	848	0.14E-02	10.80	0.13E-02
2.0	46515	128.7	115.9	103.0	3159	4.10	1807	0.81E-03	21.60	0.82E-03
3.0	50000	117.3	109.2	101.0	4151	4.72	3098	0.58E-03	35.02	0.64E-03
4.0	48218	112.6	105.9	99.2	5220	5.04	3638	0.53E-03	41.11	0.52E-03
5.0	50726	109.0	103.7	98.5	6290	5.24	4861	0.46E-03	54.36	0.44E-03
6.0	46744	108.3	103.3	97.8	7460	5.30	4572	0.48E-03	50.97	0.39E-03
7.0	48189	107.4	102.5	97.7	8630	5.36	5189	0.45E-03	57.69	0.34E-03
8.0	49037	105.6	101.4	97.2	9686	5.47	6010	0.42E-03	66.46	0.31E-03
9.0	46540	105.2	101.0	96.8	10822	5.51	5669	0.43E-03	62.58	0.28E-03
10.0	48189	104.4	100.8	97.2	11985	5.53	6832	0.40E-03	75.35	0.26E-03

Note: The above parameters are based on local heat flux values and have been calculated from data given in Data Set No.4.

**** DATA TABLE NO.6 ****

FLOW RATE	HEAT FLUX	WALL TEMP	FILM TEMP	FLUID TEMP	RE	PR	h_o	THERMAL RESIST.	$NU/PR^{1/3}$	COLBURN 1/h
1.0	40568	196.4	162.2	128.0	2293	2.69	583	0.20E-02	7.75	0.12E-02
2.0	42659	142.2	127.0	112.0	3728	3.42	1400	0.97E-03	17.57	0.76E-03
3.0	43604	127.9	117.4	106.9	4898	3.95	2124	0.73E-03	25.62	0.59E-03
4.0	43912	120.2	111.7	103.3	5807	4.49	2770	0.62E-03	32.30	0.49E-03
5.0	43912	166.2	109.1	102.0	6911	4.73	3230	0.57E-03	37.10	0.42E-03
6.0	44526	113.3	106.9	100.4	7968	4.94	3622	0.54E-03	41.11	0.37E-03
7.0	43911	111.5	105.7	100.0	9113	5.05	4057	0.50E-03	45.83	0.33E-03
8.0	43461	110.5	104.9	99.3	10260	5.13	4135	0.50E-03	46.46	0.30E-03
9.0	45166	109.0	104.0	99.0	11370	5.22	4867	0.46E-03	54.54	0.28E-03
10.0	43912	107.6	103.0	98.5	12433	5.31	4959	0.46E-03	55.28	0.26E-03

Note: The above parameters are based on average heat flux values and have been calculates from data given in Data Set No.5.

**** DATA TABLE NO.7 ****

FLOW RATE	HEAT FLUX	WALL TEMP	FILM TEMP	FLUID TEMP	RE	PR	$\eta_0 h$ THERMAL RESIST.	NU/$PR^{1/3}$	COLBURN 1/h
1.0	51781	193.6	160.8	128.0	2272	2.72	796	.15E-02	10.55	0.12E-02
2.0	46515	141.2	126.6	112.0	3719	3.43	1632	.87E-03	20.47	0.76E-03
3.0	51078	125.9	116.4	106.9	4793	4.04	2748	.62E-03	32.95	0.59E-03
4.0	49607	118.7	111.0	103.2	5730	4.55	3334	.58E-03	38.72	0.50E-03
5.0	50868	114.3	108.2	102.0	6800	4.81	4277	.49E-03	48.92	0.43E-03
6.0	50270	111.9	106.1	100.4	7865	5.01	4602	.47E-03	52.07	0.38E-03
7.0	51631	109.5	104.8	100.0	8960	5.14	5645	.44E-03	63.45	0.34E-03
8.0	47324	109.6	104.5	99.3	10188	5.17	4891	.46E-03	54.90	0.30E-03
9.0	53188	106.9	103.0	99.0	11185	5.31	7213	.40E-03	80.38	0.28E-03
10.0	49000	106.3	102.4	98.5	12304	5.37	6375	.41E-03	70.84	0.26E-03

Note: The above parameters are based on local heat flux values and have been calculated from data given in Data Set No.5.

**** DATA TABLE NO.8 ****

FLOW RATE	HEAT FLUX	WALL TEMP	FILM TEMP	FLUID TEMP	RE	PR	$\eta_o h$	THERMAL RESIST.	NU/PR$^{1/3}$	COLBURN 1/h
1.0	49914	189.8	158.2	126.5	2235	2.77	796	0.15E-02	10.51	0.12E-02
1.5	50726	153.5	134.9	116.3	2898	3.27	1389	0.98E-03	17.63	0.98E-03
2.0	46516	139.0	125.1	111.3	3841	3.46	1718	0.84E-03	21.49	0.74E-03
2.5	48189	130.4	119.3	108.3	4253	3.77	2224	0.71E-03	27.18	0.66E-03
3.0	49052	124.5	115.2	105.9	4673	4.16	2731	0.62E-03	32.50	0.60E-03
3.5	49000	121.0	112.8	104.5	5189	4.39	3070	0.58E-03	36.00	0.54E-03
4.0	48189	118.2	110.8	103.5	5712	4.57	3395	0.55E-03	39.39	0.50E-03
4.5	49914	115.5	109.0	102.6	6213	4.73	3997	0.51E-03	45.91	0.46E-03
5.0	49051	114.0	107.9	101.8	6759	4.84	4150	0.50E-03	47.38	0.43E-03
5.5	49051	112.7	107.0	101.3	7318	4.93	4397	0.48E-03	50.00	0.40E-03
6.0	49000	112.0	106.5	101.0	7929	4.97	4648	0.47E-03	52.72	0.37E-03
7.0	49051	109.1	104.4	99.8	8913	5.18	5416	0.44E-03	60.78	0.34E-03
8.0	47378	108.9	104.0	99.3	10117	5.21	5324	0.44E-03	59.61	0.30E-03
9.0	49863	106.8	102.8	98.8	11145	5.33	6562	0.41E-03	73.06	0.28E-03
10.0	49000	106.0	102.3	98.5	12283	5.37	6849	0.40E-03	76.13	0.26E-03

Note: The above parameters are based on local heat flux values and have been calculated from data given in Data Set No.6.

**** DATA TABLE NO.9 ****
INCHANNEL THERMOCOUPLE NO.2
DATA SET NO.2

FLOW RATE	BACK PLATE TEMP	WALL TEMP	FLUID TEMP	OBSERVED TEMP	CALIBRATION FACTOR	INSTALLATION PARAMETER X 10^5
1.0	197.1	184.2	120.2	169.0	0.237	99.2
2.0	148.9	137.0	108.8	131.0	0.211	47.8
3.0	134.5	121.3	104.2	119.2	0.124	29.0
4.0	128.1	115.1	102.0	112.8	0.178	21.5
5.0	124.3	111.2	100.5	109.0	0.209	16.7
6.0	121.8	109.1	99.7	106.6	0.267	14.0
7.0	120.3	106.9	99.0	104.7	0.279	11.0
8.0	119.0	106.6	98.5	102.0	0.567	7.2
9.0	118.0	104.0	98.4	103.0	0.172	8.9

**** DATA TABLE NO.10 ****
INCHANNEL THERMOCOUPLE NO.2
DATA SET NO.4

FLOW RATE	BACK PLATE TEMP	WALL TEMP	OBSERVED TEMP	FLUID TEMP	CALIBRATION FACTOR	INSTALLATION PARAMETER X 10^5
1.0	180.0	167.9	149.0	107.0	0.310	89.0
2.0	139.7	127.7	117.3	101.3	0.394	34.5
3.0	129.2	116.3	110.3	99.8	0.363	21.0
4.0	124.4	112.0	105.5	98.3	0.475	15.0
5.0	121.6	108.6	103.3	97.8	0.485	11.0
6.0	119.2	107.2	101.5	97.2	0.568	9.3
7.0	119.1	106.7	101.0	97.2	0.600	7.9
8.0	117.8	105.2	100.0	96.7	0.611	6.7
9.0	117.0	105.0	99.3	96.4	0.659	6.3
10.0	116.5	104.1	99.7	96.8	0.603	6.0

**** DATA TABLE NO.11 ****
INCHANNEL THERMOCOUPLE NO.2
DATA SET NO.5

FLOW RATE	BACK PLATE TEMP	WALL TEMP	OBSERVED TEMP	FLUID TEMP	CALIBRATION FACTOR	INSTALLATION PARAMETER X 10^5
1.0	205.5	192.2	172.5	121.1	0.277	99.2
2.0	149.1	137.2	130.3	108.4	0.238	47.2
3.0	136.4	123.3	119.5	104.5	0.202	29.4
4.0	128.9	116.1	112.5	101.4	0.245	22.4
5.0	125.3	112.2	103.5	100.5	0.318	15.7
6.0	122.8	109.9	106.0	99.2	0.363	13.6
7.0	121.2	108.5	104.5	98.9	0.384	10.8
8.0	120.2	108.0	103.7	98.4	0.451	11.1
9.0	119.2	105.5	101.5	98.2	0.546	6.3
10.0	118.2	105.6	102.0	97.8	0.462	8.7

**** DATA TABLE NO.12 ****
INCHANNEL THERMOCOUPLE NO.2
DATA SET NO.6

FLOW RATE	BACK PLATE TEMP	WALL TEMP	OBSERVED TEMP	FLUID TEMP	CALIBRATION FACTOR	INSTALLATION PARAMETER
1.0	201.0	188.2	169.5	119.9	0.273	99.4
1.5	162.0	149.0	141.0	111.8	0.214	57.6
2.0	147.0	135.1	129.0	107.8	0.223	45.6
2.5	139.5	127.1	122.5	105.4	0.213	35.4
3.0	134.0	121.4	117.3	103.5	0.229	28.1
3.5	130.8	118.2	114.0	102.5	0.266	23.5
4.0	128.0	115.7	112.0	101.7	0.263	21.4
4.5	126.3	113.4	110.0	101.0	0.267	18.1
5.0	124.6	112.0	108.5	100.3	0.300	16.7
5.5	123.7	111.1	107.0	99.9	0.366	14.4
6.0	122.8	110.2	106.3	99.5	0.361	13.9
7.0	120.5	107.9	104.0	98.7	0.423	10.7
8.0	119.2	107.0	103.3	98.4	0.434	10.3
9.0	118.2	105.4	102.5	97.9	0.388	9.1
10.0	117.5	104.9	102.0	97.8	0.404	8.7

**** DATA TABLE NO.13 ****
INCHANNEL THERMOCOUPLE NO.3
DATA SET NO.2

FLOW RATE	BACK PLATE TEMP	WALL TEMP	OBSERVED TEMP	FLUID TEMP	CALIBRATION FACTOR	INSTALLATION PARAMETER X 10^5
1.0	198.0	185.1	176.3	126.8	0.150	98.4
2.0	151.5	139.6	130.3	112.4	0.340	38.5
3.0	137.5	124.3	116.5	106.7	0.442	19.1
4.0	130.3	117.4	110.0	103.9	0.548	12.2
5.0	126.7	113.7	107.5	102.0	0.531	10.9
6.0	124.0	111.3	105.0	100.9	0.606	8.3
7.0	121.5	108.2	103.5	100.0	0.573	6.7
8.0	120.4	108.0	102.5	99.5	0.643	6.3
9.0	119.2	105.8	101.5	99.2	0.658	4.3

**** DATA TABLE NO.14 ****
INCHANNEL THERMOCOUPLE NO.4
DATA SET NO.2

FLOW RATE	BACK PLATE TEMP	WALL TEMP	OBSERVED TEMP	FLUID TEMP	CALIBRATION FACTOR	INSTALLATION PARAMETER X 10^5
1.0	197.5	184.6	148.5	127.3	0.630	42.2
2.0	150.7	138.7	119.4	112.6	0.739	14.6
3.0	137.0	123.8	110.7	106.8	0.772	7.5
4.0	130.0	117.1	106.5	104.0	0.808	5.0
5.0	125.9	112.8	104.0	102.0	0.823	3.8
6.0	123.0	110.3	103.0	101.0	0.785	4.1
7.0	121.0	107.6	101.5	101.1	0.815	2.7
8.0	120.0	107.5	100.5	99.5	0.880	2.0
9.0	118.8	104.8	100.0	99.3	0.872	1.3

**** DATA TABLE NO.15 ****
INCHANNEL THERMOCOUPLE NO.4
DATA SET NO.4

FLOW RATE	BACK PLATE TEMP	WALL TEMP	OBSERVED TEMP	FLUID TEMP	CALIBRATION FACTOR	INSTALLATION PARAMETER X 10^5
1.0	174.0	163.6	148.0	110.3	0.292	79.8
2.0	140.7	130.4	117.7	103.1	0.465	31.3
3.0	130.0	119.0	106.3	101.1	0.707	10.5
4.0	125.0	114.6	103.0	99.2	0.754	7.8
5.0	122.0	109.0	101.5	98.6	0.717	5.8
6.0	120.3	110.0	95.3	97.8	-	-
7.0	119.5	107.1	100.5	97.4	0.679	6.5
8.0	118.0	105.4	99.7	97.2	0.699	5.0
9.0	117.0	104.4	99.0	96.8	0.709	4.8
10.0	116.5	104.1	99.3	97.2	0.691	4.4

**** DATA TABLE NO.16 ****
INCHANNEL THERMOCOUPLE NO. 4
DATA SET NO. 5

FLOW RATE	BACK PLATE TEMP	WALL TEMP	OBSERVED TEMP	FLUID TEMP	CALIBRATION FACTOR	INSTALLATION PARAMETER X 10^5
1.0	205.0	101.7	160.0	128.5	0.501	60.9
2.0	152.0	140.0	122.0	112.2	0.649	21.0
3.0	138.3	125.2	114.5	107.1	0.591	14.5
4.0	130.7	117.9	108.5	103.4	0.647	10.4
5.0	127.0	113.9	105.5	102.1	0.713	6.7
6.0	124.0	110.1	103.7	100.5	0.669	6.3
7.0	122.0	108.7	102.5	100.1	0.719	4.7
8.0	121.0	108.8	101.0	99.4	0.830	3.4
9.0	120.0	106.3	100.5	99.1	0.802	2.7
10.0	118.5	105.9	100.0	98.6	0.803	3.0

**** DATA TABLE NO.17 ****
INCHANNEL THERMOCOUPLE NO. 4
DATA SET NO.6

FLOW RATE	BACK PLATE TEMP	WALL TEMP	OBSERVED TEMP	FLUID TEMP	CALIBRATION FACTOR	INSTALLATION PARAMETER X 10^5
1.0	201.0	188.2	151.0	127.0	0.607	48.2
1.5	165.0	152.0	128.0	116.6	0.678	22.9
2.0	150.0	138.1	119.0	111.5	0.717	16.2
2.5	142.0	129.6	113.8	108.4	0.746	11.2
3.0	136.5	123.9	110.4	106.0	0.755	8.9
3.5	133.0	120.4	108.3	104.6	0.768	7.5
4.0	130.0	117.6	106.5	103.6	0.796	5.9
4.5	127.7	114.8	105.3	102.7	0.784	5.3
5.0	124.7	112.1	104.0	101.8	0.787	4.4
5.5	124.7	112.1	103.6	101.3	0.786	4.7
6.0	124.0	111.4	103.3	101.1	0.792	4.7
7.0	121.0	108.4	101.4	99.8	0.810	4.5
8.0	120.3	108.2	101.0	99.4	0.823	3.3
9.0	119.0	106.2	100.1	98.8	0.824	3.3
10.0	118.0	105.4	99.7	98.6	0.828	2.7